

BSc Thesis Civil Engineering

Comparison of traditional Concrete Bridge and innovative 3D printed Steel Bridge

Determine overall life cycle properties of Concrete bridge and 3D printed Steel Bridge using a parametric calculation tool

Piscorschi Renat
BSc Civil Engineering

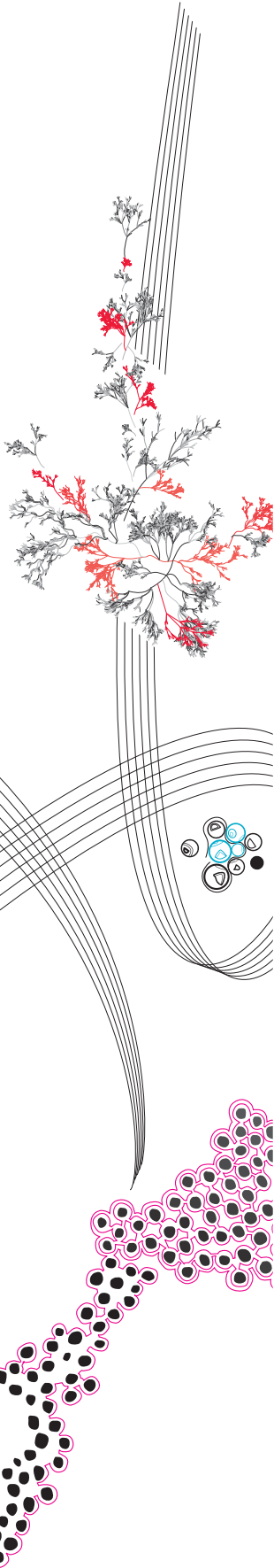
Supervisor:
Dr I. (Irina) Stipanović

External Supervisor:
S. (Sandra) Škarić Palić

Examination Committee:
Dr L. (Lara) Wöhler

July 5, 2022

Department of Civil Engineering and Management
Faculty of Engineering Technology (CTW)



Preface

The research in "Comparison of the traditional Concrete Bridge and innovative 3D printed steel Bridge design solutions" was provided in line with the literature investigations and the expert's requirements. That contributed to constructing the parametric tool that outlines the best alternative concerning several judging criteria such as structural properties, costs, and environmental impact. The final product concludes the graduation requirements of the bachelor's program in Civil Engineering at the University of Twente.

The research project engages in modeling, analyzing, and writing the dissertation at the behest of Infra Plan Consulting from April 2022. Infra Plan Consulting provides consultancy in data analytics, maintenance planning projects, and infrastructure management. The host company framed the research objective, and questions that predefined the research flow. With the substantial support of the external supervisor Sandra Škarić Palić, crucial research indications were given that defined the life cycle costs (LCC) model's critical aspects and the distribution of maintenance costs over the entire life cycle of the functional units.

The research project combines a majority of different disciplines. Keeping the high pace and precision of analysis and calculations would be impossible without the support and experience committed by experts and professors directly or indirectly involved in the research. Given this chance, I express sincere gratitude to Gerrit Snellink. He has crucially contributed to the project's starting point with valuable indications and essential feedback concerning the structural design that significantly optimized the concrete bridge's geometrical parameters, ensuring a reliable comparison analysis with the 3D-printed steel bridge.

My supervisor from the University of Twente, Irina Stipanović, merits enormous appreciation for her time, effort, feedback, and moral support in preparing the research proposal and final dissertation. Her energetic guidance and vast experience enhanced my academic competencies to the next level.

Finally, I consider that the results of this research project have a strong potential to enhance the engineers' potential to make better-informed decisions concerning economic perspective and reduce the impacts of their service on the environment.

Renat Piscorschi

June 2022, Enschede

Summary

The transportation infrastructure is a component of an essential value for developing societies since it promotes people's transportation, trading, and well-being. A high-speed developing industry permanently generates new construction methodologies that outline the efficiency and effectiveness of currently used procedures. Given that, the infrastructure experts have to ensure the functional reliability of multiple components while simultaneously retaining reasonable costs and environmental impact levels throughout the entire structural elements' life cycle. Therefore, considering the need to curb the costs and environmental impact, the infrastructure owners address the life cycle costs (LCC) and life cycle assessment (LCA) tools that assure the application of the best infrastructure alternative concerning multiple design requirements.

Currently, most bridges are commonly built of steel or concrete. Nevertheless, 3D printing technology is emerging as an alternative construction procedure that aspires to become the future fundamental tool in the infrastructure industry. Several claims favor 3D printing technology concerning the possible benefits from financial, structural, and environmental perspectives. Despite this, a wide range of engineering uncertainties concerning deciding on design alternatives is generated, mainly suspecting the extent to which the benefits of the newly appeared construction procedures overthrow the existing techniques. Consequently, this dilemma results in an inherent need for a broad range of analyses to choose the most suitable alternative in line with input requirements. Thus, this research project compares the life cycle of 100 years for two structural alternatives, the traditionally built concrete bridge, and the 3D printed steel bridge.

The research project's objective is to develop a parametric LCC and LCA tool operating functional units of concrete and a 3D-printed steel bridge. It aims to ease the process for infrastructure owners to outline the best alternative regarding adjustable input parameters that influence the financial and environmental impact of different bridge design solutions. This results in classifying the life cycle components into ten adaptable classes affecting the total costs and energy use incurred throughout different life cycle phases: 1) Activity duration; 2) Activity distance; 3) Activity unit price; 4) Volume of structural components; 5) Numbers of workers required per activity; 6) Activity frequency; 7) Dimensions of structural elements; 8) Activity production; 9) Price of recycling components; 10) Discount factor.

The postulated hypothesis was that the 3D printed bridge would inquire higher costs due to the price of the material, which was an inherent assumption given that the steel price is several times bigger than that of concrete. Additionally, concerning the environmental impact, it was assumed that the concrete bridge would retain a more substantial effect on multiple midpoints (National Institute for Public Health and the Environment, 2018). This assumption was based on a low recycling ratio of 75%, which is essentially lower than that of the 3D-printed steel bridge that could be fully recycled. Consequently, based on the literature and experts' knowledge, the LCC and LCA models were created, allowing for further inspection of the numerical results of the decisive factors of each functional unit. This inspection brought the following conclusion.

The price of the 3D-printed steel bridge partially matched the initial assumption. Since steel is a more expensive material within the production phase of the bridge life cycle, the traditionally built concrete bridge was significantly cheaper. However, since the concrete is often subject to maintenance, the overall costs of the traditionally built concrete bridge were higher than the 3D printed bridge. The discount factor implication partially generated this unexpected outcome. Considering that the maintenance costs are distributed all over the bridge's life cycle, costs in the future were substantially increased, which affected the final cost of the concrete bridge.

The majority of adjustable input parameters have different sensitivity rates for both alternatives due to the different life cycle scenarios and construction materials. However, the discount factor and the number of engaged workers throughout the bridges' life cycles were the most sensitive variables for both alternatives. Nevertheless, any similar variation of these parameters would not potentially influence the preferable design alternative choice.

From the environmental perspective, the 3D printed steel bridge heavily affects multiple midpoints criteria. The core environmental impact occurs during the production phase, where the 3D printing methodology's effect on most of the assessment criteria is extensively overrunning the environmental results of the concrete bridge. For instance, the impact of the welded bridge on climate change is 86% more significant than the concrete bridge. Next, a significant effect on environment takes place during the end-of-life phase. The concrete bridge has a more considerable impact during the end-of-life stage due to its relatively low recycling rate compared to steel, nevertheless, the total impact on the environment of the welded bridge is still more substantial.

Overall, the research outcome shows that the parametric tool can be used, which would serve as a support for decision-making process of infrastructure managers and designer. Furthermore, conclusions stemming from such tools will contribute to determining the cost-cutting alternative and environmentally more friendly solutions.

Contents

| | | |
|----------|---|-----------|
| 1 | Introduction | 9 |
| 1.1 | Background | 9 |
| 1.2 | General | 9 |
| 1.3 | Context | 10 |
| 1.4 | Location | 10 |
| 1.5 | Construction procedures | 12 |
| 1.5.1 | 3D-printed steel footbridge | 12 |
| 1.5.2 | A traditionally constructed concrete footbridge | 13 |
| 1.6 | Problem statement | 14 |
| 1.7 | Research objective | 14 |
| 1.8 | Research Scope | 14 |
| 1.9 | Limitations | 15 |
| 1.9.1 | General limitations | 15 |
| 1.9.2 | System boundary | 15 |
| 1.10 | Life span | 16 |
| 1.11 | Relevance | 16 |
| 2 | Methodology and Research Design | 17 |
| 2.1 | Research Model | 17 |
| 2.2 | Research Design | 17 |
| 2.3 | Literature review | 18 |
| 2.3.1 | Data collection methods | 18 |
| 2.4 | Data Analysis | 20 |
| 2.5 | Data Validation | 20 |
| 2.6 | Thesis outline | 20 |
| 3 | Determination of geometric parameters | 22 |
| 3.1 | 3D printed steel bridge | 22 |
| 3.1.1 | Geometrical characteristics for the 3D printed bridge | 22 |
| 3.2 | Traditionally constructed Concrete bridge | 23 |
| 3.2.1 | Geometrical characteristics for the Concrete bridge | 24 |
| 3.3 | Calculation of the Active loads | 24 |
| 3.4 | Cost-Load ratio | 25 |
| 3.5 | Conclusion | 25 |
| 4 | Development of the LCC tool | 26 |
| 4.1 | Life Cycle Costs | 26 |
| 4.1.1 | Cost breakdown structure | 26 |
| 4.1.2 | Production phase | 27 |
| 4.1.3 | Construction phase | 27 |
| 4.1.4 | Use phase | 28 |
| 4.1.5 | End-of-life phase | 29 |
| 4.2 | Life cycle costs distributed over 100 years | 30 |
| 4.3 | Discount Rate | 32 |
| 5 | Case Study LCC | 33 |
| 5.1 | Main input parameters | 33 |
| 5.1.1 | Production phase input | 33 |
| 5.1.2 | Construction phase input | 34 |
| 5.1.3 | Use phase input | 35 |
| 5.1.4 | End-of-life phase | 36 |
| 5.2 | Intermediate input parameters | 37 |
| 5.3 | Output parameters | 38 |

| | | |
|----------|--|-----------|
| 5.4 | Concluding remarks | 40 |
| 6 | LCC results of the case study | 41 |
| 6.1 | Total LCC of bridge design alternatives | 41 |
| 6.2 | Economic cost category distribution | 42 |
| 6.3 | Sensitivity analysis | 43 |
| 6.3.1 | Activity duration | 43 |
| 6.3.2 | Activity distance to travel | 44 |
| 6.3.3 | Activity unit price | 44 |
| 6.3.4 | Number of personnel | 44 |
| 6.3.5 | Activity frequency | 44 |
| 6.3.6 | Geometric characteristics | 44 |
| 6.3.7 | Cost of disposal | 44 |
| 6.3.8 | Discount factor | 44 |
| 6.3.9 | The volume of structural components | 45 |
| 6.3.10 | Technical properties of 3D printing | 45 |
| 6.4 | Sensitivity analysis results | 45 |
| 6.5 | Life cycle costs representation | 46 |
| 7 | Development of the LCA tool | 49 |
| 7.1 | Goal | 49 |
| 7.2 | Life cycle assessment | 49 |
| 7.3 | Life span | 49 |
| 7.4 | System Boundaries | 49 |
| 7.5 | Assumptions | 49 |
| 7.6 | Set up LCA Model | 50 |
| 7.7 | Phases: | 50 |
| 7.7.1 | Production and Construction phase | 50 |
| 7.7.2 | Use phase | 51 |
| 7.7.3 | End-of-life phase | 51 |
| 8 | Case study LCA | 53 |
| 8.1 | Input and Output of the LCA tool | 53 |
| 8.2 | LCA results of the case study | 54 |
| 9 | Discussion and Conclusion | 56 |
| 9.1 | Discussion - The usefulness of the parametric tool | 56 |
| 9.2 | Conclusions | 57 |
| 9.3 | Recommendations | 57 |
| A | Appendix | i |
| B | Structural Mechanics | i |
| B.1 | Introduction | i |
| B.2 | Preliminary design | ii |
| B.3 | Active and Dead Loads | iv |
| B.3.1 | Snow Load | iv |
| B.3.2 | Imposed Load (caused by cyclists/pedestrians) | iv |
| B.3.3 | Wind Load | v |
| B.3.4 | Railings Load | vi |
| B.3.5 | Railings Load | vii |
| B.4 | Loads combination | viii |
| B.5 | Principal Reinforcement Beams | xi |
| B.6 | Principal Reinforcement Plates | xiv |
| B.7 | Reinforcement Optimization | xvi |

| | | |
|----------|--|----------------|
| B.8 | Shear force reinforcement in Beam | . xviii |
| B.9 | Shear force reinforcement in Plates | . xx |
| B.10 | Structure's strength control (S/R) | . xxi |
| | B.10.1 Beam Check | . xxi |
| | B.10.2 Plate Check | . xxii |
| B.11 | Anchorage | . xxiv |
| | B.11.1 Beams | . xxiv |
| | B.11.2 Plates | . xxvi |
| B.12 | Crack Control | . xxviii |
| | B.12.1 Beam | . xxviii |
| | B.12.2 Plate | . xxix |
| B.13 | Conclusion | . xxx |
| C | LCC results of Case Study | . xxxii |
| C.1 | Production and Construction phase costs | . xxxii |
| C.2 | Use phase costs | . xxxiii |
| C.3 | End-of-life phase costs | . xxxiii |
| C.4 | Concrete bridge activities distribution | . xxxiv |
| C.5 | 3D printed bridge activities distribution | . xxxv |
| C.6 | Cost Categories | . xxxvi |
| C.7 | Concrete bridge Uncertainty | . xxxvi |
| C.8 | 3D printed bridge Uncertainty | . xxxvii |
| C.9 | LCC varination of 3D and Concrete bridges | . xxxvii |
| C.10 | Maximum and Minimal LCC deviation for Concrete bridge | . xxxviii |
| C.11 | Maximum and Minimal LCC deviation for 3D printed bridge | . xxxviii |
| C.12 | Initial deviation for Concrete bridge | . xxxix |
| C.13 | Initial deviation for 3D Printed bridge | . xxxix |
| C.14 | LCC comparison for Concrete and 3D Printed bridges | . xxxix |
| C.15 | Concrete bridge activity costs calculation | . xl |
| C.16 | 3D printed bridge activity costs calculation | . xl |
| C.17 | Cycle Cost distribution (wider perspective), Concrete bridge | . xli |

List of Figures

| | | |
|----|--|------|
| 1 | Life cycle integrated system | . 10 |
| 2 | Location of the bridge, satellite view, | . 11 |
| 3 | Location of the bridge, 3D perspective, | . 11 |
| 4 | Bridges alternatives (3D printed Steel-left and Concrete-right) modeled at the construction location | . 11 |
| 5 | MX3D vision, | . 12 |
| 6 | Comparison of common and cantilevered manufacturing direction, | . 13 |
| 7 | Telecrane installing a concrete bridge, | . 13 |
| 8 | Life cycle phases | . 15 |
| 9 | System boundary | . 16 |
| 10 | Research Model | . 17 |
| 11 | 3D representation of the Concrete bridge design | . 19 |
| 12 | GaBi software interface, | . 20 |
| 13 | Thesis outline | . 21 |
| 14 | Overview of the MX3D metal 3D printed footbridge, (Rolands Kromanis, 2021) | . 23 |
| 15 | Ending Design Loop, (Snellink, 2021) | . 23 |
| 16 | Life cycle cost breakdown | . 26 |
| 17 | LCC per phase for 3D printed and concrete bridges for 100 years service life | . 41 |
| 18 | Economic Impact for different bridge component | . 43 |
| 19 | Sensitivity Tornado, Concrete bridge | . 45 |

| | | |
|----|--|-------|
| 20 | Sensitivity Tornado, 3D printed bridge | 46 |
| 21 | Histogram Life Cycle Cost distribution, Concrete bridge | 47 |
| 22 | Histogram Life Cycle Cost distribution, 3D printed bridge | 47 |
| 23 | Production process, 3D printed bridge, | 50 |
| 24 | Production process, Concrete bridge | 50 |
| 25 | Use phase, Concrete bridge | 51 |
| 26 | Use phase, 3D printed bridge | 51 |
| 27 | Disposal process, Concrete bridge | 52 |
| 28 | Disposal process, 3D printed bridge | 52 |
| 29 | Input and Output of the calculation tool | 53 |
| 30 | Climate change impact | 55 |
| 31 | Territorial ecotoxicity impact | 55 |
| 32 | Ending Design Loop | i |
| 33 | Preliminary Design - Top View | iii |
| 34 | Preliminary Design - Side View | iii |
| 35 | Preliminary Design - Front View | iii |
| 36 | Railings detailed perspective | vi |
| 37 | Uniformly distributed load diagram for beam | xi |
| 38 | Shear force diagram for beam | xi |
| 39 | Moment diagram for beam | xi |
| 40 | Distance d | xii |
| 41 | Uniformly distributed load diagram for plate | xiv |
| 42 | Shear force diagram for plate | xiv |
| 43 | Moment diagram for plate | xv |
| 44 | Shear force reinforcement beam | xix |
| 45 | Side view of beam, location of stirrups | xix |
| 46 | Anchoring Beam | xxv |
| 47 | Anchoring Plate | xxvii |
| 48 | Final Design - Top View | xxx |
| 49 | Final Design - Side View | xxx |
| 50 | Final Design - Front View | xxx |
| 51 | Beam with final reinforcement | xxx |
| 52 | Plate with final reinforcement | xxx |
| 53 | Histogram Production-Construction phase costs | xxx |
| 54 | Histogram Use phase costs | xxx |
| 55 | Histogram End-of-life phase costs | xxx |
| 56 | Concrete bridge activities distribution per costs categories | xxx |
| 57 | 3D printed bridge activities distribution per costs categories | xxx |
| 58 | Costs categories | xxx |
| 59 | Uncertainty Concrete bridge | xxx |
| 60 | Uncertainty 3D printed bridge | xxx |
| 61 | Maximum and Minimum LCC deviation from the mean value | xxx |
| 62 | Maximum and Minimal LCC deviation, Concrete bridge | xxx |
| 63 | Maximum and Minimal LCC deviation, 3D printing bridge | xxx |
| 64 | Initial LCC (no discount factor application) Concrete bridge | xxx |
| 65 | Initial LCC (no discount factor application) 3D printed bridge | xxx |
| 66 | LCC comparison for Concrete and 3D printed bridges | xxx |

List of Tables

| | | |
|---|--|----|
| 1 | Geometrical characteristics of the 3D printed steel bridge | 22 |
| 2 | Geometrical characteristics of the traditionally built Concrete bridge | 24 |
| 3 | Dynamic loads acting on the bridge | 25 |
| 4 | Cost-load ratio per construction alternative | 25 |

| | | |
|----|---|-------|
| 5 | Discount rate (2.5%) implication over the yearly incurred costs | 32 |
| 6 | Concrete bridge components | 33 |
| 7 | 3D printed bridge components | 33 |
| 8 | Transportation Concrete bridge, construction phase | 34 |
| 9 | Transportation 3D printed Bridge, construction phase | 34 |
| 10 | Time in use Concrete bridge, construction phase | 34 |
| 11 | Time in use 3D printed bridge, construction phase | 35 |
| 12 | Input parameters Concrete bridge, use phase | 35 |
| 13 | Input parameters 3D printed bridge, use phase | 35 |
| 14 | Transportation Concrete bridge, end-of-life phase | 36 |
| 15 | Time in use Concrete bridge, end-of-life phase | 36 |
| 16 | Transportation 3D printed bridge, end-of-life phase | 36 |
| 17 | Times in use 3D printed bridge, end-of-life phase | 37 |
| 18 | Material Cost Concrete bridge | 37 |
| 19 | Material Cost 3D printed bridge | 37 |
| 20 | Wages for workers Concrete bridge | 38 |
| 21 | Wages for workers 3D printed bridge | 38 |
| 22 | Rental costs for Concrete bridge | 38 |
| 23 | Rental costs for 3D printed bridge | 38 |
| 24 | Disposal for Concrete bridge | 38 |
| 25 | Disposal for 3D printed bridge | 38 |
| 26 | Cost Schedule for Concrete bridge activities | 39 |
| 27 | Cost Schedule for 3D printed bridge activities | 40 |
| 28 | Midpoints results for Concrete Bridge | 54 |
| 29 | Midpoints results for 3D printed Bridge | 54 |
| 30 | Volume of Railing Components | vii |
| 31 | Parameterize Loads on 1 Plate to kN/m^2 | viii |
| 32 | Parameterize Loads on 1 Beam to kN/m | ix |
| 33 | Thickness of cover | xii |
| 34 | Area of Reinforcement bars [mm^2] | xiii |
| 35 | Area of reinforcement bars in [mm^2] for plates | xv |
| 36 | Plates dimensions iterations | xvi |
| 37 | Beams dimensions iterations | xvii |
| 38 | Optimal dimensions of structural components | xvii |
| 39 | Shear force capacity for stirrups B500 in N/mm^2 | xix |
| 40 | Minimal value of concrete shear force capacity | xx |
| 41 | Table used to calculate μ , (Snellink, 2021) | xxiii |
| 42 | Bonding conditions | xxiv |
| 43 | Maximum bar spacing, (Snellink, 2021) | xxix |

1 Introduction

The defined concepts in the proposal will be developed as a starting line. This chapter introduces the research topic, the research objective, and the research questions. A general overview of the background concepts of the research is presented in Paragraph 1.1. Next, in Paragraph 1.3 describes the context of the problem of the research.

Subsequently, the research questions and objectives are defined in Paragraph 1.8 and Paragraph 1.7. The following Paragraph 1.9 describes the research project's overall limitations and brings an overview of the life cycle phases for the functional units of the study. This chapter ends with the relevance of the research in Paragraph 1.11.

1.1 Background

This Paragraph start with a general description of the objective of such infrastructure components as bridges, followed by the importance of their analyses and comparison among different structural alternatives. Next, the context and the location of the analyzed functional units are described. Finally, the focus lies in describing the construction procedures investigated for the research project.

1.2 General

Since the beginning of time, bridges have been considered essential structures for the transport infrastructure system. These have undergone immense transformations, such as improved materials, larger spans, and enhanced construction procedures. Although the construction of bridges is a lot easier in modern times, bridge engineering involves precise physics, extensive resources, and detailed planning throughout the life cycle (Matthew L. Deloney, 2020).

Since bridges are part of transport infrastructure systems, these structures are vital components to the successful functioning of an economy. Not only are they expected to provide the required structural function, but bridges must also be conceived such that they can efficiently retain the economic and environmental benefits. This fact highlights the historical development of the bridge construction techniques throughout their life cycle, commencing with unstable and short-running wood structures to massive suspension, long-lasting, cost, and environmental impact narrowed bridges. The high pace of structural and functional improvements demonstrates the successful application of bridges as structural components and the contribution of their continuous research.

Nowadays, every bridge design goes in line with multiple structure cycles, which characterizes the total life span of the construction. The life cycle of the bridge is compounded from four different phases: the production phase, the construction phase, the operation phase, and finally, the bridge's demolition, also known as the end-of-life phase. Therefore, an incitive goal of each bridge project would be to extend its life cycle and minimize the overall costs and environmental impact incurred during the structure's life span.

Currently, numerous building techniques exist. However, their significant similarities cause differentiation among two influential categories of the bridge construction industry: traditionally designed bridges using reinforced concrete or the cutting-edge technology of 3D-printing operating welded steel. As a result, due to the trade-off between lifetime, costs, and sustainability, multiple engineering domains are brought together to develop an innovative solution to optimize the whole process. Thus the LCC and LCA examinations of both procedures and consequent comparison would answer the question concerning the best construction alternative.

1.3 Context

The context of the research project analyzes two different bridge construction techniques, the 3D printed (welded) bridge, and a traditionally built concrete bridge, concerning the conducted life cycle study based on different technological and social aspects of the construction alternatives. Numerous literature sources present various methods of incorporating the structural, economic, and environmental factors into one integrated system, varying from a stand-alone post to a full-fledged merge of structural, economic, and environmental factors into a jointly bounded entity (Marin and Mazzanti, 2015). The model of interacting components (see Figure 1) represents the core objective of the parametric research tool. Subsequently, the model uncertainties are further analyzed on the effect of structural, economic, and environmental constraints that contributes to determining the best construction solution.

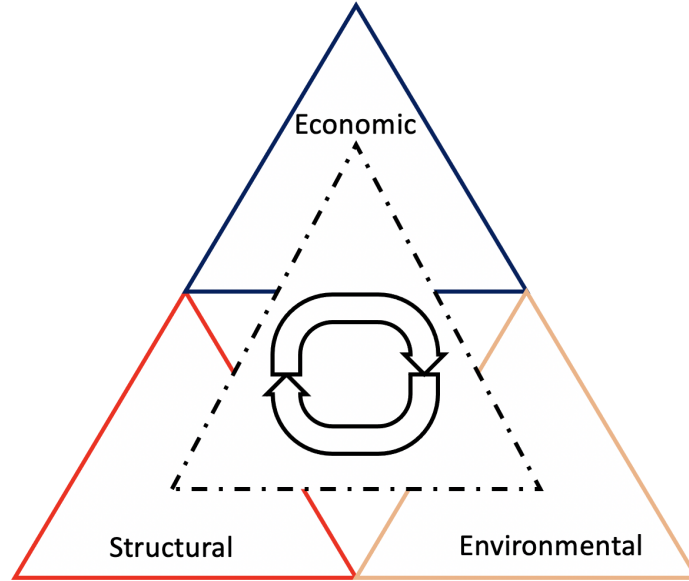


FIGURE 1: Life cycle integrated system

1.4 Location

Amsterdam is the world-known capital of the Netherlands. It is also famous for its infrastructure and numerous canals, some of which are considered a world heritage (UNESCO, 2010). Amsterdam is operating an intense infrastructure system, according to (Star Board, 2020), having over one thousand bridges. One newly-designed element of the Amsterdam infrastructure is the world's first 3D-printed steel bridge. This bridge spans the oldest canal, the Ouderzijds Achterburgerwal, in the Wallen district, Amsterdam's best-known red-light district. De Wallen is a famous tourist destination due to its location in the heart of Amsterdam, which counts 11.8 million trippers per day (Senay Boztas, 2019). Moreover, it is the focal point of the ongoing debate in the larger city about balancing the tourism industry with livability for residents and accessibility for workers (Rolands Kromanis, 2021).

The research project will be conducted based on the data from two construction alternatives: the 3D-printed steel bridge, also known as a welded bridge, and the traditionally built reinforced concrete bridge, which prototype will be analyzed and compared to the aforementioned 3D-printed solution. In Figures 2 and 3, the bridge location can be seen, additionally, in Figure 4, both design decisions are modeled at the construction location.

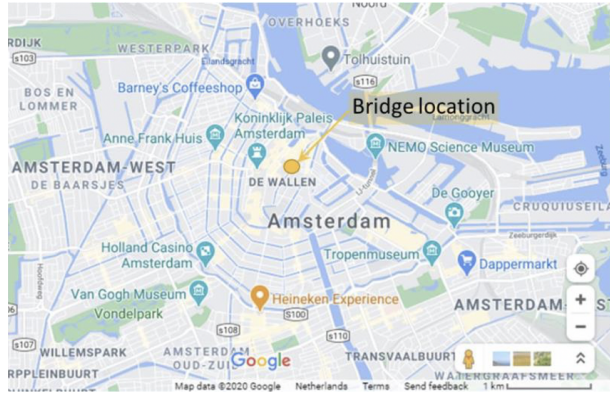


FIGURE 2: Location of the bridge, satellite view, (Rolands Kromanis, 2021)

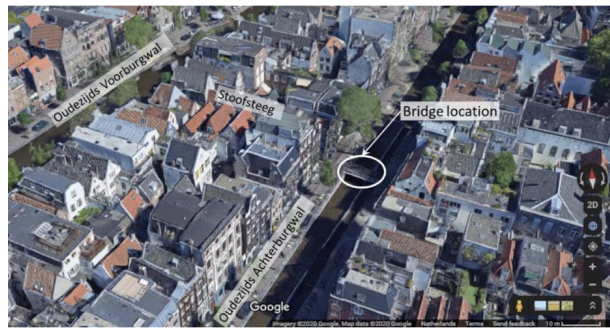


FIGURE 3: Location of the bridge, 3D perspective, (Rolands Kromanis, 2021)



FIGURE 4: Bridges alternatives (3D printed Steel-left and Concrete-right) modeled at the construction location

1.5 Construction procedures

Construction project management is an essential component of construction engineering. Although it requires significant technological expertise, it always involves human connection. Nowadays, the construction industry requires enhanced management and decision-making procedures concerning multiple life cycle elements: production, design, construction methodology, budgeting, scheduling, and many more (Blank et al., 2000).

Since the beginning of times, diverse construction approaches have been shaped with respect to various materials, which differ in their properties, such as strength, weight, durability, and even resistance against corrosion. Therefore, infrastructure owners should select these materials based on the external condition and the design requirements. Considering that, a bridge construction method could be classified based on the principal materials used in its primary structure (Dr. Homayoun Abrishami, 2017). Following the research objective, two alternatives for construction methodologies are to be investigated, mainly traditional concrete and 3D-printed steel.

1.5.1 3D-printed steel footbridge

The 3D printing is one of the fastest developing niches of civil engineering. For steel construction, 3D printing, also known as Wire + Arc Additive Manufacturing (WAAM), is very well suited due to high construction rates and relatively low costs (Waldschmitt et al., 2021).

The bridge of the Dutch company MX3D, situated in Amsterdam, is one of the best-known building projects in the area of WAAM. Given that the MX3D steel bridge is an industry pioneer, the entire bridge construction took place in a factory hall under laboratory circumstances. Following their vision, bridges are built directly on the construction site by mobile welding robots (see Figure 5) (Waldschmitt et al., 2021).



FIGURE 5: MX3D vision, (Waldschmitt et al., 2021)

Manufacturing sequences for 3D printing techniques must be defined prior to production. For this purpose, the structure to be manufactured is split into layers. Existing slicing software automatically creates the layers and G-Code for standard printers. Because the geometry produced by the welding robot cannot be predicted accurately, the slicing must be adjusted several times during the manufacturing process. Following the welding procedure, the bridge is divided into iso-curves. It is described geometrically by polynomial functions, which allow the robot to calculate the x- and y-coordinates of any iso-curve for any z-height. With the shape of the bridge, the curvature angle is subject to constant transformations, and thus also the layer height (see Figure 6).

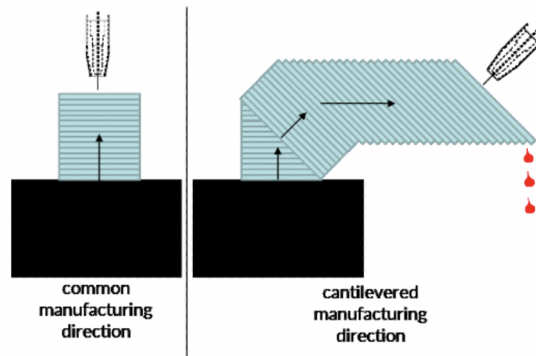


FIGURE 6: Comparison of common and cantilevered manufacturing direction, (Waldschmitt et al., 2021)

A vertical manufacturing direction is always advantageous so that the layers lie on top. Large structural spans are challenging to produce since the metal is melted or liquefied thus, there is a risk of dripping. The current and arc voltage is employed to assure a high construction pace resulting in a deposition rate generally equal to 0.5-2.0 kg/h (Gardner et al., 2020).

1.5.2 A traditionally constructed concrete footbridge

The construction of concrete bridges can be divided into two main classes: Cast in Situ and Precast. Cast in Situ concrete is poured and cast on-site, while precast concrete is prefabricated in a factory off-site. Considering the situation covered in this research project, all structural elements of the concrete bridge will be Precast. Therefore, this construction method requires the implication of heavy machinery that carries and installs the bridge's components.

A concrete slab that spans the crossing and is reinforced with a steel bar forms the foundation for the bridge's construction. The slab may have a simple, solid rectangular shape or be thinner and strengthened on its underside by built-in beams that span the bridge. The top surface of the concrete slab can serve as the walkway surface for footbridges, eliminating the need for a separate deck. The availability of mobile telecranes ensures that the precast concrete elements can be lifted appropriately and installed in the defined location (DFID, 2004) (see Figure 7).



FIGURE 7: Telecrane installing a concrete bridge, (VEDA Associates, 2014)

1.6 Problem statement

Following the context framework, the research problem has been determined.

The technology used in the 3D-printed bridge in Amsterdam can be considered a cutting-edge technology of the new construction era. Nevertheless, the engineers' wide usage, knowledge, and experience with the traditional constructing procedure retain a considerable weight in front of the newly applied method, implying a decisive factor in not shifting towards 3D-printing technology. This problem could be solved through a quantitative tool that compares two design alternatives and outlines the most optimal solution concerning the whole life cycle impacts.

1.7 Research objective

The uncertainty in the efficiency and effectiveness of the applied design and construction solution is a common problem in the infrastructural industry. This concern is directly related to the production and the structural works that significantly influence the entire economical impacts throughout the bridge's life cycle. Besides that, the construction procedure is a decisive aspect that defines the usage level in terms of repairing and maintenance works frequency, which influences one of the prominent parts of the environmental impacts. Therefore it is necessary to acquire a deep insight into the components and processes inquired during the life cycle of both design alternatives to provide better-targeted solutions.

The research project focuses on reducing the uncertainty concerning the decision-making about design alternatives while considering two options, traditional concrete and newly developed 3D printed bridges. In order to achieve the solution to the problem mentioned above, the following research objective has been formulated:

"This research project aims to gain insight into the advantages of the newly applied 3D-printed steel over traditional concrete construction alternatives by analyzing the lifecycle, environmental, and economic impacts of both types of bridges."

1.8 Research Scope

This research project focuses on developing a parametric tool that determines the optimal bridge design solution. Since the use of different materials within the construction process generates multiple comparing criteria, the two functional units are comparable. Subsequently, they can be investigated with respect to a various range of output performance indicators. For example, diverse electricity and fuel consumption results from the overall consumption of the functional unit throughout its life cycle. Besides, the structural and durability properties of the bridge materials influence the required frequency and extent to which the maintenance works are required, also affecting the recycling ratio. As a result of setting the input parameters, the parametric model provides a deeper understanding of the core factors that affect the environmental and economic outcomes of the calculation tool. Furthermore, these results can be compared and used for deciding the matter of the infrastructure owners' long-term interests. The research objective constructed in Paragraph 1.7 results in the following research questions:

"What is the overall economic and environmental performance of the welded bridge compared to the traditionally built concrete bridge throughout the life cycle?"

In order to design a parametric model that can outline the best design alternative and investigate functional units' impacts on multiple performance indicators, several sub-questions are formulated. This will help narrow down each specific element of the main question and helps structure the report.

- Which bridge design solution requires higher maintenance costs?
- Which life cycle phases are most economically affecting the total costs?
- Which design solution is subject to the biggest cost deviation?
- What are the impacts of the construction technology and used materials during the construction phase?

Before addressing the above mentioned questions, a structural characteristics examination for both design solutions and construction methods must be executed. This will help define multiple parameters of the parametric tool and achieve higher precision of the final output.

”What are the welded bridge’s structural properties compared with the traditionally built concrete bridge?”

- What are the geometrical characteristics of each design alternative?
- Which design alternative retains the most effective cost-load ratio?
- Which design alternative is most suitable for the long-term run?

1.9 Limitations

1.9.1 General limitations

This research project does not directly answer whether and when the design alternative is preferred. Instead, it delivers a parametric tool that can calculate the LCC and LCA for both alternatives, given the construction procedure and structural characteristics as the starting input parameters. Given that the output of the calculation tool is directly dependent on the construction procedure, the different input variables are systematically adjusted so that the final results are consistent concerning comparing performance indicators. The comparison between two functional units, mainly the 3D-printed steel and traditionally constructed concrete bridges, are operated to adjust the calculation tool, which would retain the feasibility of one alternative competing with another. However, it must be stressed that the calculation results are expected to be intensely impacted by the assumptions and requirements specific to each alternative. Considering that the data collection represents one of the main challenges for the construction of the parametric tool, thus, within the given time span of the project, the researcher aims to collect the most reliable data based on the literature research and experts’ knowledge.

1.9.2 System boundary

The functional unit of this research project is the bridge built to accommodate the daily crossing of the Ouderzijds canal for 100 years. The different life cycle phases must be defined before implementing the parametric tool to calculate the LCA and LCC performance indicators. Therefore, the research project covers the following phases: acquiring raw materials, production of structural components, bridge construction, maintenance, and end-of-life (see Figure 8).



FIGURE 8: Life cycle phases

For the LCC and LCA, it has been decided to distinguish three main phases: the construction phase (combining raw material acquisition, the production of the structural components, and the bridge constructions), followed by the use phase, and the end-of-life phase. The construction phase begins with the basis of the construction method, mainly purchasing raw materials and producing required structural components. Since these components are fabricated, the bridge construction works can start. Consequently, after finalizing the infrastructure works, the use phase takes over, representing the most extended phase spanning almost the entire life span of the bridge. The life cycle is concluded with the end-of-life phase, where the functional unit is demolished, after which a particular fraction of material is recycled, transported to the landfill, or reused for different purposes. The entire system boundary is shown in Figure 9.

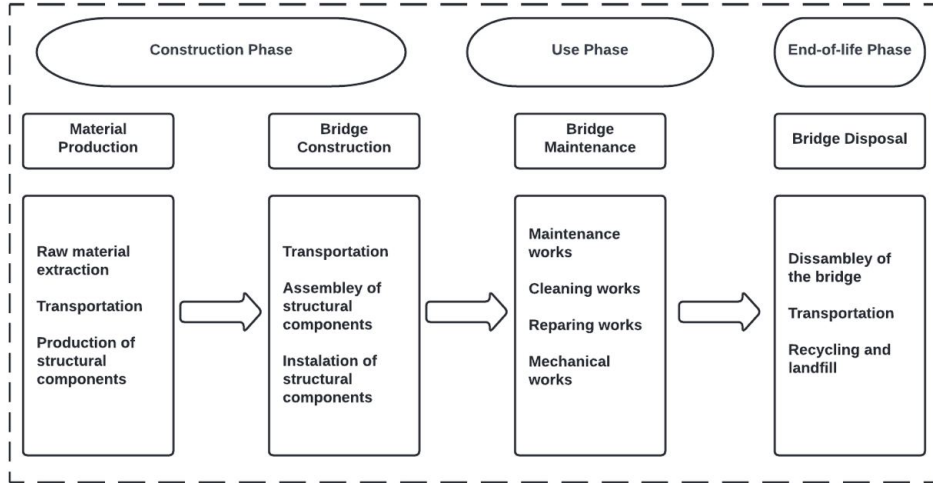


FIGURE 9: System boundary

1.10 Life span

The life span of bridges is a flexible variable depending on multiple factors. The construction procedure, materials, location, and structural requirements significantly influence the bridge's life span. A reliable structural design and correct maintenance ensure a concrete bridge with a life span of 100 years (Kim and Tae, 2020). Given the material for 3D printing, a steel bridge generally operates a life span of slightly more than 100 years (AISI, 2007).

Considering the scope of the research project, both functional units, mainly the 3D-printed steel and traditionally built concrete bridge, will be investigated for a life span of 100 years.

1.11 Relevance

The parametric tool generates a straightforward assessment process to determine the benefits and weaknesses of both construction alternatives concerning specific case life cycle scenarios. For the scope of feasibility examination of construction procedures - as demanded by Infra Plan Consulting - the goal is to assess items on a high abstraction level for prompt investigation at the early design-management stage.

Following the above mentioned requirements, the calculation tool will be developed in line with the pre-defined model purposes. Based on the results of the calculations, the research will outline the potential decisions concerning the necessary extent of the performance indicators for the infrastructure owners. Additionally, the provided sensitivity analysis embedded in the calculation tool will deliver an idea of the most sensitive factors influencing the economic and environmental impacts and inspect whether the variables' uncertainty can influence the prevalent preferable alternative. Consequently, this evaluation will outline components of the construction methods that could be adjusted in order to improve the overall performance of the design and construction alternative.

2 Methodology and Research Design

The research problem was identified and explained in the previous Chapter 1, formulating the research questions. The project research will be executed using quantitative research. Mainly, desk research is the primary method used in design-based research. The emphasis will be on quantitative research because it aims to shed light on the circumstances and magnitude of the performance difference between two construction methods, 3D-printed steel and concrete bridges, in terms of LCC and LCA.

This Chapter focuses on combining problem context and the research question to develop a systematic approach to performing the research. An overview of the methodical answering of the research questions is provided concerning modal data collection, analysis, validation, and the research system's integrated scheme.

2.1 Research Model

The research model is generated in line with examining the research context and objective. Given the project's context, the scientific literature on life cycle costs, environmental impact assessment, and preliminary research on the considered construction alternatives serve as the foundation for the investigation model. Consequently, the results from the predefined design process are used as inputs for the parametric LCC and LCA assessment tool. As soon as the calculation procedure is established, the obtained results can be used to assess the LCA and LCC performance parameters. Based on the calculation results, conclusions can be drawn as well as recommendations concerning the potential improvements of the parameters that cause the most significant impact on the final results (see Figure 10)

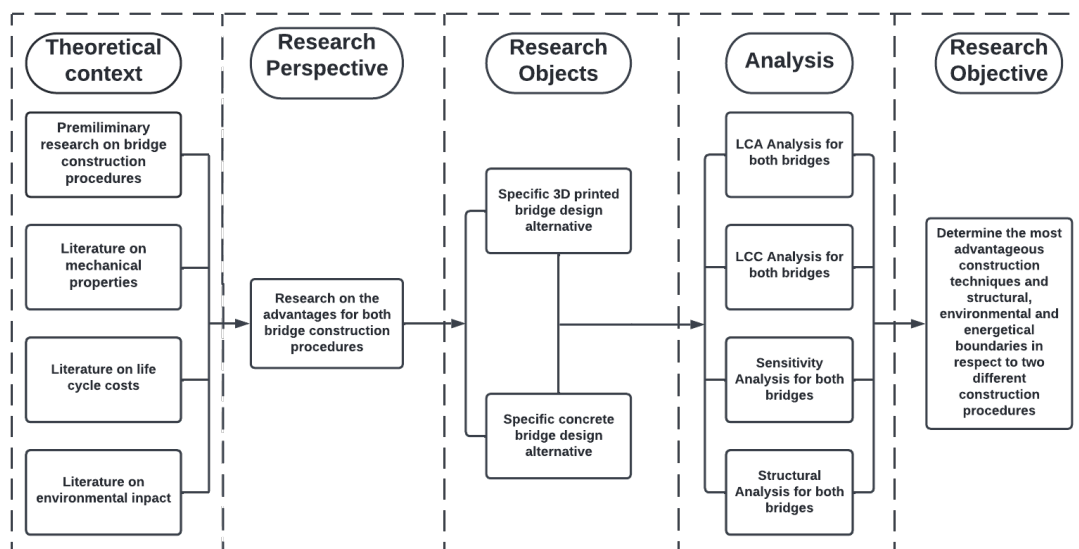


FIGURE 10: Research Model

2.2 Research Design

A quantitative research design is used to conduct the research. Design-based research, in particular, is mainly conducted through desk research. The emphasis will be on quantitative research to get insight into the situations, and extent of the performance differences in terms of LCC and LCA between the two construction alternatives, 3D-printed steel and traditionally built concrete bridges. Following the defined research objective, geometrical parameters of structural components (based on mechanical calculations for traditionally built concrete bridge and based on a literature review for 3D-printed steel bridge) are required. Besides, the researcher operates the computer-based LCA model to determine the

environmental impact of both alternatives within different life cycle phases. Final results are presented with the help of multiple visual aids such as graphs and images.

2.3 Literature review

Throughout the research project, numerous variables and data were identified. For the selection of papers, search engines/databases such as Google Scholar, UTwente library, and the literature shared by the Infra Plan Consulting were used in the research scope. Literature collection for this purpose has been divided into three groups for each construction alternative: literature concerning structural mechanics, mainly mechanical properties, material and construction guidance, literature about life cycle costs, and literature regarding the sustainability of infrastructural components. For both construction alternatives, there are three steps followed: Literature Collection, Identification, and Selection.

The collection of literature was done by searching phrases and keywords in the search engines mentioned above. The following are the keywords and phrases that were used: "structural properties of the material", "maintenance of the bridge in the Netherlands", "construction guideline for the bridge in the Netherlands", "life cycle costs of the bridge in the Netherlands", "material recycling in the Netherlands", "environmental impact of the infrastructural components", "life cycle assessment of the bridge in the Netherlands". Articles the search engines identified connected to the query were picked for additional investigation if these words/phrases appear in the title, abstract, or keywords. A total of 85 papers were chosen to be examined further to decide whether they were relevant to the investigation. This was determined by reading the papers' and books' abstracts or summaries. After doing this, 64 documents were selected as applicable for reading (to identify LCA and LCC characteristics for design alternatives). A list of the selected documents can be found in References section.

2.3.1 Data collection methods

In order to get a deep comprehension of the research components within the assigned period and limited resources, the strategy opted for was to gather different types of data but as detailed as possible. Since the research combines multiple engineering disciplines, the data collection varies with respect to different investigated parts of the project. Therefore, to clarify the general approach of the project, data collection methods per core research question are explained separately.

"What are the welded bridge's structural properties compared with the traditionally built concrete bridge?"

This question could be considered complex since it combines multiple research domains simultaneously. Based on the available literature, relevant data, and insights gathered from consultations with experts involved in the structural design, the required input variables, technical assumptions, and the accompanying calculations will be described.

In the beginning, both design alternatives' geometrical parameters are calibrated so that further comparison would be reliable. Considering that the 3D-printed bridge has already been designed, the traditionally concrete bridge will have similar dimensions with minor differences coming from the design decisions. Specific input values would be needed to determine the mechanical properties of both design solutions, for instance, material properties and imposed loads on the structure. Thus, the required variables are determined based on the available literature and official construction guidelines in the Netherlands. Using multiple digital tools, such as *Microsoft Excel* software and *SketchUp* software (see Figure 11), the structural design will be visualized and checked for complying with the required safety norms predefined by NEN, 2022 codes.

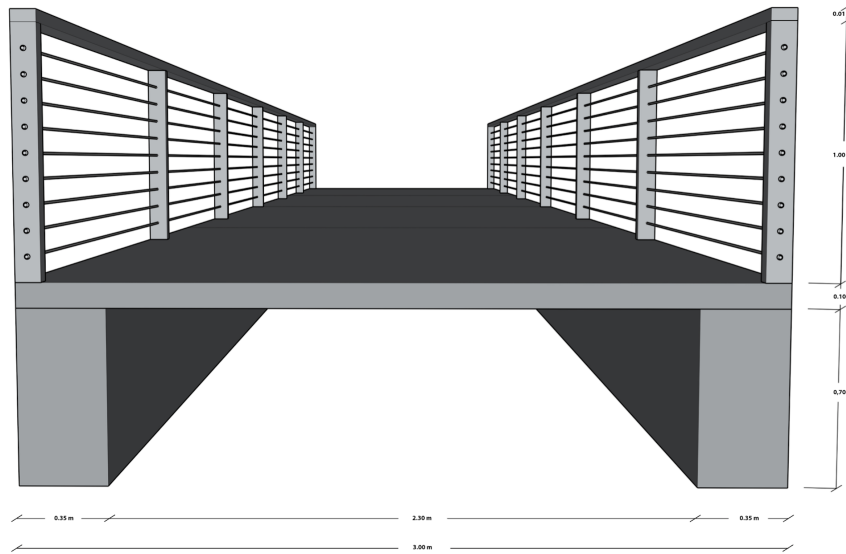


FIGURE 11: 3D representation of the Concrete bridge design

The primary data collection method for this question concerning the 3D-printed steel bridge is based on a literature study. Mainly, geometric parameters and material properties are selected from the available sources.

In this way, the required input parameters are set. These are used to generate the structural calculations using *Microsoft Excel* software and further compare structural properties for both design alternatives. Furthermore, the structural design parameters yield numerical parameters necessary to provide the inputs for the LCC and LCA calculation tool.

"What is the overall economic and environmental performance of the welded bridge compared to the traditionally built concrete bridge throughout the life cycle?"

Multiple engineering subfields are to be combined to determine the overall economic and environmental performance of the welded steel bridge compared to the traditionally built concrete bridge. Following the first research question, geometric parameters and construction procedures of both bridges' alternatives function as a base case. This implies that the electricity and fuel consumption, frequency of maintenance works, amount of required construction workers, and other functional criteria are known. As a result, some of the input parameters further used to calculate both design alternatives' overall costs and sustainability levels are determined.

In order to calculate the rest of the performance indicators, the relevant research papers and documents present at Infra Plan Consulting are studied for insights concerning activity price, necessary repair, maintenance works, recycling ratios, and the influence of economic parameters throughout the life cycle. This results in all necessary variables for calculating the total economic and environmental impact. The final LCC results are determined through the *Microsoft Excel* software, and the final LCA results are found through the *GaBi* software (see Figure 12). Consequently, the representation of the research outcome is done via figures following the representation templates present in the literature and adjusted with the help of experts from Infra Plan Consulting.

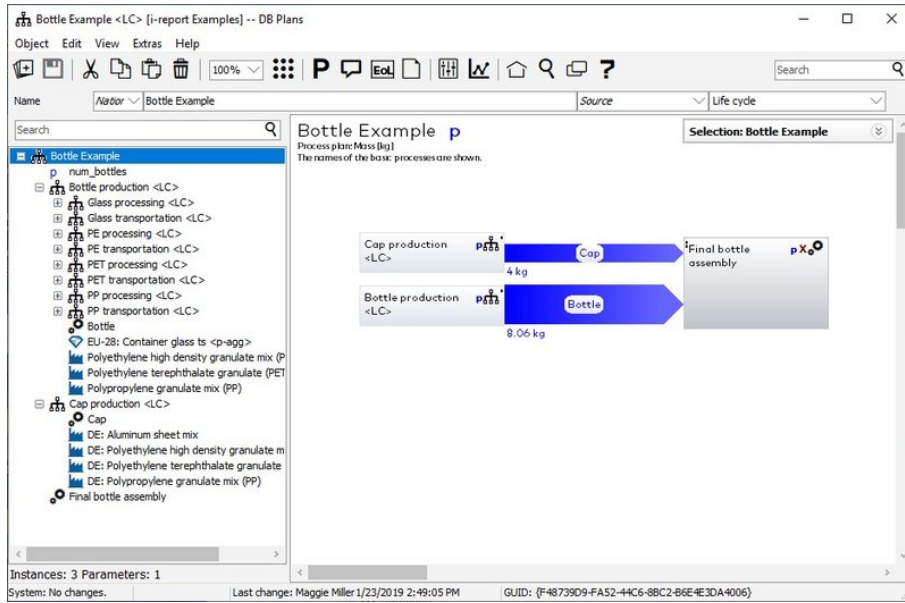


FIGURE 12: GaBi software interface, (Sphera, 2022)

2.4 Data Analysis

Obtained data is analyzed through the aforementioned digital tools. Furthermore, a sensitivity analysis is executed. The list of uncertain variables is defined based on the insights gained from the literature research and experts from multiple engineering domains. Consequently, the predefined variables are categorized depending on their nature and properties. Considering the distribution from the mean (initial) values, the lowest and the highest boundary of the uncertainty variables are used for the sensitivity analysis. Next, every set of uncertainty variables is fixed in the parametric tool, retaining the remaining variables unchanged. After multiple iterations (the number of iterations equals to the number of uncertainty sets), the most sensitive parameters sharply influencing the mean (initial) total cost of the parametric tool are determined. These results deliver an understanding of what variables are most critical to the accurate selection, and also, these might communicate the general applicability of the parametric tool in determining the most suitable construction alternative.

2.5 Data Validation

Given the nature of the project, the most significant part of the parametric tool input parameters is approximated. This implies that uncertainty variable sets are applied numerically deviating from the initial mean values of the calculation. Therefore, the sensitivity analysis aims to determine the magnitude of the uncertainties' effect on the final results of the analyzing tool. Additionally, a considerable amount of input parameters of the model are literature-based, therefore, the sources of the parameters and assumptions are presented and discussed with experts from Infra Plan Consulting.

2.6 Thesis outline

The research design and data collection methods described in Paragraph 2.2 and Paragraph 2.4 are visualized in the following thesis outline (see Figure 13).

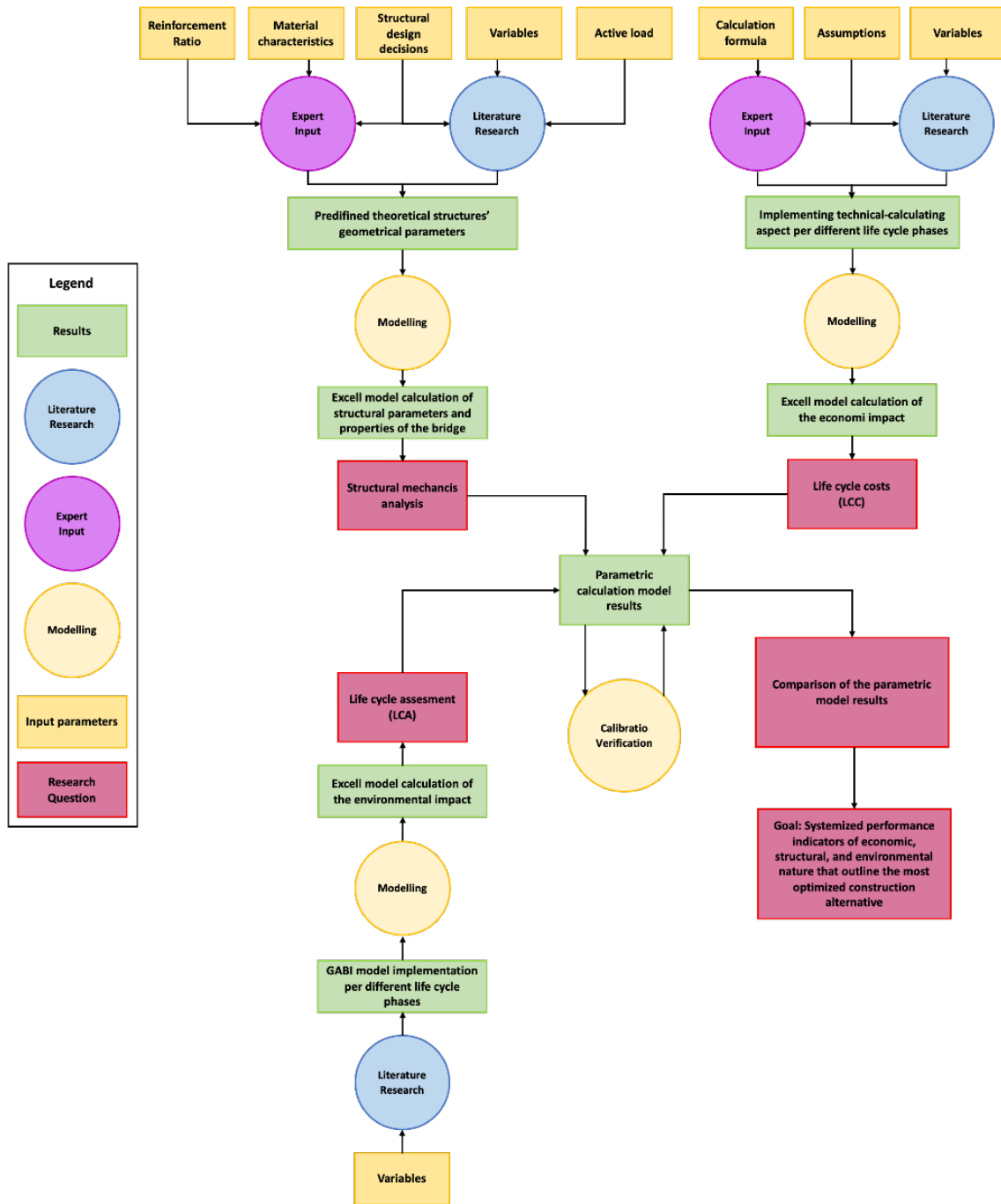


FIGURE 13: Thesis outline

3 Determination of geometric parameters

This chapter describes the calculation procedures and literature research to determine the geometrical characteristics of both design alternatives, mainly traditionally built concrete and 3D printed steel bridges. Further, the geometric characteristics are used in the LCC and LCA calculation tools that outline the benefits of one construction method over another.

The literature review based on the bridge’s study offers precise measurements of the structural components used throughout the life cycle. Considering the scope of the research project, the geometrical characteristics of the 3D-printed bridge will be determined via research. Next, the concrete bridge’s dimensions will be adjusted to make the comparison of the two design alternatives objective. Thus, the initial geometric parameters of the concrete bridge will mostly correspond to those of the second construction method. Given that the research project does not use a specific concrete bridge, the structural model and calculation procedure of the designed concrete bridge are explained in Appendix B.

The literature research for geometric characteristics and material properties of the 3D printed steel bridge are described in Paragraph 3.1, followed by the structural design and calculations used to determine the appropriate dimensions of the concrete bridge’s structural elements is developed in Paragraph 3.2. The chapter is closed by concluding remarks based on a comparison of the structural properties of both design alternatives in Paragraph 3.4.

3.1 3D printed steel bridge

Following the construction procedures described in Chapter 2, the 3D printed steel bridge is designed as a footbridge spanning the canal in Amsterdam city. Given that, the geometric parameters and the material properties are investigated based on the available research papers. In this research, the 3D-printed steel bridge represents the starting point for the dimensions and structural properties of the analyzed functional units.

3.1.1 Geometrical characteristics for the 3D printed bridge

The geometrical properties of the 3D printed bridge are predefined by the MX3D company that has designed and tested the infrastructure component (MX3D, 2020). Following the literature research, the bridge’s mass and the density of the operated steel (Davis, 1998) are found from the (Gardner et al., 2020). Given that, the overall volume of the bridge can be determined. The bridge’s volume represents a crucial variable for the later comparison of the structural properties of the bridges.

The 3D-printed bridge consists of two railings located on the edges of the structure, as well as one deck and four spirals found on the corners of the bridge (see Figure 14). The overall geometric characteristics of the 3D printed bridge are represented in the Table 1 , which follows the numerical values found in (Gardner et al., 2020).

| Component | Material | Volume [m ³] | Density [kg/m ³] | #components | Mass [kg] |
|-----------|----------------------------|--------------------------|------------------------------|-------------|-----------|
| Bridge | stainless steel grade 304L | 0.98 | 8000 | 1 | 7800 |

| Component | Length [m] | Width [m] | Height [m] | Diameter [m] | #components |
|------------------------------|------------|-----------|------------|--------------|-------------|
| Deck | 12.5 | 2.5 | [-] | [-] | 1 |
| Railing | 10.5 | 0.1 | 1.2 | [-] | 2 |
| Lateral structure (spirrals) | [-] | [-] | 1.2 | 1 | 4 |

TABLE 1: Geometrical characteristics of the 3D printed steel bridge

The total area of the bridge is another essential variable for the correct calculation of the required costs throughout the life cycle of the bridge. Thus, the total area of the 3D-printed bridge is calculated according to Equation (1), which sums the components’ areas and subtracts the calculation overlaps.



FIGURE 14: Overview of the MX3D metal 3D printed footbridge, (Rolands Kromanis, 2021)

$$A_{tot} = 2 * A_{railings} + A_{deck} + 4 * A_{spirrals} - Overlaps = 141.65m^2 \quad (1)$$

3.2 Traditionally constructed Concrete bridge

In this Paragraph, we develop and explain the structural design of the concrete bridge. Initial dimensions will be set starting with the boundary conditions concerning the bridge's length, width, and use purpose. Given that the bridge should comply with the Dutch regulations set by the eurocodes (NEN, 2022), the structural design must be safe for its users. Besides the durability of the bridge, the contexts of sustainability, effectiveness, and cost have to be as beneficial as possible. Therefore, the calculations will follow the ending design loop (see Figure 32), followed by several iterations. The bridge dimensions will be adjusted to optimize the overall quantities of materials used throughout the construction phase.

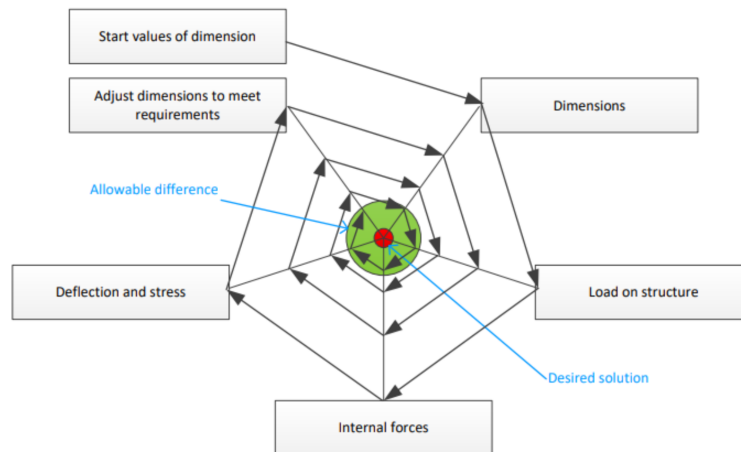


FIGURE 15: Ending Design Loop, (Snellink, 2021)

The structural design and its optimization will be executed according to the following steps:

1. Set the initial design of structural with the rules of thumb
2. Determine the active and dead loads acting on the structure
3. Determine the principal reinforcement for structural components
4. Determine the most optimal dimensions for the principal reinforcement for structural components

5. Determine the shear force reinforcement
6. Determine the most optimal dimensions for the shear force reinforcement for structural components
7. Check the structure's strength (S/R)
8. Determine the Anchorage for structural components
9. Check crack control

3.2.1 Geometrical characteristics for the Concrete bridge

By conducting the steps mentioned above, the initial dimensions of the bridge's structural components are modified, affecting the bridge's bearing capacity. Thus, several iterations with different dimensions are performed. However, to attract the reader, only the calculation based on initial and final dimensions is delivered. These steps are presented in detail in the Appendix B, explaining each design and engineering decision properly.

Given the starting point, the purpose, and the approximate dimensions of the structural components followed from the 3D printed steel bridge, the geometrical characteristics and material properties of the traditionally constructed concrete bridge were determined in compliance with the Dutch regulations and are preset in Table 2.

| Component | Material | Volume [m ³] | Density [kg/m ³] | #components | Mass [kg] |
|-----------|----------------------------|--------------------------|------------------------------|-------------|-----------|
| Bridge | stainless steel G304 | 0.31 | 8000 | 1 | 2480 |
| Bridge | reinforced concrete C20/26 | 9.92 | 2400 | 1 | 23800 |

| Component | Length [m] | Width [m] | Height [m] | Diameter [m] | #components |
|-----------------|------------|-----------|------------|--------------|-------------|
| Beam | 12.2 | 0.35 | 0.76 | - | 2 |
| Deck | 3.05 | 3 | 0.1 | - | 4 |
| Railing columns | 0.05 | 0.1 | 1 | - | 7 |
| Railing top | 12.2 | 0.1 | 0.05 | - | 2 |
| Railing wires | 12.2 | - | - | 0.01 | 9 |

TABLE 2: Geometrical characteristics of the traditionally built Concrete bridge

The concrete bridge consists of two concrete beams, four concrete deck plates located over the beams, and two steel railing systems installed on the edges of the bridge. Similar to the 3D printed bridge, the total area of the traditionally built concrete bridge is an essential variable for further calculations. Therefore, the total area of the concrete bridge is calculated with the following formula and can be seen in Equation (2), which similar to the total area of the 3D printed bridge sums the components' areas and subtracts the calculation overlaps. .

$$A_{tot} = 2 * A_{railings} + A_{deck} + 2 * A_{beams} - Overlaps = 113.33m^2 \quad (2)$$

3.3 Calculation of the Active loads

The load the bridge needs to withstand is determined according to the Dutch construction requirements, mainly the Eurocodes defined by (NEN, 2022). There are several classes of loads, such as self-weight induced by the structural components and dynamic loads generated by snow wind and pedestrians passing or standing on the bridge. Given the scope of the research project, the loads generated by the bridge's self-weight are not considered for the comparison of the structural properties of the design alternatives. Therefore, only the dynamic loads will be analyzed. This specific analysis (related to dynamic loads) is conducted because the loads caused by the bridge's self-weight significantly vary per material. Thus, dynamic loads present in the Table 3 are used to retain the objective comparison of mechanical properties. Considering the fact that two design alternatives tend to retain similar geometric parameters, it is assumed that the dynamic loads on both structures are of the same magnitude. The detailed calculation of the dynamic loads can be found in Appendix B.3.

| Load | Magitude | Units |
|--------------|----------|-------------------|
| Snow load | 0.56 | kN/m ² |
| Wind Load | 0.52 | kN/m ² |
| Imposed Load | 5 | kN/m ² |

TABLE 3: Dynamic loads acting on the bridge

3.4 Cost-Load ratio

Applying the geometrical parameters and dynamic loads concerning both bridge alternatives generates the possibility of comparing different design alternatives methods with respect to the costs-load ratio. The cost-load ratio is calculated by dividing the total incurred cost during the production and construction phases of the bridge by the summation of the dynamic loads acting on the structure.

The combination of dynamic loads obviously depends on multiple conditions and can not occur simultaneously. For instance, neither of the bridges can be fully loaded by people standing on the bridge deck during a heavy storm, thus, a precise combination of dynamic loads is explained in Appendix B.4. Nevertheless, to visualize the difference between the loads and costs concerning design and construction alternatives, a summation of all possible dynamic loads is applied. As a result, the cost-load ratio is represented in Table 4.

| Bridge Alternative | Production and Construction Costs [€] | Dynamic Load [kN/m ²] | Cost-Load ratio [€m ² /kN] |
|-----------------------------|---------------------------------------|-----------------------------------|---------------------------------------|
| 3D-printed Steel Bridge | 24660.05 | 6.08 | 4054.59 |
| Traditional Concrete Bridge | 15755.07 | 6.08 | 2590.44 |

TABLE 4: Cost-load ratio per construction alternative

As seen in Table 4, the cost-load ratio is significantly larger for 3D printed bridge compared with the traditionally constructed concrete bridge. Mainly, the 3D printed bridge's cost-load ratio is €1460 per kN/m^2 , higher than its alternative. Given that the dynamic loads are equal for both construction procedures, the significant difference in the cost-load ratio is generated by a higher cost incurred during the production and construction phases of the 3D-printed steel bridge. This leaves an advantage for the traditionally concrete bridge, which shows to be cheaper in the first phases of its life cycle.

3.5 Conclusion

In this chapter, the method for determining the dimensions of the bridges considering two different design approaches, using different structural materials and different construction techniques, was described. All structural elements of the bridge design comply with all required Dutch construction norms. Additionally, the traditionally built concrete bridge has been checked on its strength and can withstand all potential load combinations (see Appendix B).

The cost-load ratio has been determined based on the costs incurred during the production and construction phases and the summation of the dynamic loads. This has resulted in the first performance indicator for outlining the most optimal design alternative.

Following the determined geometrical characteristics for both alternatives, the components of LCC and LCA calculation tools and their functionality are described in Chapter 4 and Chapter 7. Besides, to test the reliability of the results, validation tests are applied. As a result, the case study determines how 3D-printed steel and traditionally built concrete bridges compete concerning different performance indicators.

4 Development of the LCC tool

This Chapter describes the LCC tool developed based on one of the branches of the research model elaborated in the Chapter 2. The LCC tool design is based on four phases of the bridge life cycle, mainly the production, construction, use, and end-of-life phases. Considering the phases of the bridge life cycle mentioned above, the total costs incurred throughout a time span of 100 years make up the total LCC costs. This Chapter describes the necessary input parameters and equations to calculate different costs concerning the life cycle phase and their nature. In the Paragraph 4.1, the costs for different phases will be discussed. Following, the calculation procedures to determine the economic impact are described in the Paragraph 4.2. Next, the calculation of the discount rate impact is developed in Paragraph 4.3. An overview of additional insights concerning LCC calculation tool can be found in Appendix C.

4.1 Life Cycle Costs

Throughout the bridge life cycle, multiple types of costs are occurring. Given that the bridge needs to be produced, constructed, maintained, and recycled, the economic impact consists of multiple costs. Therefore, having the purpose of easing the understanding of the LCC calculation tool, the costs are explained per each phase of the life cycle. The life cycle phases follow a similar order as shown in Figure 9, namely the production, construction, use, and end-of-life phases.

4.1.1 Cost breakdown structure

The cost breakdown structure is developed to clarify the origin of the economic impact per each bridge's life cycle phase. In Figure 16, the life cycle costs of the analyzed functional unit are shown in a cost breakdown structure. The initial costs take place during the production phase, where the financial impact is generated by manufacturing and processing activities. Next, the costs incurred during the construction phase are divided into three categories: construction labor costs, transportation/machinery costs, and rental costs. Followed by the most extended phase spanning the entire life cycle of the bridge, the costs generated during the use phase are split into three categories: energy, material, and maintenance personnel. The cost encountered throughout the end-of-life phase is generated by the disposal costs, demolition labor costs, transportation/machinery costs, and rental costs. The structural components are recycled, landfilled, or reused depending on the construction alternative.

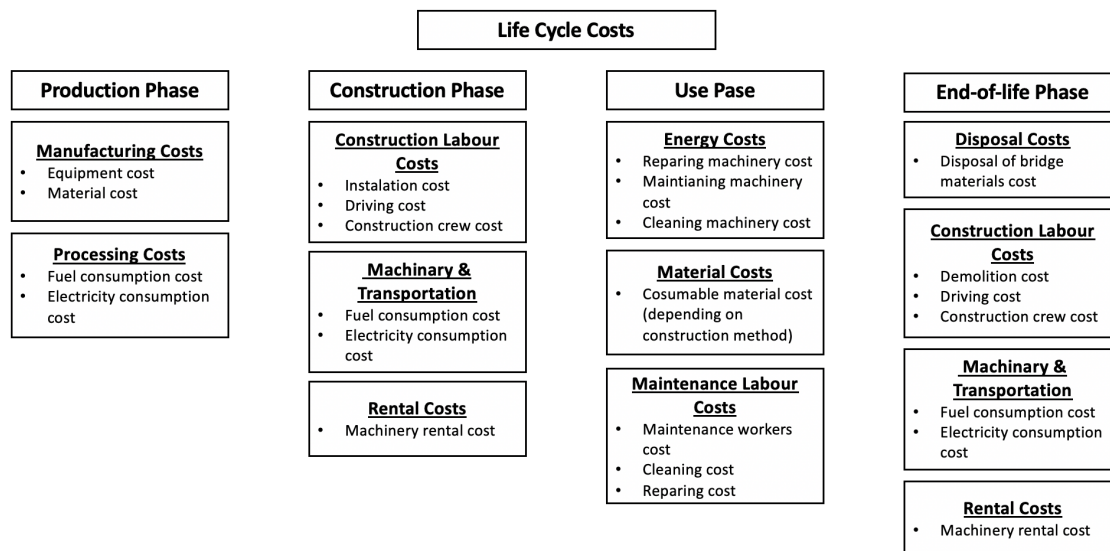


FIGURE 16: Life cycle cost breakdown

4.1.2 Production phase

The cost incurred during the production phase could also be named the initial construction costs, which implies the costs necessary for producing the complete structural components of the functional unit. These costs are generated by two main factors, the costs of the material (manufacturing costs) and the cost of the consumed energy (fuel or electricity) (processing costs) for producing the structural elements.

The energy consumption for producing the structural element is calculated to estimate the costs subject to the production phase. The next step is to determine the cost concerning the operated material for the production of the structural elements. Given the geometrical characteristics and the material properties from Chapter 3 per each of the two bridge alternatives, the material costs are determined. This is achieved via a simple multiplication of two variables: the price of one kilogram or one cubic meter of each material used to produce structural components and the materials' mass or volume. Given the differences between the production methodologies of the two bridge alternatives, this calculation procedure allows for determining cost correctly without applying any additional steps concerning construction methodological differences.

The production costs are calculated according to the Equation (3). Notice that the discount rate is not applied yet, since it is not necessary at this point. The discount rate is applied to the costs which occur in the future. This implication is explained in detail in the later section of this Chapter, in Paragraph 4.3.

$$PPC = \sum_{i=n}^m CUP_i \times CqM_i + \sum_{j=k}^z CES_j \times CUPE_j \quad (3)$$

Where:

PPC = Total Production Phase Costs (€)

i = material type n until material type m

j = structural component k until component z

CUP_i = Cost unit price of material i (€)

CqM_i = The quantity of construction material i (kg or m³)

CES_j = Consumption of energy by structural element j (kWh)

$CUPE_j$ = Cost unit price of energy sources for structural element j (€/kWh)

4.1.3 Construction phase

According to (Waldschmitt et al., 2021) and (Blank et al., 2000) the construction procedures of the 3D-printed steel and traditionally built concrete bridge have several specific differences that need to be adjusted in the calculation tool. Mainly, the transportation of the structural elements, the installation of the functional unit, and the required mechanical equipment used during the construction works vary with respect to the applied construction method. Therefore, the LCC tool must split the incurred costs per category such that differences retained by the bridge's alternative construction method do not affect the correctness of the calculation procedure. This implies that the expected costs during the construction phase must be divided into construction labor costs, transportation/machinery costs, and rental costs.

Labor generates the highest construction costs. For example, the duration of construction works instantly implies the presence of the construction crew that follows the structural protocol and installs the bridge. Besides, delivering the required machinery for components installation, construction works, and transportation of the prefabricated structural elements requires professional personnel. Thus, to determine the economic impact magnitude of the construction labor costs, the working activity duration concerning the amount of required personnel needs to be determined. Next, the personnel's wage per activity is needed depending on the type of labor. As a result, by multiplying the two variables mentioned above, the total costs required for the construction crew, truck drivers, and machinery operators, namely construction labor costs, can be determined.

Similar to the labor costs, the rental cost varies with respect to the construction procedure, mainly due to the potential differences in the required machinery. Following the construction labor costs, the rental

costs potentially represent the second-highest economic impact during the construction phase. In order to determine the rental costs, two variables are required, namely the rental duration and the hourly cost of the rental component.

Last but not least, the third cost category of the construction phase combines two components, transportation, and machinery. To overcome potential issues with the calculation procedure while varying the construction method, it has been decided to merge the energy consumption for transportation and for operating the machinery. Therefore, multiple variables are required to determine the energy consumed throughout the processes mentioned above, such as covered distances, amount of time required to operate or transport, vehicle type, energy cost, consumption rates, etc. Nevertheless, to clarify the research project for the reader, the calculation cost incurred for the transportation and machinery is simplified to the final variables, mainly the energy consumption and cost unit price of the energy source.

Considering the remarks and explanation of all three construction phase cost categories, the Equation (4) is deduced.

$$CPC = \sum_{y=r}^p WAd_y \times W_y + \sum_{j=k}^z CRd_j \times RC_j + \sum_{i=n}^m CEVM_i \times CUPE_i \quad (4)$$

Where:

CPC = Total Construction Phase Costs(€)

y = working activity r until activity p

j = rental component type k component type z

i = Vehicle/Machinery type n until Vehicle/Machinery m

CR_j = Component j rental duration (hour)

RC_j = Rental cost of component j (€/hour)

WAd_y = Working activity y duration (hour)

W_y = Wage for activity (€/hour)

$CEVM_i$ = Consumption of energy by Vehicle/Machinery i (L or kWh)

$CUPE_i$ = Cost unit price of energy sources for Vehicle/Machinery i (€/L or €/kWh)

4.1.4 Use phase

First, the maintenance scenario that accurately describes the estimated necessary Maintenance over the bridges' life cycle must be determined. Compared to other bridges' life cycle phases, the use phase is directly pointing up due to a significant difference in its duration. The use phase is extended almost throughout the entire life cycle of the bridge. Therefore, the LCC tool needs to be adjusted very carefully to reproduce precisely the economic impact caused by the processes and operations during the use phase of the bridge. Moreover, by analyzing the research papers concerning the Maintenance of the concrete bridge (Richard E. and Paul D., 2006) and the steel bridge (Hoyle Tanner, 2017), it inherently indicates that the maintenance processes significantly vary for different types of materials. This maintenance variation increases the difficulty regarding implementing a similar calculation for both types of construction procedures. Therefore, the costs incurred throughout the use phase are divided into three subgroups: material, maintenance, and energy.

Similarly to the cost systematization for the construction phase, the cost categories of the use phase are described in descending order concerning the potential financial magnitude. Due to the nature of the application, frequency rates, and duration of the activities, either the material costs either maintenance personnel costs are considered to have the most significant influence on the total cost throughout the use phase of the bridge. In order to determine the material costs, multiple variables are required. Nevertheless, to ease comprehension of the applied calculation procedure for the reader, the final simplified variables are described. Mainly the cost unit price of the applied material, activity frequency, functional object, and the usage percentage of the functional object. The first two required terms are straightforward, however, the next two require additional explanation. The functional object represents the location or the structural component where the material is applied. In contrast, the usage percentage of the functional object represents the numerical value implying the number of structural components

that require a material application. For example, it is impossible that the entire concrete bridge area is defective and needs to be replaced.

The following two cost categories are almost similar to those described in the Paragraph 4.1.3 for the construction phase. The Maintenance labor costs and Energy costs are calculated similarly as in the Paragraph 4.1.3. Hence, due to the nature of maintenance work, the activity frequency variable is embedded in the Equation (5). This procedure ensures that neither use phase costs are lost due to the differences in maintenance scenarios for both construction alternatives.

The total cost incurred throughout the use phase is therefore calculated by Equation (5):

$$UPC = \sum_{y=r}^p CUPM_y \times AF_y \times FO_y \times UFO_y + \sum_{j=k}^z WAd_j \times W_j \times AF_j + \sum_{i=n}^m CEVM_i \times CUPE_i \times AF_y \quad (5)$$

Where:

UPC = Total Use Phase Costs (€)

y = material type r until material p

j = working activity k until activity z

i = Vehicle/Machinery type n until Vehicle/Machinery m

$CUPM_y$ = Cost unit price of material y (€/functional unit)

AF_y = Activity y frequency (times in 100 years)

FO_y = Functional object y (functional unit)

UFO_y = Usage percent of functional object y (%)

WAd_j = Working activity j duration (hour)

W_j = Wage for activity (€/hour)

AF_j = Activity j frequency (times in 100 years)

$CEVM_i$ = Consumption of energy by Machinery i (L or kWh)

$CUPE_i$ = Cost unit price of energy sources for Machinery i (€/L or €/kWh)

AF_i = Activity i frequency(times in 100years)

4.1.5 End-of-life phase

The fourth subcategory of the life cycle costs is end-of-life costs. In order to ease the calculation procedure, the end-of-life costs are divided into four cost categories: disposal, demolition, transportation/machinery, and rental costs. For this section, most cost categories of the end-of-life are calculated the same way as the costs incurred during the construction phase, except the disposal costs. Concerning different types of material, the disposal of the structural components can result in a negative value, implying that the recycling of the material is partially returning the initial investments. Thus, this feature is embedded into the calculation tool and explained in the later chapters.

The disposal costs require the recycling percentage, price per cubic meter of recycling material, and the amount of material to be recycled in cubic meters. Obtaining these values from predefined geometrical characteristics of the bridge as well as the literature research allows us to determine the total costs generated within the boundaries of the disposal cost category and determine the overall cost per end-of-life phase via Equation (6) :

$$EPC = \sum_{s=u}^v CUPR_s \times V_s + \sum_{j=k}^p WAd_y \times W_y + \sum_{j=k}^z CRd_j \times RC_J + \sum_{i=n}^m CEVM_i \times CUPE_i \quad (6)$$

Where:

EPC = Total End-of-life Phase Costs(€)

s = disposal component u until component v

y = working activity r until activity p

j = rental component type k component type z

i = Vehicle/Machinery type n until Vehicle/Machinery m

$CUPR_s$ = Cost unit price of recycling component s (€/m³)
 V_s = Volume of component s (m³)
 CR_j = Component j rental duration (hour)
 RC_j = Rental cost of component j (€/hour)
 WAd_y = Working activity y duration (hour)
 W_y = Wage for activity (€/hour)
 $CEVM_i$ = Consumption of energy by Vehicle/Machinery i (L or kWh)
 $CUPE_i$ = Cost unit price of energy sources for Vehicle/Machinery i (€/L or €/kWh)

4.2 Life cycle costs distributed over 100 years

Before calculating the impact caused by the discount rate, the distribution of the registered costs throughout the bridge's lifetime has to be set. This implies that the activity frequency and duration need to be known beforehand. Therefore, the LCC calculation tool has to retain a function that distributes the costs concerning activity frequency and duration. The starting point of the desired cost distribution functions lies in the expected result. Thus, it has been decided that the starting year of the first iteration, the ending year of the first iteration, and the time boundary between the first and the second interaction must be determined. In order to determine the variables mentioned above, activity frequency is required. Next, the cost can be distributed with assumptions and parametric calculations. Given the activities' nature and frequency, the cost distribution function will be tested per different life cycle phases. The variables' frequency unit is measured in times per 100 years, which eases the distribution procedure. This implies that the allocation function distributes activities per year.

The duration of activities from different life cycle phases needs to be determined. According to (Dr. Homayoun Abrishami, 2017), the production of the bridge structural components takes around two years. Thus, considering that the infrastructure owners decide to start the bridge life cycle phase, the first two years are dedicated to modeling and manufacturing the bridge's structural components. The construction phase can be initiated as soon as the bridge's structural elements are manufactured and ready for transportation. This implies that the production and construction phases overlap in the same year. Therefore, the starting year of the construction works can be determined. Mainly there will be a one-year difference between the production and construction phases. Following the (Dr. Homayoun Abrishami, 2017) and (Waldschmitt et al., 2021), both bridge construction alternatives with the predefined geometrical properties (see Paragraph 3.1.1 and Paragraph 3.2.1) indicates that the entire process putting the structure into service takes up to one year. As a result, the starting year and the duration of the activities during the production and construction phase are determined.

The research literature is applied to determine the duration of the activities during the use and end-of-life phases. Multiple literature sources for both construction alternatives resulted in the following conclusion there are no activities whose duration is larger than one year. In this way, the duration of the user activities and end-of-life phases are determined. The required starting year for the calculation functions demands the application of several straightforward assumptions. Firstly, considering the scope of the research project, the starting year of the bridge life cycle is set to be 2022. This implies that the production phase is started in the same year and ends in the next year, mainly in 2023. Regarding the conclusion above, the construction phase starts in 2023. Obviously, the end-of-life phase, in which activities duration is shorter than one year, will take place in the last year of the life cycle. Thus the starting year of the end-of-life phase activities is 2122.

The activities which belong to the use phase occur multiple times per life cycle, therefore, knowing their duration, the starting year of the first iteration can be determined via Equation (7).

$$SY_{1i} = 2022 + \lfloor 100/AF_i \rfloor \quad (7)$$

Where:

i = activity index

SY_{1i} = Starting year of the first iteration for activity i

AF_i = Activity i frequency (times in 100 years)

The logic behind the Equation (7) implies that the starting year can be calculated as the summation between the starting year of the bridge life cycle (2022) and the division of the bridge lifetime (100 years) by the activity frequency. This way, the activities belonging to the use phase take place at a specific time after the structure is installed. This is obvious since there is no sense in applying for any maintenance works instantly after construction phase's termination.

The next aim is to determine the period between the first and the second activity iteration. Given that the activities belonging to the construction phase and end-of-life take place once per life cycle, the time boundary between "the first and second" iteration obviously, result in 100 years, representing the entire life span of the bridge. For the production phase, the activity duration might last longer. However, since the activities of the production phase take place only once during the bridge's life cycle, determining the period between "the first and the second activity iteration" is inherently explicit. The following Equation (8) is used in the LCC calculation tool for the aforementioned life cycle phases (which occur once in the life time of the bridge).

$$TB_i = \lfloor 100/AF_i \rfloor \quad (8)$$

Where:

i = activity index

TB_i = Time boundary between the first and the second activity i iteration (years)

AF_i = Activity i frequency (times in 100 years)

In contrast, the use phase activities start in different years and have varied frequency rates. Therefore, the following Equation (9) was applied to determine the time boundary between the first and the second activity iteration.

$$TB_i = \lfloor (2122 - EF_{1i})/AF_i \rfloor \quad (9)$$

Where:

i = activity index

TB_i = Time boundary between the first and the second activity i iteration (years)

EF_{1i} = Ending year of the 1st activity iteration

AF_i = Activity i frequency (times in 100 years)

As a result, the starting year of the first iteration, the ending year of the first iteration, and the time boundary between the first and the second iteration is determined for all activities that occur throughout the bridge life cycle. Thus the function for the cost distribution over the bridge's life cycle can be created.

The Equation (9) returns the year when an iteration of the activity takes place. A mathematical condition restricts the number of iterations. Mainly the equation's result can not overcome the year 2122. If the function result exceeds 2122, this implies that the activity occurs after the bridge disposal, which is illogical. Moreover, the function is a combination of known variables, namely the starting year of the first iteration and the time boundary between the first and the second activity iteration. Besides, a new variable is applied, standing for the iteration order.

$$Y_i = \lfloor SY_{1i} + (N_i - 1) \times TB_i \rfloor \leq 2122 \quad (10)$$

Where:

Y_i = Year when activity i iteration $N_{(i)}$ takes place (years)

i = Activity index

SY_{1i} = Starting year of the first iteration for activity i

N_i = Iteration number of activity i from 0

TB_i = Time boundary between the first and the second activity i iteration (years)

Applying the Equation (10) mentioned above to the life cycle activities establishes the precise schedule during which year the activity starts and ends. Therefore, the total costs of activities are divided by activity frequencies and spread all over the life cycle phase. As a result, the costs incurred per year during the entire life cycle phase can be determined.

4.3 Discount Rate

As soon as the yearly incurred cost is determined, the discount rate can be applied to visualize the impact of the time over the entire LCC. According to the (Jawad and Ozbay, 2005), multiple variables are required to calculate the discount rate's impact, mainly the present-day activity cost, the number of discount periods, and the discount factor. Considering that the first two variables are already determined, the literature review in line with consultations with experts from Infra Plan Consulting was applied for the application of the discount factor. (Jaap de Wit, 2012). Consequently, the implication of the discount factor could be applied to determine the final total cost for both construction alternatives according to the Equation (11).

$$TC = \sum_{t=2022}^T TC_t \times \left(1 + \frac{r}{100}\right)^{(t-2022)} \quad (11)$$

Where:

TC = Total cost (€)

t = Year of the life cycle from 0 until the end-of-life cycle T

TC_t = Total cost incurred during year t (€)

r = The discount factor (%)

An example of the parametric tool operation can be seen in Table 5. Initially, the costs schedule is created, where each activity belonging to different life cycle phases is scheduled on the years determined by the frequency corresponding with that activity. The tool can then discount the scheduled cost depending on the year in which the costs are planned. This calculation is done with the Equation (11). Its effect can be observed as the costs exponentially increase with respect to the number of years since the beginning of the life cycle.

| Year | 2022 | 2023 | 2024 | ... |
|------------------------------|-------------------|--------------------|-----------------|------------|
| Construction | € 4,376.02 | € 11,101.52 | € 0.00 | ... |
| Use phase | € 0.00 | € 31.65 | € 112.66 | ... |
| End of life | € 0.00 | € 0.00 | € 0.00 | ... |
| Total Costs | € 4,376.02 | € 11,133.17 | € 112.66 | ... |
| Total Cost (discount) | € 4,376.02 | € 11,411.50 | € 118.37 | ... |

TABLE 5: Discount rate (2.5%) implication over the yearly incurred costs

5 Case Study LCC

In Chapter 1, the research model defines the parametric calculation tool as the research objective. The base of the parametric tool has been explained in Chapter 4. Furthermore, the described formula is used to analyze the base case concerning two design alternatives: the 3D printed steel bridge and the traditionally constructed concrete bridge. The base case has been selected in line with Infra Plan Consulting to depict the core differences between the two design alternatives. This Chapter describes the input parameters used to calculate the final economic impact of both constructions. Consequently, the LCC model output concerning the case study is explained.

The developed parametric tool consists of two parts, the input parameters, also used for calculating the environmental impact (in Chapter 7), and the output performance indicators that ensure a proper comparison between two bridge alternatives. Starting with the Paragraph 5.1, the input parameters and their differences for both bridges are described. The output of the LCC calculation tool is explained in Paragraph 5.3. The Chapter is closed with some concluding comments in the Paragraph 5.4.

5.1 Main input parameters

The LCC calculation tool starts with the structural parameters of the bridge and its geometrical characteristics. Following the Chapter 3, the geometric elements of the bridge are defined. Therefore, the different construction elements are further used to set the input parameters of the parametric tool. Given the complexity of the calculation, only the main input parameters are discussed. The rest variables can be found in the Appendix C. The main input parameters are also elaborated in the order of the life cycle phases, namely, the production, construction, use, and end-of-life phases.

5.1.1 Production phase input

Starting with the production phase, the energy consumed throughout the process is required. The following parameters were entered in the parametric tool based on the literature research. Notice that the volume of the bridge alternatives is not included since this variable is automatically calculated based on the predefined geometrical characteristics.

See Table 6 for the Concrete bridge and Table 7 for the 3D printed steel bridge.

| Component | Material | Density [kg/m ³] | Mass [kg] | Frequency [times in 100y] | Energy consumption [kWh] | Sources |
|-------------------|----------------------------|------------------------------|-----------|---------------------------|--------------------------|--|
| Beams reinforced | reinforced concrete C20/25 | 2400 | 15662.63 | 1 | 2277.35 | (MPA The Concrete Centre, 2019) |
| Plates reinforced | reinforced concrete C20/25 | 2400 | 8832.31 | 1 | 1284.22 | (MPA The Concrete Centre, 2019) |
| Railings | Stainless Steel grade G304 | 8000 | 1673.98 | 1 | 6980.49 | (Fruehan and Fortini, 2000) (Davis, 1998) |

TABLE 6: Concrete bridge components

| Component | Material | Density [kg/m ³] | Mass [kg] | Frequency [times in 100y] | Energy consumption [kWh] | Sources |
|-----------|----------------------------|------------------------------|-----------|---------------------------|--------------------------|--|
| Bridge | Stainless steel grade 304L | 8000 | 7800 | 1 | 32526 | (Fruehan and Fortini, 2000) (Davis, 1998) |

TABLE 7: 3D printed bridge components

The overall consumption per unit of mass or volume is required to determine the consumed energy during the production phase. These variables are embedded in the calculation model and are found based on the literature research. According to (MPA The Concrete Centre, 2019), 145.4 kWh/tonne of electricity are consumed for the concrete elements. In contrast, according to (Fruehan and Fortini, 2000), 4.17 kWh/kg of electricity is consumed by the steel elements.

5.1.2 Construction phase input

The construction procedures for the traditional concrete bridge and alternative 3D-printed steel bridge strongly differ, mainly the installation procedure, transportation means, and machinery used during the construction phase (Blank et al., 2000).

Nevertheless, the input for both design alternatives can be systematized such that the calculation tool does not require additional information. Therefore, the input parameters of the construction phase are divided into two categories: transportation and time in use. The transportation category encounters the covered distances and fuel consumption of vehicles that contributed to the delivery or installation of the structural components. The input parameters for the concrete bridge are shown in Table 8, for the 3D printed bridge in Table 9.

| Component | Transportation Origin | Distance to travel [km] | Distance from [km] | Transportation Type | Fuel Type | Frequency | Total distance traveled [km] | Source |
|-----------|-----------------------|-------------------------|--------------------|---------------------|-----------|-----------|------------------------------|--------------------|
| Beams | Coonstar Beton Waren | 80 | 80 | Heavy Transport | Diesel | 1 | 160 | (Constar, 2022) |
| Plates | Coonstar Beton Waren | 80 | 80 | Heavy Transport | Diesel | 1 | 160 | (Constar, 2022) |
| Railings | Tata Steel | 30 | 30 | Heavy Transport | Diesel | 1 | 60 | (Tata Steel, 2022) |
| Bridge | Koninklijke Saan | 18 | 18 | Crane | Diesel | 1 | 36 | (Saan, 2022) |

TABLE 8: Transportation Concrete bridge, construction phase

| Component | Transportation Origin | Distance to travel [km] | Distance from [km] | Transportation Type | Fuel Type | Frequency | Total distance traveled [km] | Source |
|-----------|-----------------------------------|-------------------------|--------------------|---------------------|-----------|-----------|------------------------------|--------------|
| Bridge | Dynamostraat 46 1014 BK Amsterdam | 10 | 10 | Boat | Diesel | 1 | 20 | (MX3D, 2020) |
| Bridge | Koninklijke Saan | 18 | 18 | Crane | Diesel | 1 | 36 | (MX3D, 2020) |

TABLE 9: Transportation 3D printed Bridge, construction phase

Due to the nature of the 3D-printed steel bridge that is transported as one single element (MX3D, 2020), transportation requires fewer rounds, reducing the number of hours the vehicles and personnel are engaged. The time in use defines the amount of time that the machinery or the transport was used. In this case, the calculation model systematized the input parameters for later calculation of the costs. For instance, knowing the time in use, the workers' salaries can be defined, see Table 10 and Table 11.

| Scenario | Time [h] | Total distance traveled [km] | Frequency per 100 years | Fuel Consumption | Units | Total Consumption | Units | Source |
|------------------------------|----------|------------------------------|-------------------------|------------------|------------------|-------------------|-------|--------------------|
| Truck Beams transportation | 3.5 | 160 | 1 | 30 | L/100km (Diesel) | 48 | L | (Constar, 2022) |
| Truck Plates transportation | 3.5 | 160 | 1 | 30 | L/100km (Diesel) | 48 | L | (Constar, 2022) |
| Truck Railing transportation | 1.5 | 60 | 1 | 30 | L/100km (Diesel) | 18 | L | (Tata Steel, 2022) |
| Amount of time Crane travels | 1 | 36 | 1 | 20 | L/100km (Diesel) | 7.2 | L | (Saan, 2022) |
| Amount of time Crane is used | 5 | [-] | 1 | 12 | L/h (Diesel) | 60 | L | (Saan, 2022) |
| Machinery 1 (for concrete) | 5 | [-] | 1 | 4.2 | kW | 21 | kWh | (STIHL, 2020c) |
| Machinery 2 (for concrete) | 5 | [-] | 1 | 5 | kW | 25 | kWh | (STIHL, 2022) |

TABLE 10: Time in use Concrete bridge, construction phase

| Scenario | Time [h] | Total distance traveled [km] | Frequency per 100 years | Fuel Consumption | Units | Total Consumption | Units | Source |
|------------------------------|----------|------------------------------|-------------------------|------------------|------------------|-------------------|-------|----------------------|
| Boat Bridge transportation | 5 | 20 | 1 | 7 | L/h (Diesel) | 35 | L | (QUICK Silver, 2020) |
| Amount of time Crane travels | 1 | 36 | 1 | 20 | L/100km (Diesel) | 7.2 | L | (Saan, 2022) |
| Amount of time Crane is used | 4 | [-] | 1 | 12 | L/h (Diesel) | 48 | L | (Saan, 2022) |
| Machinery 1 (for steel) | 5 | [-] | 1 | 3.8 | kW | 19 | kWh | (STIHL, 2020e) |
| Machinery 2 (for steel) | 5 | [-] | 1 | 4.2 | kW | 21 | kWh | (STIHL, 2020d) |

TABLE 11: Time in use 3D printed bridge, construction phase

5.1.3 Use phase input

During the whole lifetime of the bridge, multiple maintenance operations are required, such as repairing, cleaning, and plastering the potentially affected zones. The most extended phase of the bridge life cycle is the use phase. Obviously, the materials used throughout the complete maintenance works retain the highest economic impact for the use phase. Nevertheless, considering that multiple materials are used at different phases, the parametric tool develops a separate input category with cost that concerns materials used throughout the whole life cycle of the bridge (see Paragraph 5.2). Thus, the starting input for the use phase consists of one category, time in use.

As mentioned above, multiple maintenance operations are applied. Hence the nature and scope of the maintenance work significantly vary with respect to construction procedure. Based on (Weyers and Strategic Highway Research Program (U.S.), 1993), and (Transit NZ, 2001), the maintenance operation for both design alternatives are defined, the time in use and frequency of the maintenance operations are the core input. In this way, the energy consumption, wages of the working personnel, and (partially) the material consumption can be determined. Therefore, the following input parameters have been defined for the base case for the concrete bridge (see Table 12) and the 3D printed bridge (see Table 13).

| Scenario | Time [h] | Total distance traveled [km] | Frequency per 100 years | Fuel Consumption | Units | Total Consumption | Units | Source |
|--------------------------------------|----------|------------------------------|-------------------------|------------------|-------|-------------------|-------|----------------|
| Machinery 1 (cleaning deck) | 1.5 | [-] | 100 | 4.1 | kW | 615 | kWh | (Sika, 2020) |
| Machinery 1 (plastering concrete) | 4 | [-] | 20 | 2.1 | kW | 168 | kWh | (STIHL, 2020c) |
| Machinery 3 (reinforcement concrete) | 2 | [-] | 7 | 2.4 | kW | 33.6 | kWh | (STIHL, 2020f) |
| Machinery 4 (corrosion removal) | 2 | [-] | 50 | 2.8 | kW | 280 | kWh | (TEKNOS, 2013) |
| Machinery 5 (cleaning parapets) | 1 | [-] | 100 | 4.1 | kW | 410 | kWh | (STIHL, 2020b) |

TABLE 12: Input parameters Concrete bridge, use phase

| Scenario | Time [h] | Total distance traveled [km] | Frequency per 100 years | Fuel Consumption | Units | Total Consumption | Units | Source |
|--|----------|------------------------------|-------------------------|------------------|-------|-------------------|-------|----------------|
| Machinery 1 (pressure washer deck) | 1.5 | [-] | 100 | 4.1 | kW | 615 | kWh | (STIHL, 2020c) |
| Machinery 2 (pressure washer joints) | 1 | [-] | 100 | 4.1 | kW | 410 | kWh | (STIHL, 2020b) |
| Machinery 3 (air blast flushing steel) | 1 | [-] | 100 | 2 | kW | 200 | kWh | (STIHL, 2020e) |
| Machinery 4 (painting isolated areas) | 2 | [-] | 34 | 2.1 | kW | 142.8 | kWh | (TEKNOS, 2013) |
| Machinery 5 (corrosion removal) | 2.5 | [-] | 25 | 2.8 | kW | 175 | kWh | (STIHL, 2020b) |

TABLE 13: Input parameters 3D printed bridge, use phase

Notice that the parameter defining the total traveled distance is empty. This design decision for the parametric tool allows for preserving of the systematical structure for input parameters per each phase of the bridge life cycle.

5.1.4 End-of-life phase

Similar to the construction phase, the input for the primary end-of-life phase costs calculation consists of two input parameter categories—mainly the transportation and the time in use. Thus, the input variables for the base case for the concrete bridge can be seen in Tables 14 and 15 and for the 3D printed bridge in Tables 16 and 17.

| Component | Transportation Origin | Distance to travel [km] | Distance from [km] | Transportation Type | Fuel Type | Frequency | Total distance traveled [km] | Source |
|-----------|-----------------------------|-------------------------|--------------------|---------------------|-----------|-----------|------------------------------|--------------------|
| Beams | Disposal point, Amsterdam | 14 | 14 | Heavy Transport | Diesel | 1 | 28 | (Constar, 2022) |
| Plates | Disposal point, Amsterdam | 14 | 14 | Heavy Transport | Diesel | 1 | 28 | (Constar, 2022) |
| Railings | Stationsplein 45, Rotterdam | 79 | 79 | Heavy Transport | Diesel | 1 | 158 | (Tata Steel, 2022) |
| Bridge | Koninklijke Saan | 18 | 18 | Crane | Diesel | 1 | 36 | (Saan, 2022) |

TABLE 14: Transportation Concrete bridge, end-of-life phase

| Scenario | Time [h] | Total distance traveled [km] | Frequency per 100 years | Fuel Consumption | Units | Total Consumption | Units | Source |
|------------------------------|----------|------------------------------|-------------------------|------------------|------------------|-------------------|-------|----------------------------|
| Truck Beams transportation | 2 | 28 | 1 | 30 | L/100km (Diesel) | 8.4 | L | (Jairo Posada-Henao, 2013) |
| Truck Plates transportation | 2 | 28 | 1 | 30 | L/100km (Diesel) | 8.4 | L | (Jairo Posada-Henao, 2013) |
| Truck Railing transportation | 3 | 158 | 1 | 30 | L/100km (Diesel) | 47.4 | L | (Jairo Posada-Henao, 2013) |
| Amount of time Crane travels | 1 | 36 | 1 | 20 | L/100km (Diesel) | 7.2 | L | (KOBELKO, 2020) |
| Amount of time Crane is used | 5 | [-] | 1 | 12 | L/h (Diesel) | 60 | L | (KOBELKO, 2020) |
| Machinery 1 (for concrete) | 5 | [-] | 1 | 4.2 | kW | 21 | kWh | (STIHL, 2020c) |
| Machinery 2 (for concrete) | 5 | [-] | 1 | 5 | kW | 25 | kWh | (STIHL, 2022) |
| Machinery 3 (for steel) | 2 | [-] | 1 | 3 | kW | 6 | kWh | (STIHL, 2020a) |
| Machinery 5 (for steel) | 2 | [-] | 1 | 3.6 | kW | 7.2 | kWh | (STIHL, 2020e) |

TABLE 15: Time in use Concrete bridge, end-of-life phase

| Component | Transportation Origin | Distance to travel [km] | Distance from [km] | Transportation Type | Fuel Type | Frequency | Total distance traveled [km] | Source |
|-----------|----------------------------|-------------------------|--------------------|---------------------|-----------|-----------|------------------------------|---------------------|
| Bridge | Stationsplein 45 Rotterdam | 79 | 79 | Heavy Transport | Disel | 1 | 158 | (Google Maps, 2022) |
| Bridge | Koninklijke Saan | 18 | 18 | Crane | Disel | 1 | 36 | (Saan, 2022) |

TABLE 16: Transportation 3D printed bridge, end-of-life phase

| Scenario | Time [h] | Total distance traveled [km] | Frequency per 100 years | Fuel Consumption | Units | Total Consumption | Units | Source |
|------------------------------|----------|------------------------------|-------------------------|------------------|------------------|-------------------|-------|----------------------|
| Truck Beams transportation | 3 | 158 | 1 | 30 | L/100km (Diesel) | 47.4 | L | (QUICK Silver, 2020) |
| Amount of time Crane travels | 1 | 36 | 1 | 20 | L/100km (Diesel) | 7.2 | L | (KOBELKO, 2020) |
| Amount of time Crane is used | 6 | [-] | 1 | 12 | L/h (Diesel) | 72 | L | (KOBELKO, 2020) |
| Machinery 1 (for steel) | 3 | [-] | 1 | 4.2 | kW | 12.6 | kWh | (STIHL, 2020e) |
| Machinery 2 (for steel) | 3 | [-] | 1 | 3 | kW | 9 | kWh | (STIHL, 2020c) |
| Machinery 3 (for steel) | 4 | [-] | 1 | 3.6 | kW | 14.4 | kWh | (STIHL, 2020a) |
| Machinery 5 (for steel) | 4 | [-] | 1 | 3.6 | kW | 14.4 | kWh | (STIHL, 2020e) |

TABLE 17: Times in use 3D printed bridge, end-of-life phase

5.2 Intermediate input parameters

Given that the main input parameters are set, the LCC tool requires additional variables for further calculations to generate the final economic performance indicators. For instance, the material price, number of personnel, wages, and cost of rental equipment are the chain variables between the base input and the output of the parametric model.

Considering that the 3D-printed steel bridge represents an integral structural unit of steel, and considering the maintenance procedures required for steel bridges, the 3D-printed bridge alternative requires fewer materials (Attema and Kosgodagan Acharige, 2017) than the traditionally concrete constructed bridge. Since the different types of materials are used for specific design and construction alternatives, the amount of materials differs per construction model. Thus the material price and respective units used for the cost calculation for the 3D printed bridge are shown in Table 19. For the concrete bridge, the material input values are shown in Table 18.

| Material | Price | Unit | Source |
|----------------------------------|---------|------------------|-----------------------------|
| Reinforced Concrete | 125 | €/m ³ | (Knudsen and Jensen, 2007) |
| Stainless steel G304 (railings) | 1.625 | €/kg | (Constar, 2022) |
| Water for the cleaning machinery | 0.00087 | €/L | (Vollebergh and Dijk, 2017) |
| Concrete Paint | 37 | €/m ² | (Charlie Morgan, 2022) |
| Repair Mortar (polymer) | 1856 | €/m ³ | (Rob B. Polder, 2008) |

TABLE 18: Material Cost Concrete bridge

| Material | Price | Unit | Source |
|--------------------------------------|---------|------------------|-----------------------------|
| Stainless steel grade 304L | 1.8 | €/kg | (Constar, 2022) |
| Water for the cleaning machinery | 0.00087 | €/L | (Vollebergh and Dijk, 2017) |
| Paint isolated areas of rusted steel | 3.06 | €/m ² | (MetalExpert, 2022) |

TABLE 19: Material Cost 3D printed bridge

The engaged personnel throughout the bridge life cycle potentially have a severe economic impact on the final bridge cost. Thus, to determine the extent to which the final bridge cost is affected by the workers, the working hours and the different wages must be determined. Following multiple resources and literature research, the base case input has been defined. Considering the different amounts of construction and maintenance work, the number of working hours and workers differ per bridge alternative. The input parameters for working hours for the concrete bridge can be seen in Table 20. Besides, the wages per job type for 3D printed bridge can be seen in Table 21.

The LCC tool requires the parameters concerning the rental of transport or machinery. To calculate the rental costs of the construction machines, the price per hour and the number of hours of rental are required. Based on the rental obligation defined by the (Saan, 2022) company and discussion with the experts from Infra Plan Consulting, the following input parameters have been established for the base

| Worker | Wage [€/h] | Source |
|---------------------------------|------------|----------------------------|
| Truck. Driver | 14.8 | (Nationale Beroepen, 2022) |
| Crane Driver | 23.5 | (ERI, 2022) |
| Constructor (construction crew) | 21.7 | (ERI, 2022) |
| Cleaner. (pressure washer) | 12.2 | (QPS, 2022) |
| Concrete. maintenance worker | 20.1 | (Nationale Beroepen, 2022) |

TABLE 20: Wages for workers Concrete bridge

| Worker | Wage [€/h] | Source |
|--------------------------------|------------|----------------------------|
| Truck Driver | 14.8 | (Nationale Beroepen, 2022) |
| Boat Driver | 21.5 | (ERI, 2022) |
| Crane Driver | 23.5 | (ERI, 2022) |
| Constructor (onstruction crew) | 21.7 | (ERI, 2022) |
| Cleaner (pressure washer) | 12.2 | (QPS, 2022) |
| Steel maintenance worker | 20.1 | (ERI, 2022) |

TABLE 21: Wages for workers 3D printed bridge

case. Mainly, the rental input parameters for the concrete bridge can be seen in Table 22, and for the 3D printed bridge in Table 23.

| Component | Time [h] | Price [€/hour] | Source |
|---------------------------------|----------|----------------|--------------|
| Crane rental construction-phase | 6 | 146 | (Saan, 2022) |
| Crane rental end-of -life phase | 6 | 146 | (Saan, 2022) |

TABLE 22: Rental costs for Concrete bridge

| Component | Time [h] | Price [€/hour] | Source |
|---------------------------------|----------|----------------|--------------|
| Crane rental construction-phase | 5 | 146 | (Saan, 2022) |
| Crane rental end-of -life phase | 7 | 146 | (Saan, 2022) |

TABLE 23: Rental costs for 3D printed bridge

According to the life cycle described in Chapter 1, the end-of-life phase implies the disposal or recycling of the material after demolishing the structural components. Thus, to determine the cost of the demolition and disposal of different materials, the cost per kg or cubic meter of recycling/disposal of material is required as an input parameter for the parametric tool. Thus, the disposal rates for the concrete bridge can be found in Table 24, and for the 3D printed steel bridge in Table 25.

| Component | Price [€/m ³] | Source |
|-------------------|---------------------------|---------------------|
| Concrete Disposal | 35 | (Hu and Maio, n.d.) |
| Steel Recycling | -6800 | (NSC, 2020) |

TABLE 24: Disposal for Concrete bridge

| Component | Price [€/m ³] | Source |
|-----------------|---------------------------|-------------|
| Steel Recycling | -6800 | (NSC, 2020) |

TABLE 25: Disposal for 3D printed bridge

Last, the discount rate is another input variable that is required for providing the cost calculation. Thus, the input discount rate for both bridge alternatives equals 2.5% (Jawad and Ozbay, 2005).

5.3 Output parameters

Following the formulae described in Chapter 4 and the primary input and intermediate input variables required for the parametric tool, the final output values can be determined. Thus, the LCC tool generates two core tables used to determine the final cost of the bridge. The able shows the total cost incurred per activity during the life cycle. Besides, given a certain amount of repetitions, the cost of one activity

iteration and the time between iterations is determined. The describing the mentioned above parameters for traditionally constructed concrete bridges and the 3D printed bridge can be found in Appendix C.15 and C.16. The net and final Table represent the distribution of the activity costs over the entire lifetime of the design alternative and calibrates the incurred yearly costs with respect to the discount rate. The entire Tables with the costs scheduled and distributed over the life cycle of the bridge can be found in the attached *Excel File*. An example of the above output can be seen in Table 26 for the traditionally constructed concrete bride and the 3D printed steel bridge Table 27.

| | | | | | | | |
|--------------|---------------------------------------|----------------|-----------------|---------------|--------------|---------------|-------------|
| | Component/Activity | 2022 | 2023 | 2024 | 2025 | 2026 | 2027 |
| Production | Beams reinforced | 125.25 | 125.25 | | | | |
| | Plates reinforced | 70.63 | 70.63 | | | | |
| | ... | ... | ... | | | | |
| Construction | Crane driven from the origin and back | | 14.68 | | | | |
| | Crane operated | | 122.4 | | | | |
| | Machinery 1 | | 2.31 | | | | |
| | ... | | ... | | | | |
| Use | Cleaning machinery | | 0.67 | 0.67 | 0.67 | 0.67 | ... |
| | Cleaning Material | | 0.01 | 0.01 | 0.01 | 0.01 | ... |
| | Repair Mortar Material | | | | | | ... |
| | ... | | ... | ... | ... | ... | ... |
| End-of-life | Construction crew | | | | | | |
| | Concrete Disposal | | | | | | |
| | Steel Recycling | | | | | | |
| | ... | | | | | | |
| Calculations | Year | 2022 | 2023 | 2024 | 2025 | 2026 | 2027 |
| | Construction | 4376.02 | 11101.52 | | | | |
| | Use phase | | 31.64 | 112.66 | 31.65 | 112.66 | ... |
| | End of life | | | | | | |
| | Total Costs in € | 4376.02 | 11133.17 | 112.66 | 31.64 | 112.66 | ... |
| | Year | 2022 | 2023 | 2024 | 2025 | 2026 | 2027 |
| | Construction | 4376.02 | 11379.06 | | | | |
| | Use phase | | 32.44 | 118.36 | 34.08 | 124.36 | ... |
| | End of life | | | | | | ... |
| | Discount Rate in € | 4376.02 | 11411.50 | 118.36 | 34.08 | 124.36 | ... |

TABLE 26: Cost Schedule for Concrete bridge activities

The cost schedule table is further used to determine the total costs of the functional unit incurred throughout the entire life cycle. The discount rate is applied to the yearly costs in the bottom row. The effect of the discount rate can be seen by comparing the initial costs with the cost after the discount rate application. In this way, the parametric tool retains all variables to calculate the final cost for both design alternatives. Besides, the years with the most significant economic impact can be determined. These are expected to be those years when multiple activities cost iteration overlap. The impact of the discount rate increases with respect to the number of years since the beginning of the life cycle. This inherently shows that the discount rate's impact is distributed exponentially. A detailed explanation of the discount rate follows in Chapter 6.

| | Component/Activity | 2022 | 2023 | 2024 | 2025 | 2026 | 2027 |
|--------------|--|----------------|-----------------|--------------|---------------|---------------|-------------|
| Production | Bridge production phase | 1788.93 | 1788.93 | | | | |
| | Stainless steel grade 304L | 7020 | 7020 | | | | |
| | ... | ... | ... | | | | |
| Construction | Boat driven from the MX3D to the bridge and back | | 71.4 | | | | |
| | Crane driven from the origin and back | | 14.69 | | | | |
| | Crane operated | | 97.92 | | | | |
| | ... | | ... | | | | |
| Use | Bridge flushing with (air blast) | | 12.2 | 12.2 | 12.2 | 12.2 | ... |
| | Painting isolated areas | | | | 80.4 | | ... |
| | Removal salt residue | | 0.01 | 0.01 | 0.01 | 0.01 | ... |
| | ... | | ... | ... | ... | ... | ... |
| End-of-life | Crane driven from the origin and back | | | | | | |
| | Crane operated during | | | | | | |
| | Machinery 1 | | | | | | |
| | ... | | | | | | |
| Calculations | Year | 2022 | 2023 | 2024 | 2025 | 2026 | 2027 |
| | Construction | 8808.93 | 15464.52 | | | | |
| | Use phase | | 44.07 | 44.07 | 221.82 | 145.34 | ... |
| | End of life | | | | | | |
| | Total Costs in € | 8808.93 | 15508.58 | 44.07 | 221.82 | 145.34 | ... |
| | Year | 2022 | 2023 | 2024 | 2025 | 2026 | 2027 |
| | Construction | 8808.93 | 15851.13 | | | | |
| | Use phase | | 45.17 | 46.30 | 238.87 | 160.43 | ... |
| | End of life | | | | | | ... |
| | Discount Rate in € | 8808.93 | 15896.30 | 46.30 | 238.87 | 160.42 | ... |

TABLE 27: Cost Schedule for 3D printed bridge activities

5.4 Concluding remarks

The parametric LCC parametric tool described in this Chapter aims to quickly and easily assess the life cycle costs of two bridge alternatives, mainly the traditionally built concrete bridge and the 3D printed steel bridge. The overall costs calculation tool results in multiple economic performance indicators that further can be used to evaluate the bridge alternatives concerning specific requirements. The economic performance indicators are systematically described in the Chapter 6 by comparing two design and construction alternatives and representing their economic impact throughout the life cycle.

6 LCC results of the case study

In this Chapter, the results of the case study are discussed. The Chapter starts with an overview of the resulting output for the traditional constructed concrete bridge and 3D printed steel bridge. Next, in Paragraph 6.2 the cost are analyzed with respect to the activity costs schedule and their distribution over the life cycle time, given the impact of the discount factor. Here the overall costs per different life cycle phases are compared. Consequently, in Paragraph 6.3 the sensitivity analysis is applied to determine the most sensitive parameters of the parametric tool. Lastly, the concluding remarks regarding the overall results of the LCC tool are discussed in Paragraph 6.5.

6.1 Total LCC of bridge design alternatives

Considering the output parameters explained in Chapter 5, the total life cycle cost for each bridge alternative are determined. To ease the comprehension of the results for the reader, a primary research project assumption must be explained. Mainly, the parametric tool outlines the cost differences between two bridge design alternatives. This implies that the costs of similar processes applied for both construction procedures are disregarded. For example, the examinations and controls of the bridge structural elements and energy consumed by the lighting, sensors, and surveillance devices might be identical or different. In other words, the parameters mentioned above vary per bridge depending on the infrastructure owner's request and therefore are irrelevant for outlining the most cost-optimized alternative.

To outline the parametric tool possibilities and get an idea of the general economic competitiveness of the different bridge alternatives, the total costs of the two construction methods have been determined over a life cycle of 100 years. After the calculation of the total costs of each bridge alternative, the distribution of the costs per life cycle phase is investigated. The results are represented in Figure 17.

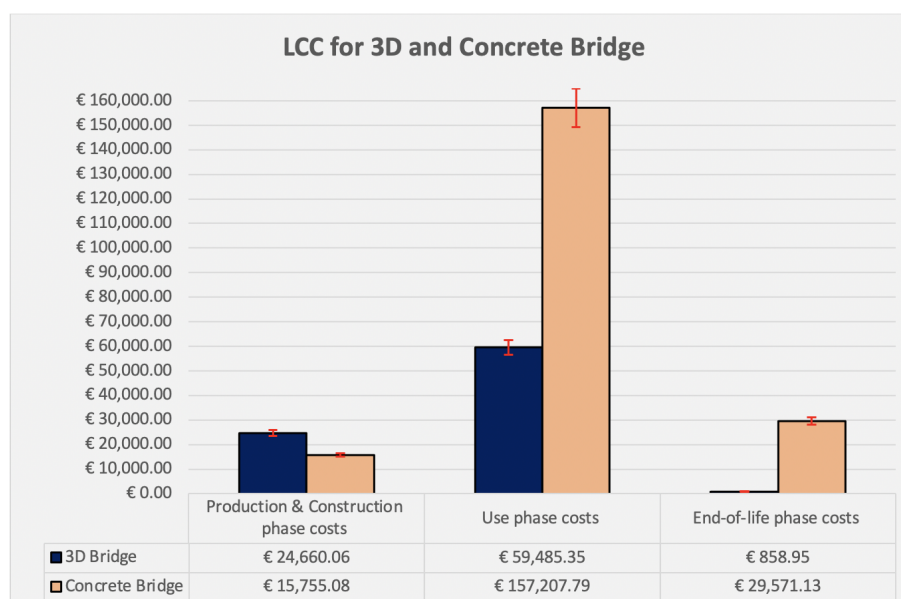


FIGURE 17: LCC per phase for 3D printed and concrete bridges for 100 years service life

A few aspects can be seen while considering the results above, which are predicated on the idea that the input variables are constant and genuinely reflect reality.

The first thing that can be noticed is that the concrete bridge has a higher total cost LCC. Namely, the total cost of the traditionally built concrete bridge equals €202500. In contrast, the 3D printed steel bridge incurred a total life cycle cost equal to €85000. The initial research project expected the steel bridge to retain a higher price. Nevertheless, due to a long life cycle period, the costs during the use phase for the concrete bridge severely influence the total costs, see Figure 17. The costs of the

concrete bridge during the use phase an almost three times higher than those incurred by the 3D printed steel bridge. This difference occurs due to the bridge's main material component. According to (Dr. Homayoun Abrishami, 2017), steel requires fewer maintenance procedures compared to concrete, which inherently generates a significant economic impact concerning all concrete elements.

Another subject of attention is the costs incurred during the end-of-life phase. Similar to the use phase, during the last phase of the bridge life cycle, the costs of the traditionally built concrete bridge heavily override those of the 3D printed bridge. This phase cost difference is induced by one of the calculation tool features. According to the calculation of the costs for the end-of-life phase, the bridge's structural components are demolished and recycled or reused. The 3D-printed bridge is made of steel, which recycling is materially compensated (Bowyer, 2015).

In this way, the income generated from the steel recycling compensates the cost generated by the transportation of the bridge to the recycling site, the personnel salaries and the energy consumption.

In contrast, following the (Maio et al., 2017) after the demolition of the concrete bridge, the concrete particles are considered to be reused for instance for other purposes such as filling the roads. Besides, the traditionally built concrete bridge retains steel elements, which are recycled and paid back to the infrastructure owners. Nevertheless, due to the relatively small amount of steel in the structure and reusing rates, the costs of the transportation and demolition work remain dominant components of the end-of-life phase.

The LCC results are subject to potential variation. Thus the error bars aim to indicate the expected range of the final costs per different life cycle phases concerning the uncertainty input variables described in the Paragraph 6.3. As a result of the probabilistic calculations, there is a 90% chance that the LCC result is bounded between two values, see the error bars in Figure 17. A detailed visualization per each phase for both bridge design alternatives of the error bars can be found in Appendix C.1, C.2, and C.3.

Finally, the third observation concerns the construction and production phases. These have been unified for a more convenient visual representation. As shown in Figure 17, during the initial two phases of the life cycle, the 3D printed steel bridge incurred more considerable economic impact than the concrete bridge. The reason for this difference would lay in the product price of different materials. The steel price is significantly higher than concrete, implying that the steel bridge production would require a higher financial contribution (Douma Staal, 2022). Thus, the traditional concrete bridge is roughly by 40% more costly than the 3D printed steel bridge.

Considering the above observation, both design alternatives show different cost results per different life cycle phase. These performance indicators might be essential for applying a specific construction procedure.

6.2 Economic cost category distribution

The final LCC values are determined per each of the construction alternatives. Nevertheless, a secondary objective of the parametric tool is to determine the cost categories with the highest economic impact on the LCC. In this way, the infrastructure owners can adjust the parameters which are part of the most cost-affecting category and, as a result, decrease the total costs per alternative.

In order to determine the most impacting activities that influence the total life cycle costs, a systematic activity distribution must be applied. Thus, five-component categories have been defined: Construction/Disposal, Transportation, Electricity, Labour/Rent, and Material. The detailed activity distribution per different economic impact categories can be found in Appendix C.15 and C.16. Following the Figure 18 representing the economic impact per different activity categories, several observations can be produced.

Firstly, the two categories with the highest financial magnitude present Labour/Rent and Material. Due to the frequent maintenance works and materials required for repairing the structural unit, the above categories would register the highest costs. The incurred costs for the material category for 3D printed

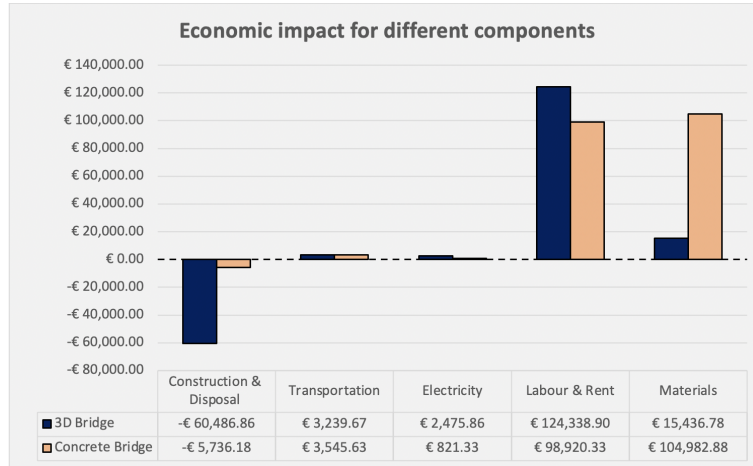


FIGURE 18: Economic Impact for different bridge component

steel bridges validate this relation, mainly due to infrequent maintenance works for steel bridges, fewer materials are required, which results in lower costs.

Another thing that can be noticed from the results is that the Construction/Disposal cost category results in negative values, which implies that the activities of this category generate income instead of costs. This unusual effect is caused by several factors, mainly the disposal rates and the discount factor. The costs incurred in the first years of the bridge life cycle (mainly the costs of construction and production) are not subject to the severe impact of the discount rate (explained in Paragraph 6.3). In contrast, the activities that take place in the last years of the life cycle retain a big difference between initial costs and costs after applying the discount rate. Due to the income generated by recycling materials after the bridge demolition (in the last years of the life cycle), the construction phase costs are counterbalanced, resulting in negative cost value.

Last but not least, the Transportation and Electricity costs category has an insignificant impact on the final LCC.

Combining the above observations, to improve the economic performance of the analyzed bridge alternative, infrastructure owners would directly visualize the cost category target, which requires adjustments to decrease the financial effect. In this way, the process of economic decisions and application of the particular construction method would become more reliable and objective.

6.3 Sensitivity analysis

This section assesses the influence of uncertainty of the input parameters. Therefore it is decided to select the most influential input parameters by sensitivity analysis and then recalculate the results with the new values. In other words, each uncertain variable is given a percentage or amount of deviation from its mean value. Consequently, two new life cycle cost results are determined using the variable's highest and lowest numerical boundary. This way, it is possible to determine whether the uncertainty of certain input variables influences the output significantly.

The following variables have been incorporated into the sensitivity analysis. Their deviation percent from the mean value and minimal-maximum resulting values can be found in Appendix C.4 and C.5.

6.3.1 Activity duration

The construction works, cleaning, and repairing of the bridge require different amounts of time depending on the bridge's material. The natures of activities significantly vary concerning the bridge design alternatives. Given this, multiple agencies offering the required services were investigated to determine

potential deviation from the activity duration mean value. Furthermore, collaborating with the Infra Plan experts and consulting resulted in assigning a 10% up and down variation to assess the model's sensitivity to this parameter.

6.3.2 Activity distance to travel

Another uncertain variable is the extra travel distance due to detours and unknown transportation means. Since the origin and destination points are subject to variation, the traveling variable is adjusted accordingly. According to (Bosman, 2015), a considerable uncertainty makes a significant variation appropriate, therefore, a variation of -40% to +40% is used.

6.3.3 Activity unit price

Based on the various activity price values reported in the literature, the uncertainty of these numbers is estimated to be roughly 10% up and down. This is the distribution used in the sensitivity analysis for all activity unit prices.

6.3.4 Number of personnel

Similar to activity duration, the number of hired personnel significantly alters for different construction alternatives. Thus, in line with the literature research as well as discussions with the experts from Infra Plan Consulting, the deviation from the mean value of workers per activity type was established. The lowest and the highest boundaries per variable can be found in Appendix 59 and 60.

6.3.5 Activity frequency

The activity frequency variable is directly related to the use phase, mainly because activities from other phases occur only once in a lifetime of the bridge and can not be altered. Following the literature research, namely (Weyers and Strategic Highway Research Program (U.S.), 1993) for concrete and (Hoyle Tanner, 2017) for the 3D printed steel bridge, the deviations from the mean values concerning the frequency of the events is determined. Consequently, both values (minimum and maximum) have been entered into the sensitivity analysis to examine the influence of the variation of replacement frequencies.

6.3.6 Geometric characteristics

Different geometrical characteristics vary per design alternative. Following the Appendix B, the traditionally concrete bridge operates two variables subject to uncertainty. According to the calculations provided in the Appendix B, any iteration of these variables influences the geometric parameters, thus, complying with structural norms defined by (NEN, 2022), the deviation from the mean values is defined. In contrast, the geometric characteristics of the 3D printed steel bridge were based on the different literature sources. Thus after analyzing multiple sources, the percentage variation of the input values has been adjusted.

6.3.7 Cost of disposal

The disposal cost depends on the material. The adjusted recycling cost for steel is based on national averages. Therefore, according to (NSC, 2020), a variation of -20% to +20% is used.

6.3.8 Discount factor

As was already mentioned, the discount rate affects how future cash flows would affect the overall LCC. This factor has an impact on the ultimate LCC result. According to (Jawad and Ozbay, 2005), the effect of a 1% change in the discount rate is investigated. The discount factor used in previous calculations was 2.5% based on the recommended value by the (Jaap de Wit, 2012). As a result, a minimum discount factor of 1.5% and a maximum of 3.5% were considered.

6.3.9 The volume of structural components

The volume of structural components for the base case is related only to the concrete bridge. The available literature defines these parameters for the 3D printed steel bridge, which makes it irrelevant to investigate the uncertainty for these variables concerning the steel bridge. In contrast, the concrete bridge potentially has multiple ways of reducing or increasing the volume of its structural components. Following the expert in structural mechanics, Ing. Gherit Snellink, the uncertainty of these values has been defined see Appendix B.

6.3.10 Technical properties of 3D printing

The deviation from the mean values of the steel welding techniques has been set with (Gardner et al., 2020). The percentage of deviation for voltage and deposition rates has been manually calculated and applied in the parametric tool.

6.4 Sensitivity analysis results

The sensitivity analysis is applied for both bridge design alternatives, traditionally built concrete and 3D printed steel bridges. The sensitivity analysis results are presented as a tornado graph in Figures 19 and 20. From most to least influential, variables are listed with their respective influence ranges on the LCC shown next to them. Additionally, the impact is caused by the upper boundary of uncertain variables with the reddish color and the lower boundary of uncertain variables with the green color.

The sensitivity analysis results show that a variation in the discount factor has the most significant influence on the total LCC for both bridge design alternatives. Nevertheless, any similar alterations (for both construction alternatives) in the discount rate do not make enough difference to change the preferred design alternative. Secondly, after the discount factor, similarly, for both alternatives, the number of workers severely affects the total costs incurred during the life cycle of bridges. The individual impact of a variation of the discount factor is described in Paragraph 6.5.

Another observation brought by the parametric tool, the output is that other uncertain variables have a relatively small impact on the total LCC. However, these variables can not be disregarded since their low impact on the economic perspective can be offset by the environmental impact. For instance, the LCA midpoint indicators are strongly related to the geometric parameters, however, these bridge parameters have a relatively low financial effect.

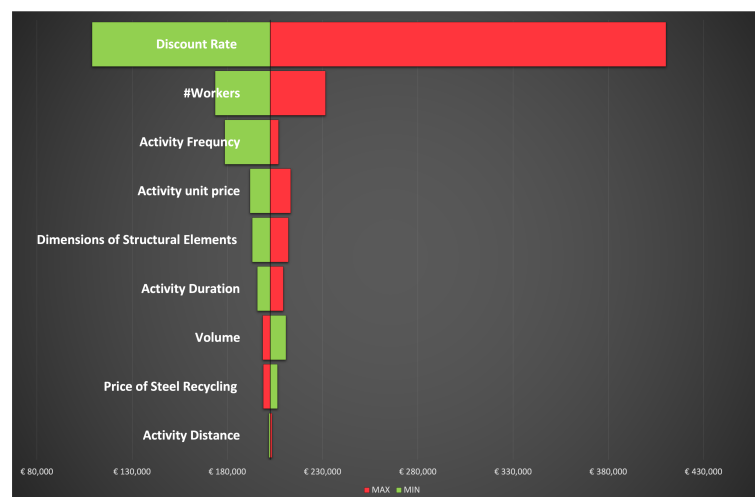


FIGURE 19: Sensitivity Tornado, Concrete bridge

A third observation is that some of the variables have a reversed effect. Notice that the variables' values increase is expressed in red. This implies that the increase in variable values is generally represented on

the right side of the figure in the direction of cost growth. Nevertheless, for example, the price of steel recycling for the 3D printed steel bridge has a reversed effect. If the price of steel recycling increases, the overall costs will decrease. This happens due to the income made on material recycling mentioned in the previous sections.

Proper visualization of the differences between the costs occurring with the mean and minimal-maximum values of the base cases can be seen in Appendix C.7 and C.8.

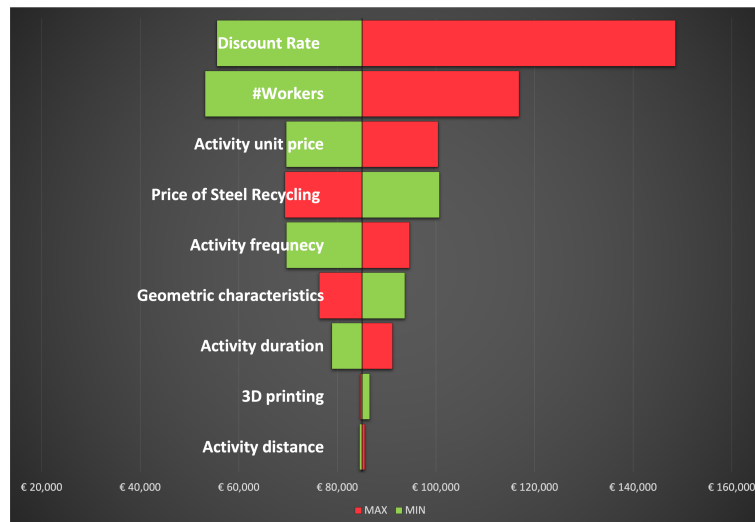


FIGURE 20: Sensitivity Tornado, 3D printed bridge

6.5 Life cycle costs representation

The discount rate and the number of workers impact the total LCC for both alternatives. The final output of the parametric tool can be seen in the Figure 21 for the traditionally concrete bridge and the Figure 22 for the 3D-printed steel bridge. The results are displayed over 100 years, and the life cycle phases of the bridge are marked with different colors. The potential impact of the lowest and highest boundary of all uncertain variables with the discount rate application is represented with a dotted line. The effect of discounting the future cash flows of the construction alternative becomes clear from the fact that the cost peak is achieved when the time approaches the end of the life cycle. For a more in-depth perception of the discount rate impact and its contribution, the reader is recommended to visualize the Appendix C.12 and C.13, where the total life cycle costs without the discount rate application are represented.

As seen in Figure 21, the use phase and the end-of-life phase costs form the most significant part of the costs incurred throughout the life cycle. Mainly, the highest peak is reached during the end-of-life phase. This takes place partially due to the discount rate. Following the dotted line representing the maximum discount rate, it can be seen that the peaks increase in parallel with the bridge's age reaching €83000 in the last year of the bridge's life cycle (see Appendix C.17). This directly implies that a potential reduction of the life cycle costs for the concrete bridge could be achieved by adjusting costs reduction on the processes that occur in the later stages of the life cycle.

Figure 22 illustrates the life cycle costs distribution for the 3D printed steel bridge. This figure retains the same technical features as the one for the concrete bridge. The main difference occurs due to the application of alternative construction procedures. In contrast, the costs reached during the construction and production phase for the steel bridge represent the most substantial economic impact. Additionally, the costs incurred throughout the use phase operate at a higher frequency but have a lower financial impact. This effect explains that the steel material does not require heavy repairing work that would result in high costs.

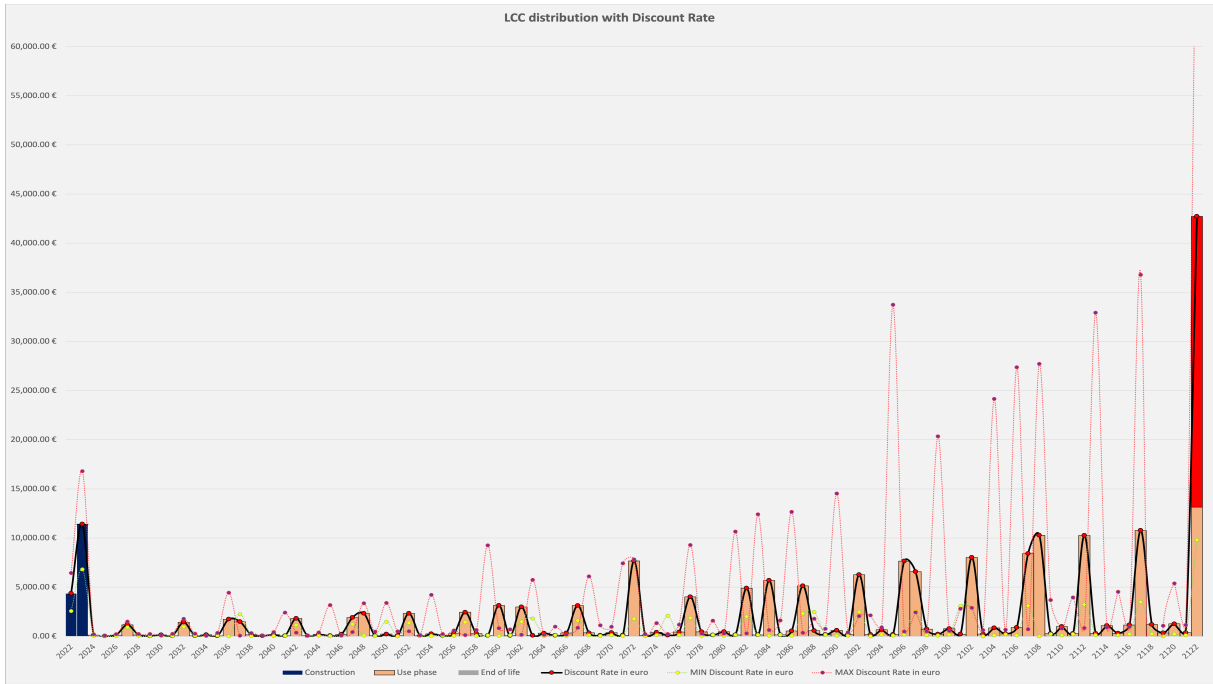


FIGURE 21: Histogram Life Cycle Cost distribution, Concrete bridge

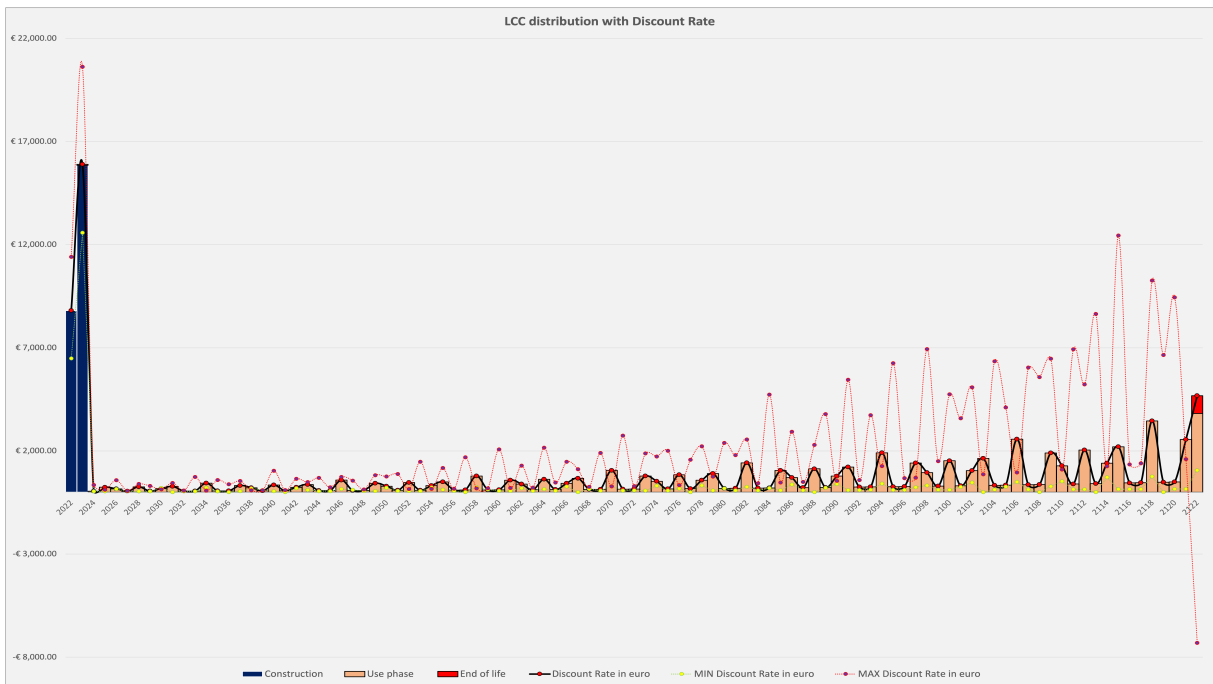


FIGURE 22: Histogram Life Cycle Cost distribution, 3D printed bridge

Another interesting observation can be deduced from the dotted line representing the maximum costs concerning the upper boundaries of all uncertain variables. Following the red dotted line, it can be observed that, similar to the concrete bridge LCC behavior, the peaks are increasing while approaching the end-of-life phase. Nevertheless, the 3D printed bridge costs can be significantly compensated during the last year of the life cycle. Given the potential uncertainty of the recycling price for the steel, and the

impact caused by the discount factor, costs can be partially compensated during the end-of-life of the 3D-printed steel bridge. Obviously, this is hardly likely to occur. However, the infrastructure owners must encounter this possibility of achieving an economic benefit from bridge disposal. Proper visualization of the differences between the costs occurring with the mean and minimal-maximum values of the base cases can be seen in Appendix C.

7 Development of the LCA tool

Conform to (BSi, 2006), a Life Cycle Assessment includes goal and scope definition, life-cycle inventory, life-cycle impact analysis, and interpretation of the results. Therefore, this Chapter discusses the goal of the LCA tool and its inventory. In Chapter 8, an analysis of the environmental impact of the case study is discussed, followed by the interpretation of the results.

7.1 Goal

This Chapter aims to develop the environmental calculation component of the parametric tool. The main focus of the environmental assessment is the performance of the environmental parameters comparison of two design alternatives, which would facilitate infrastructure owners making a balanced selection of structural alternatives. Given the scope of the research, the lifetime of the analyzed functional units is considered equal to 100 years which has been ensured via structural assessment discussed in Chapter 3 and Appendix B. Thus, the LCA aims to evaluate the environmental impact based on different input parameters set in line with predefined requirements.

7.2 Life cycle assessment

The environmental assessment of both bridge design alternatives is conducted using the *GaBi* software. The functional unit of the LCA is considered the bridge, hence altering the functional unit to a kilogram of material is also an option. The design alternative aims to design a bridge that spans the Ouderzijds Achterburgerwal, ensuring infrastructure components with a lifetime of 100 years. The environmental impacts caused by material manufacturing, construction of the bridge, transportation, maintenance, and disposal are analyzed in different manners, namely based on different life cycle phases, either on midpoint indicators (M.A.J. Huijbregts and Z.J.N. Steinmann, 2016).

7.3 Life span

The life span of the different bridges varies. The material and external factors, such as weather, location, span distance, and size, influence a bridge's life span. Given the geometrical characteristics of the functional research unit described in Chapter 3 the bridge's life span, alternatives can be set. Nevertheless, to develop the reader's more profound understanding of the lifetime parameter of the bridge, literature research is applied. According to (Kim and Tae, 2020), with a reliable structural design and under regular maintenance works the traditionally designed concrete bridge can easily have a lifetime of 100 years. In contrast, conform (Kourepinis V., 2016), properly structurally designed bridges made of steel can achieve a lifespan of slightly more than 100 years. Therefore, following the research goal, the lifespan of 100 years is selected for the analyses of the environmental impacts generated by each investigated design alternative.

7.4 System Boundaries

The system boundary definition is needed to clarify which processes are included in the LCA. Thus the Figure 9 corresponding to the system boundary of the research from the Chapter 1 in Paragraph 7.4 is operated.

7.5 Assumptions

Several simplifications have been made to retain an objective comparison and ease the calculation procedures embedded in the LCA investigation. Given that the 3D-printed steel bridge operates multiple apparatuses, namely sensors, cameras, lighting systems, and data systems (MX3D, 2020), the number of devices installed on the bridge directly depends on the infrastructure owner's requirements. For example, modeling two bridges with similar devices with similar characteristics most likely does not influence the LCA outcome. Therefore, the devices present on both bridges will be disregarded. This simplification implies that the production, construction, use, and end-of-life phases of electronic devices operated by the bridge are not within the scope of the system

7.6 Set up LCA Model

The system has clearly been defined. The *GaBi* model can be made. As explained before, the life cycle is analyzed concerning the following phases: construction (construction + production), use, and end-of-life phases. The following sections elaborate on how each phase mentioned above's environmental impact was modeled in the *GaBi* software. The information about the data is developed in the next Chapter 8.

7.7 Phases:

7.7.1 Production and Construction phase

The calculation of the LCA environmental impact starts with the production and construction phase. A critical adjustment for further modeling concerning bridge construction procedures alternatives is made. 3D bridge printing is a relatively new and complex process. Thus modeling a 3D printing procedure with the *GaBi* software would decrease the reliability of the result due to the potential errors and misinterpretations of the technical implications. Therefore, only the concrete bridge production and construction phase is modeled with *GaBi* software. The model data for the 3D printed bridge is substituted by the research based on the production process of the WAAM (see Figure 23), namely (National Institute for Public Health and the Environment, 2018).



FIGURE 23: Production process, 3D printed bridge, (Bekker and Verlinden, 2018)

As can be seen, the Figure 23 contains all data concerning raw material, material transportation, and manufacturing of concrete. The concrete bridge consists of two structural materials, namely concrete and steel. The concrete structural elements of the bridge are prefabricated with the use of electricity and then transported using a truck and a mobile crane to the construction site. Similarly, the steel elements are prefabricated and then transported to the construction site.

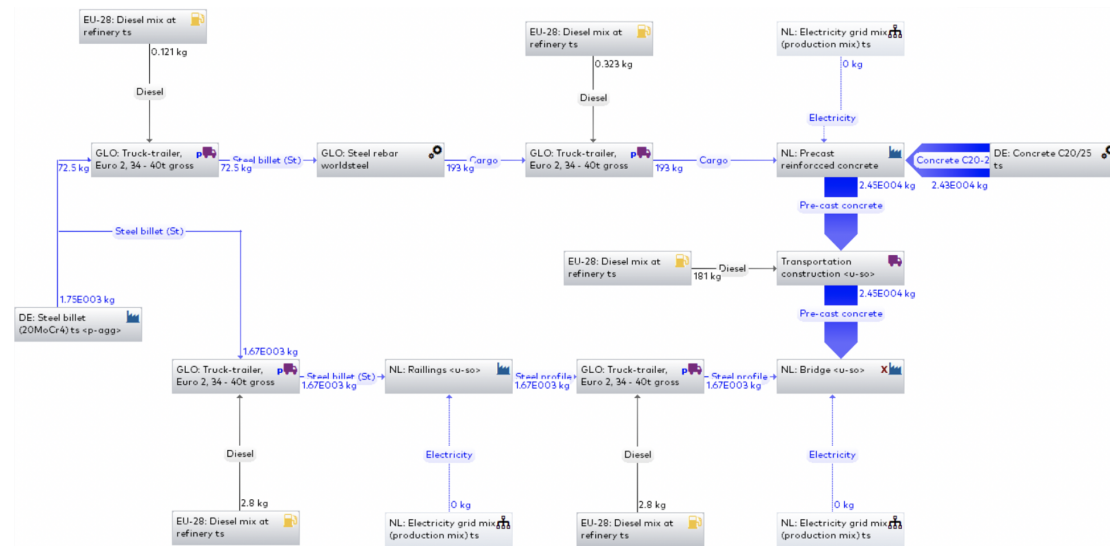


FIGURE 24: Production process, Concrete bridge

The structural elements made of concrete are the beams and deck (floor plates). These consist of premixed concrete and reinforced steel bars. Both components are manufactured separately, assembled, and then

delivered to the bridge's location. Since railings consist only of steel, their fabrication is instantly followed by direct transportation to the construction site. Therefore, the transportation means and machinery consuming electricity or fuel are directly embedded into the production and construction phase process (see Figure 24).

7.7.2 Use phase

The next phase modeled for the LCA calculation is the use phase. Considering that the electronic devices in the bridge are outside the system boundary, modeling the use phase contribution to the environmental impact is relatively simplified. As a result, the use phase electricity consumption for the maintenance works is modeled for both bridge design alternatives. The model for the use phase of the concrete bridge is indicated in the Figure 25 for the 3D printed steel bridge in the Figure 26. Notice that the use phase for both alternatives is almost similar, implying that the parametric system is well-systematized and could be easily adjusted for an alternative bridge.

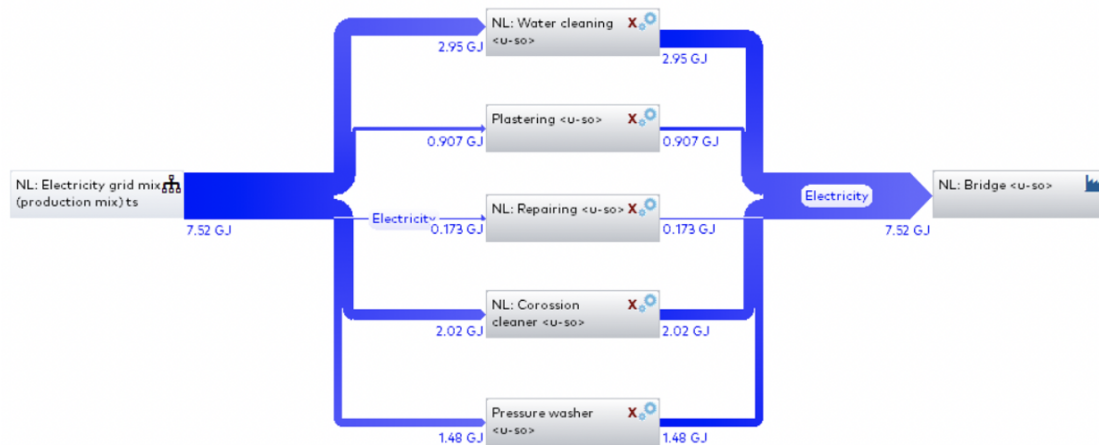


FIGURE 25: Use phase, Concrete bridge

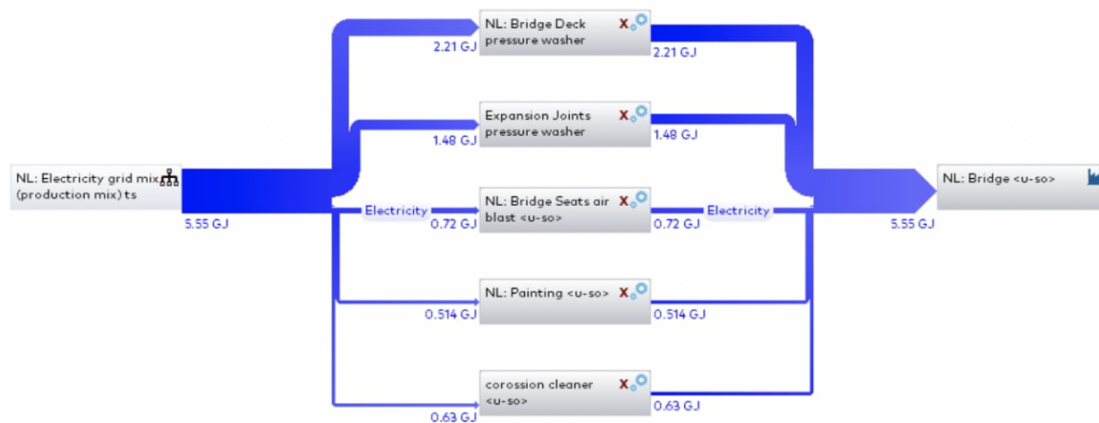


FIGURE 26: Use phase, 3D printed bridge

7.7.3 End-of-life phase

The disposal process encloses the final phase of the life cycle. During the end-of-life phase, the bridge is disassembled and transported to the disposal point by the track. The structural elements made of

concrete are reused or land filled. According to (A. Jansen, 2018), the LCA calculation directs 5% to the landfilling. The rest of the concrete is reused in different industries, such as road filling. 95% of the steel elements are subject to recycling (Tingley and Allwood, 2014). The above mentioned model decisions can be seen for the concrete bridge in Figure 27 and the 3D printed steel bridge in Figure 28.

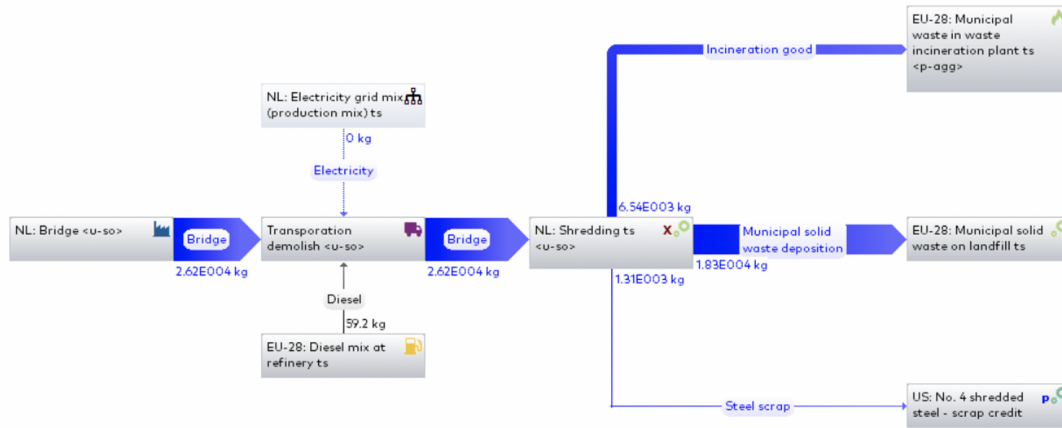


FIGURE 27: Disposal process, Concrete bridge



FIGURE 28: Disposal process, 3D printed bridge

8 Case study LCA

In Chapter 1, the research model defines the parametric calculation tool as the research objective. The base of the LCA tool has been explained in Chapter 7. Furthermore, the described *GaBi* models are used to analyze the base case concerning two bridge design alternatives: the 3D printed steel bridge and the traditionally constructed concrete bridge. According to Infra Plan Consulting, the base case has been chosen to highlight the critical distinctions between the two bridge design options. The input variables needed to determine the final environmental impact of both constructions are described in this Chapter. In light of this, the LCA model output with regard to the case study is explicated.

8.1 Input and Output of the LCA tool

All of the materials and emissions that enter the system and generate the model's output are schematized in Figure 29. Basically, there are two classifications of inputs: material and energy. The materials input category represents the matter used for the bridges' construction for the research project, these are concrete and steel. The following input category is divided into two subcategories, energy and electricity. Energy summarises the power required for essential activities throughout the life cycle, such as transportation, installation, and operation. Electricity and fuel are input variables which generalize various processes such as cleaning, assembling, and repairing.

The system's output is more complex and cannot be fully schematized. Considering that some of the used materials are partially recycled, concrete and steel serve as output variables. In contrast, a substantial amount of the products assigned to be landfilled generate waste. In other words, partially, the bridge components become useless after the end of the life cycle. Examples of these substances are CO₂ and radioactive waste. However, the complete list of the emitted substances is far longer (Bekker and Verlinden, 2018). Due to this, many effect categories are analyzed. Along with emissions and recycled materials, there will also be solid trash. For instance, concrete can no longer be used and must be disposed of immediately. Together with the other two categories, these form the system's outputs.

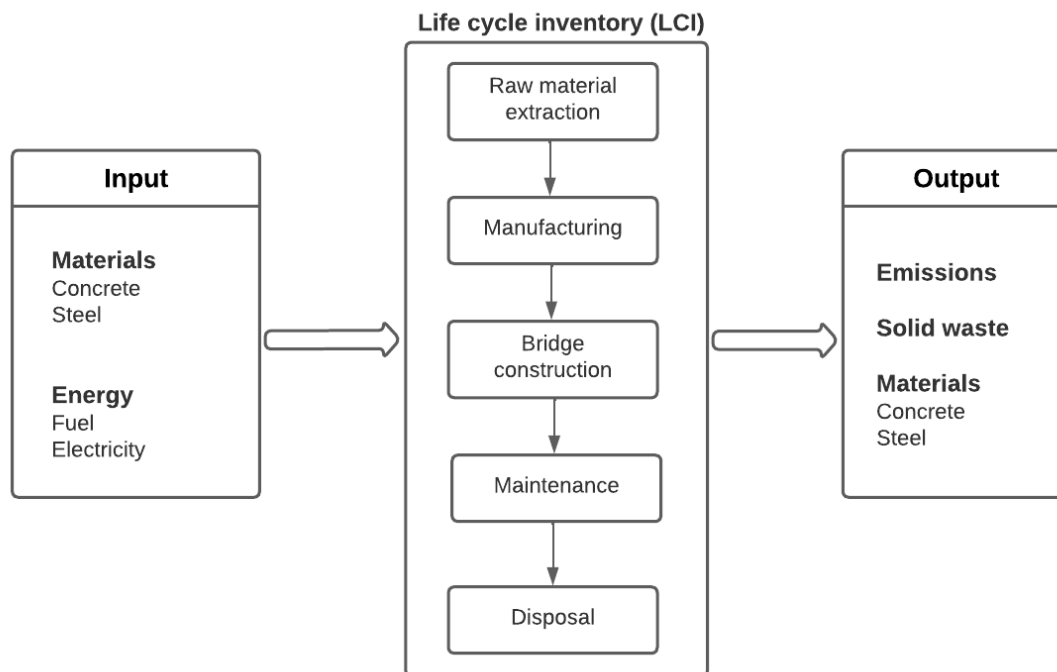


FIGURE 29: Input and Output of the calculation tool

8.2 LCA results of the case study

Since the model has been set up in *GaBi* for both design alternatives, a Life Cycle Impact Assessment can be executed. This analysis will focus on different components, namely:

- The environmental impact of the separate phases (production, use phase, end-of-life phases)
- The environmental impact of the separate midpoint indicators of the construction alternatives (climate change, ozone depletion, human toxicity, etc)

In order to determine the environmental indicators for each bridge construction procedure, the reliability of the results must be maintained. Mainly, given that the production and construction phase for the 3D printed bridge is based on the literature research, the output parameters' units differ from standard variables in *GaBi* software. Thus, all performance indicators for bridge LCA results were set similarly. This has resulted in the following results. The midpoints results with respected units and their impact per different life cycle phases for the traditionally concrete bridge is represented in Table 28, for the 3D printed steel bridge in Table 29.

| MidPoint | Unit | Production and Construction phase | Use Phase | End of Life Phase |
|---------------------------|----------------|-----------------------------------|-----------|-------------------|
| Climate Change | kg CO2 eq. | 11200 | 1200 | 19700 |
| Ozone depletion | kg CFC-11 eq. | 7.56E-11 | 8.5E-12 | 4.83E-11 |
| Terrestrial acidification | kg SO2 eq. | 10.8 | 0.709 | 5.09 |
| Human toxicity | 1.4 DB eq. | 3.09 | 0.367 | 0.778 |
| Terrestrial ecotoxicity | 1.4 DB eq. | 3610 | 179 | 4260 |
| Freshwater ecotoxicity | 1.4 DB eq. | 0.571 | 0.041 | 0.352 |
| Marine ecotoxicity | 1.4 DB eq. | 2.66 | 0.149 | 2.1 |
| Water Depletion | m ³ | 23.2 | 2.31 | 26.6 |

TABLE 28: Midpoints results for Concrete Bridge

| MidPoint | Unit | Production and Construction phase | Use Phase | End of Life Phase |
|---------------------------|----------------|-----------------------------------|-----------|-------------------|
| Climate Change | kg CO2 eq. | 82283.9624 | 246 | 93.6 |
| Ozone depletion | kg CFC-11 eq | 0.00586441 | 1.74E-12 | 2.59E-13 |
| Terrestrial acidification | kg SO2 eq | 763.385789 | 0.145 | 0.218 |
| Human toxicity | kg 1.4 DB eq. | 60484.5763 | 2.94 | 42.6 |
| Terrestrial ecotoxicity | kg 1.4 DB eq. | 22.9391227 | 36.8 | 42.4 |
| Freshwater ecotoxicity | kg 1.4 DB eq. | 1726.40105 | 0.0084 | 0.0822 |
| Marine ecotoxicity | kg 1.4 DB eq. | 1874.92115 | 0.0305 | 0.25 |
| Water Depletion | m ³ | -6672.1441 | 0.473 | 0.449 |

TABLE 29: Midpoints results for 3D printed Bridge

The impact of climate change measured in a kilogram of CO2 equivalent has been distributed per life cycle phase. Looking closely at the above tables, the most significant environmental impacts occur during the production and construction phase. In this way, the other two life cycle phases become negligible to the overall sustainability performance of both design alternatives. Another critical observation significantly outlines the preferable design alternative from the environmental perspective. For example, the midpoints results for the 3D printed steel bridge production and construction phase significantly outrun those of the traditionally constructed bridge. Given that, diving deeper into the comparison result, the most significant midpoint indicator was taken for comparing the bridge alternatives, as shown in Figure 31.

The 3D-printed steel bridge generates the majority of the midpoint environmental indicators with a significant impact. Nevertheless, an interesting observation is that for the Territorial ecotoxicity. According

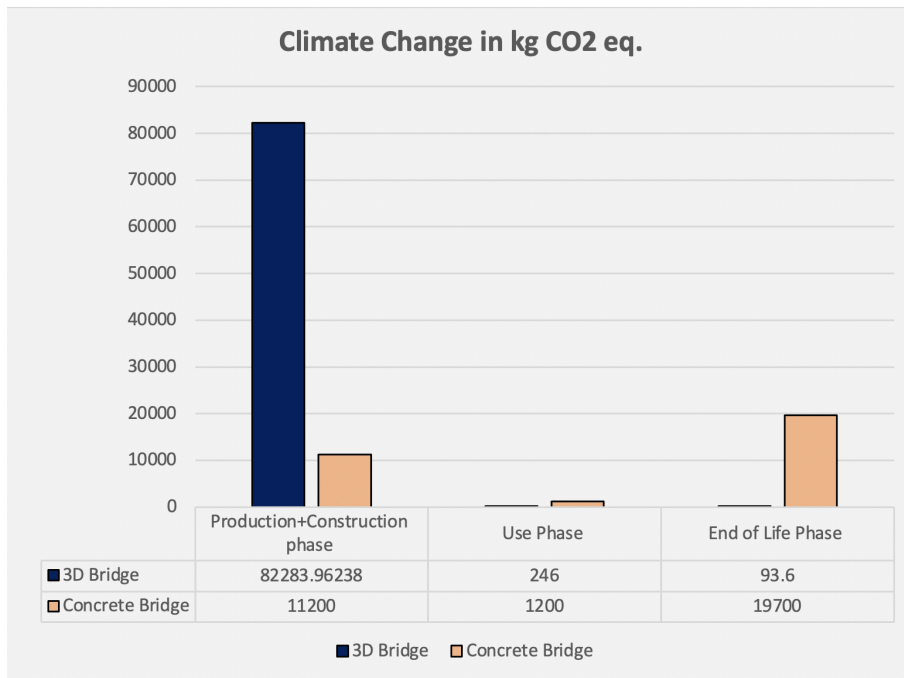


FIGURE 30: Climate change impact

to the Figure 31, the ecological parameters of the traditionally constructed concrete bridge severely overcome those of the 3D printed bridge. This intriguing result is discussed in the research concluding Chapter 9. The rest parameters can be compared in the attached *Excel File*.

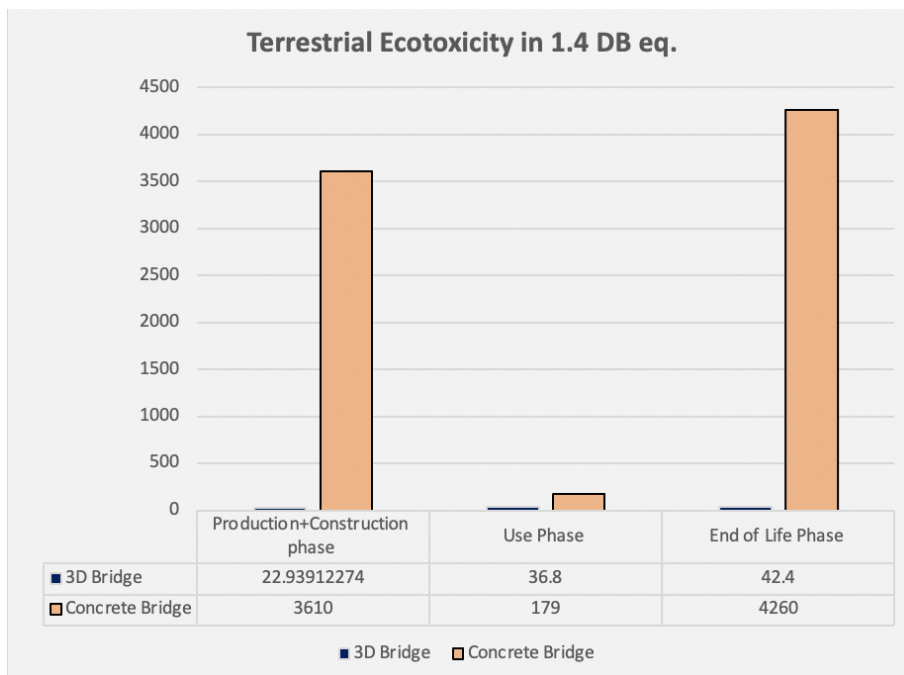


FIGURE 31: Territorial ecotoxicity impact

9 Discussion and Conclusion

9.1 Discussion - The usefulness of the parametric tool

Parametric tools that calculate overall life cycle perspectives of infrastructure components are now emerging in projects of high significance and size.

The research aimed to explore favored construction alternatives concerning structural properties, sustainability factors, and economic impact to make a list of recommendations for improving the certainty of industrial decisions and adapting it for use in the construction industry.

This research showed the need for more broad usage of these tools and the variety of scenarios in which they can be applied. Following the research goal, the resulting parametric tool facilitated the comparison of two construction alternatives based on their life cycle costs, environmental impact, and structural properties. Most of the input variables were determined with great certainty, which retained the objective comparison of the calculation results. Although that model's most influential input parameter was the discount rate, varying this input parameter does not influence the preferred construction alternative. Hence, the calculation tool also operates input variables which lack precision. Nevertheless, the sensitivity analysis incorporated in the calculation procedures indicated that these uncertain variables' contribution is insignificant, so the output could be considered consistent.

The following most significant variable was the number of workers engaged throughout the life cycle of the bridge. The influence of similar deviation from the mean (input) value of engaged workers throughout the life cycle was more significant for the 3D-printed steel bridge than for the concrete bridge. Even though the maintenance works for the steel bridge require less severe interventions, this difference in the impacts caused by the number of workers implies that the working on the steel bridge is more labor extensive and demands more implications. Obviously, since 3D bridge printing is cutting-edge technology, it would require more labor due to the greater extent of procedure uncertainties compared to the established procedure for traditional concrete bridge construction.

The environmental impact calculation operated the model's input parameters found from the structural analysis and the input parameters used for the LCC calculation. Based on the literature review, identified midpoint performance indicators showed that the most environmental influential phase of the bridge is its production and construction. The impact generated during this phase influences the preferred construction alternative based on midpoints indicators (climate change, marine toxicity, etc.) or the total environmental impact per phase. The LCA calculation showed that the environmental impact generated by the 3D printing construction procedure severely outruns the impact caused by the traditionally constructed concrete bridge.

Structural parameters analysis serves as the base for the parametric tool, giving the starting input parameters and bringing attention to potential drawbacks regarding the price and material properties. The mechanical calculations of both construction alternatives indicate multiple factors that must be considered when choosing the construction procedure. The relation between material price, volume, and load that needs to be bared (by structural elements) represent critical criteria potentially influencing the preferred design alternative. The cost load ratio indicates an essential parameter for the infrastructure owner's decision regarding the construction procedure. Last but not least, the core model assumption is based on similarities encountered throughout the life cycle of both construction alternatives. Elements and activities such as electronic devices, lightning, and maintenance controls vary with respect to the decisions made by the infrastructure owners. Therefore, the model calculations for environmental, structural, and economic performance indicators neglect the implication of elements and activities in both analyzed cases. If the user of the parametric tool encounters the assumptions and technical aspects influencing the final output, then the calculation tool can be successfully used for a quick and reliable estimation of the financial and environmental performance for different construction alternatives.

9.2 Conclusions

This research aimed to outline the most optimized construction alternative by developing a parametric calculation tool to calculate overall core performance indicators for two differently designed and constructed bridges. The parametric life cycle cost and assessment tool was developed that enables comparison of different bridge design alternatives based on the structural, materials, and cost inputs. During the literature review, it was considered to include structural properties (mechanical performance and material properties), life cycle costs (production, construction, use, and end-of-life costs), and environmental impact (midpoints environmental impact indicators). The MX3D steel bridge was used as a base case for an alternative traditionally constructed concrete bridge that was designed. Furthermore, the parameters of these design alternatives were entered into the calculation tool, which then estimated the corresponding outputs. Based on the results of the calculation tool, the following conclusions have been drawn.

Looking at the results, the 3D printed steel bridge and the concrete bridge have their own advantages and disadvantage concerning structural, economic, and environmental perspectives. Considering the structural perspective, the material price, volume, and bared load ratio show that a concrete bridge is preferable. This ratio for the 3D printed bridge has resulted roughly in €4000 m²/kN, while for the traditionally constructed concrete bridge, €2500 m²/kN. The result of this ratio indicates that to achieve the required mechanical properties for the pedestrian bridge with a span of 12.1 meters, the traditionally concrete constructed bridge is a preferable alternative from the economic perspective. In other words, both construction alternatives achieve similar mechanical characteristics, hence the 3D printed steel bridge would be less cost-mechanically effective than its concrete alternative.

Based on the relatively small 90% certainty ranges of the calculated LCC and the sensitivity analysis results, it can be concluded that the tool is reliable enough to support decision making during the bridge design alternatives selection. The discount factor, the number of workers, and maintenance activity frequency are seen to affect the total LCC significantly. In contrast, transportation distances, unit price, and duration comprise a small part of the total life cycle costs for both construction procedures.

Concerning the construction alternative, the mentioned above parameters behave differently. Mainly, their peak magnitude generates economic contribution in different life cycle phases. While the 3D printed bridge requires less maintenance than the concrete bridge, the number of workers implicated during the production and construction phases of the steel alternative makes up the most significant cost contribution to the total LCC. Overall, the concrete bridge is economically less efficient than the 3D printed bridge for the predicted 100 years of the life cycle. However, if the life cycle of the bridge were shortened to 50 years, the concrete bridge would outscore the 3D-printed bridge. The total costs of the concrete bridge reach €200000, which is two and a half times bigger than LCC of its alternative construction procedure. The reason for this difference is that the discount rate affects future costs. For example, due to the frequent maintenance work, the discount rate severely affects the use phase for the concrete bridge, increasing the overall costs of the bridge. Since the steel bridge can be integrally recycled, some of the costs can be returned. Therefore, the recycling returns combined with the discount rate impact (for the steel bridge) generate an evident economic beneficial effect, which outlines the economically preferred construction alternative.

Based on the results of the environmental impacts, it can be concluded that the environmental parameters of the use phase and the end-of-life phase barely influence the overall environmental impact. Their magnitude can hardly be compared to the magnitude during the initial two life cycle phases: production and construction. The environmental impact indicators of the 3D printed bridge at the production and construction phase are significantly larger than those for the concrete bridge, implying that the 3D printed bridge is environmentally less friendly than the traditionally constructed concrete bridge.

9.3 Recommendations

The model utilized in this research has some limitations, as indicated in the discussion paragraph. Therefore, it would be engaging in analyzing these limitations' effects more extensively. Probably, the

parametric model could be adjusted such that the calculation of the economic and environmental factors would achieve even higher accuracy, simultaneously retaining intuitive and straightforward usage. Another discussion point is the weighing of the different output parameters. Right now, it is assumed that all analysed categories are equally important. Although this hypothesis may be true in theory, investing decisions are probably less neutral in reality. Therefore, the best way to adjust this matter would be to equip the calculation tool with the weighting system, where the weights of each perspective could be adjusted according to the requirements of the infrastructure owner.

References

- A. Jansen. (2018). What is recycled concrete? <https://www.ajansenbv.com/wat-is-gerecycled-beton/>
- AISI. (2007). American Iron and Steel Insitute.
- Attema, T., & Kosgodagan Acharige, A. (2017). Maintenance decision model for steel bridges: a case in the Netherlands. *Structure and Infrastructure Engineering*, 13(2), 242–253. <https://doi.org/10.1080/15732479.2016.1158194>
- Bekker, A. C., & Verlinden, J. C. (2018). Life cycle assessment of wire + arc additive manufacturing compared to green sand casting and CNC milling in stainless steel. *Journal of Cleaner Production*, 177, 438–447. <https://doi.org/10.1016/j.jclepro.2017.12.148>
- Blank, S., Blank, M., & Luberas, L. (2000). Concrete Bridge Construction.
- Bosman, J. (2015). *FRP road bridges as a concrete alternative* (tech. rep.).
- Bowyer, J. (2015). *Understanding Steel Recovery and Recycling Rates and Limits to Recycling* (tech. rep.). www.dovetailinc.org
- BSi. (2006). *Environmental management-Life cycle assessment-Principles and framework* (tech. rep.).
- Charlie Morgan. (2022). Cement and Concrete Paints. <https://www.mymove.com/home-inspiration/painting/best-concrete-paint/>
- Constar. (2022). Concrete slabs - Constar Betonwaren. <https://constar.nl/betonplaten/>
- Davis, J. (1998). Density of Steel. https://amesweb.info/Materials/Density_of_Steel.aspx
- DFID. (2004). FOOTBRIDGES A Manual for Construction at Community and District Level.
- Douma Staal. (2022). Staalleverancier Douma Staal. <https://www.doumastaal.nl/>
- Dr. Homayoun Abrishami. (2017). Design of Reinforced Concrete Bridges CIV498H1 S Group Design Project.
- ERI. (2022). ERI Economic Research Institute. <https://www.erieri.com/>
- Fruehan, R. J., & Fortini, O. (2000). Theoretical Minimum Energies To Produce Steel for Selected Conditions.
- Gardner, L., Kyvelou, P., & Herbert, G. (2020). Testing and initial verification of the world’s first metal 3D printed bridge. *Journal of Constructional Steel Research*, 172. <https://doi.org/10.1016/j.jcsr.2020.106233>
- Google Maps. (2022). Google Maps. <https://www.google.nl/maps>
- Hoyle Tanner. (2017). Preventative Maintenance. www.hoyletanner.com
- Hu, M., & Maio, F. D. (n.d.). Fates of end-of-life concrete and their economic implications.
- Jaap de Wit. (2012). *Mobiliteitsbalans 2012 Kennisinstituut voor Mobiliteitsbeleid* (tech. rep.).
- Jairo Posada-Henao. (2013). *Fuel Consumption on Trucks* (tech. rep.). <https://www.researchgate.net/publication/281391746>
- Jawad, D., & Ozbay, K. (2005). THE DISCOUNT RATE IN LIFE CYCLE COST ANALYSIS OF TRANSPORTATION PROJECTS.
- Kim, H., & Tae, S. (2020). Scenarios for Life Cycle Studies of Bridge Concrete Structure Maintenance.
- Knudsen, A., & Jensen, F. M. (2007). Cost-effective Enhancement of Durability of Concrete Structures by Intelligent Use of Stainless Steel Reinforcement.
- KOBELKO. (2020). Model TK550-1E. <http://www.kobelco-cranes.com/>
- Kourepinis V. (2016). *Lifetime Enlargement of Steel Bridge Decks* (tech. rep.).
- Maio, D., Roekel, v., & der Stelt, v. (2017). *Closing the loop of EOL concrete* (tech. rep.).
- M.A.J. Huijbregts, & Z.J.N. Steinmann. (2016). *ReCiPe harmonized life cycle impact assessment method at midpoint and endpoint level* (tech. rep.). www.rivm.nl/en
- Marin, G., & Mazzanti, M. (2015). Structural Change and the Environment Unbundling the Contribution of Structural Change to Sustainable Consumption and Production.
- Matthew L. Deloney. (2020). How Are Bridges Built — How Are Bridges Constructed — Factors Associated with Building Bridges. <https://civiljungle.com/how-are-bridges-built/>
- MetalExpert. (2022). Rust-Oleum MetalExpert. <https://www.verfwebwinkel.nl/rust-oleum-metalexpert-3-in-1-antiroest-primer.html?id=253512056&quantity=1>
- MPA The Concrete Centre. (2019). *Concrete Industry Sustainability Performance*. www.sustainableconcrete.org.uk
- MX3D. (2020). MX3D Introducing advantages of 3D metal printing to new high-impact industries.

- National Institute for Public Health and the Environment. (2018). LCIA: the ReCiPe model — RIVM. <https://www.rivm.nl/en/life-cycle-assessment-lca/recipe>
- Nationale Beroepen. (2022). Vind ieder beroep! <https://www.nationaleberoepengids.nl/>
- NEN. (2022). NEN Connect. <https://connect.nen.nl/Search/Detail/3?compId=16755&collectionId=0&=colAdmin=False>
- NEN 1990 1-1+C2/NB+A1. (2020).
- NEN 1991-1-2. (2021).
- NEN 1992 1-1+C2/NB+A1. (2020).
- NSC. (2020). Barnsley - SteelConstruction. https://www.steelconstruction.info/Glass_Works,_Barnsley
- QPS. (2022). Current Studies - QPS. https://qpsvrijwilliger.nl/campagne-mv/?utm_cssource=search_ads&gclid=CjwKCAjwzeqVBhAoEiwAOrEmzWdkB2UCZitrG1FIOQ5J2LrWU7kYxO9ACugyC5_100IpaOw-RooqRoCtDsQAvD_BwE
- QUICK Silver. (2020). Boat Performance Datasheet.
- Richard E., & Paul D. (2006). Guide for Maintenance of Concrete Bridge Members.
- Rob B. Polder. (2008). Chatodic Protection of Reinforced Concrete Structures.
- Rolands Kromanis. (2021). *SUSTAINABLE CIVIL ENGINEERING-MODULE MANUAL 1 MODULE 6* (tech. rep.).
- Saan. (2022). Telescopic cranes - Crane rental. <https://saan.nl/onze-kranen/>
- Senay Boztas. (2019). Tourists to Amsterdam. <https://www.dutchnews.nl/news/2021/04/best-case-scenario-tourists-to-amsterdam-around-half-of-2019-peak-this-year/>
- Sika. (2020). Simple and Effective Long Lasting Concrete Repair. <https://gbr.sika.com/en/construction/concrete-repair/knowledge-articles/Blogs/simple-and-effective-long-lasting-concrete-repair.html>
- Snellink, G. H. (2021). *ENGINEERING RECGHNOLOG LECTURE NOTES ENGINEERING TECHNOLOGY READER STRUCTURAL MECHANICS CONCRETE* (tech. rep.).
- Sphera. (2022). GaBi Envision - Automation. <https://gabi.sphera.com/international/software/gabi-envision/automation/>
- Star Board. (2020). The bridges of Amsterdam - Starboard Boats. <https://starboardboats.nl/nl/de-bruggen-van-amsterdam/>
- STIHL. (2020a). HL 92.
- STIHL. (2020b). KGA 770.
- STIHL. (2020c). RE 140 PLUS.
- STIHL. (2020d). RE 90.0 2-24.
- STIHL. (2020e). SR 200.
- STIHL. (2020f). TS 500i.
- STIHL. (2022). BT 131.
- Tata Steel. (2022). Tata Steel in Europe. <https://www.tatasteeleurope.com/nl/home>
- TEKNOS. (2013). Handbook for Corrosion Protection of Steel Surfaces by Painting.
- Tingley, D. D., & Allwood, J. (2014). *Reuse of structural steel: the opportunities and challenges* (tech. rep.). <https://www.researchgate.net/publication/279441808>
- Transit NZ. (2001). Bridge inspection and maintenance steel.
- UNESCO. (2010). Seventeenth-Century Canal Ring Area of Amsterdam inside the Singelgracht - UNESCO World Heritage Centre. <https://whc.unesco.org/en/list/1349/>
- VEDA Associates. (2014). Weeley Station — VEDA Associates. <https://www.veda.co.uk/weeley-station-exmouth-footbridge-removal>
- Vollebergh, H., & Dijk, J. (2017). Taxes and fees of regional water authorities in the Netherlands.
- Waldschmitt, B., Lange, J., & Erven, M. (2021). *3D-Printing with Steel: Additive Manufacturing of a Bridge in situ* (tech. rep.). <https://www.researchgate.net/publication/354321549>
- Weyers, R. E., & Strategic Highway Research Program (U.S.) (1993). *Concrete bridge protection, repair, and rehabilitation relative to reinforcement corrosion : a methods application manual*. Strategic Highway Research Program, National Research Council.

A Appendix

B Structural Mechanics

B.1 Introduction

In this chapter, we develop and explain the structural design of the concrete bridge. Starting with the boundary conditions concerning length, width, and use purpose of the bridge, initial dimensions will be set. Given that the bridge should comply with the Dutch regulations set by the eurocodes, the structural design must be safe for its users. Besides the durability of the bridge, the contexts of sustainability, effectiveness, and cost have to be as beneficial as possible. Therefore, the calculations will follow the ending design loop, Figure 32, Snellink, 2021, followed by several iterations the bridge dimensions will be adjusted to optimize the overall quantities of materials used throughout the construction phase.

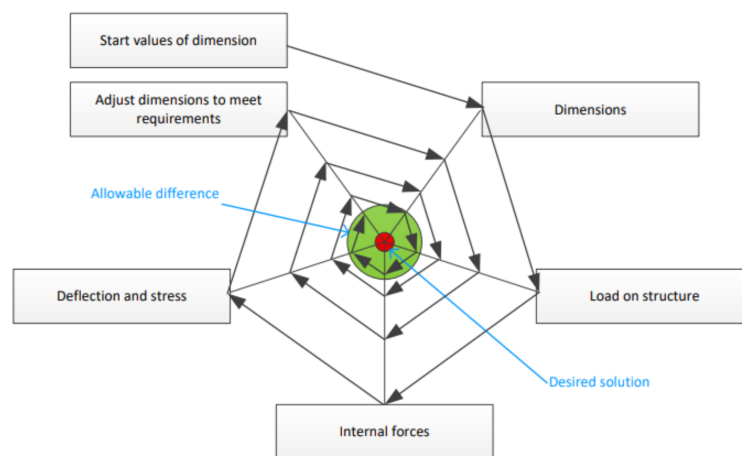


FIGURE 32: Ending Design Loop

The structural design and its optimization will be executed according to the following steps:

1. Set the initial design of structural with the rules of thumb
2. Determine the active and dead loads acting on the structure
3. Determine the principal reinforcement for structural components
4. Determine the most optimal dimensions for the principal reinforcement for structural components
5. Determine the shear force reinforcement
6. Determine the most optimal dimensions for the shear force reinforcement for structural components
7. Check the structure's strength (S/R)
8. Determine the Anchorage for structural components
9. Check crack control

By conducting the aforementioned steps, the initial dimensions of the bridge's structural components will be changed which would affect the bearing capacity of the bridge. Thus, several iterations with the different dimensions will be conducted, however, having the purpose to attract the reader, the calculation based on initial and final dimensions will be presented. All these steps will be examined in the next paragraphs given a proper explanation of each design and engineering decision.

B.2 Preliminary design

Starting with the boundary condition, the concrete bridge has to be of the same dimensions as the WAAM bridge. Both bridges aim to span the Oudezijds Achterburgwal in Amsterdam's Red Light District and allow cyclists and pedestrians to cross from one side of the canal to another, thus the length of the concrete bridge can be defined (Bekker and Verlinden, 2018).

$$L_{bridge} = 12.2m \quad (12)$$

Since the WAAM width varies over its entire length (MX3D, 2020), for the structural design of the concrete bridge the width would be based on an approximation concerning the pass-ability of the bridge.

$$W_{bridge} = 3m \quad (13)$$

Defining the main dimensions of the concrete bridge allows for specifying the types and numbers of structural components that are included in the initial configuration. Thus, the design of the concrete bridge consists of four concrete plates, and two concrete beams spanning across the canal. The preliminary dimensions of the bearing structure are estimated, although the loads acting on the bridge are unknown, the starting dimensions of the structural components can be found by using rules of thumb that comply with the ratio between the length, width, and height of structural components of the bridge. The height and width of the beams were determined in equations (15) and (16).

$$L_b = 12.2m \quad (14)$$

$$H_b = \frac{L_b}{10} = 1.2m \quad (15)$$

$$W_b = \frac{H_b}{2} = 0.61m \quad (16)$$

Over the 2 beams 4 plates of equal dimensions will be installed. Thus, the length of one plate would be equal to a quarter out of the length of the beam, $L_p = \frac{L_b}{4} = 3.05m$. The plates span the width of the bridge, 3 meters. The plates are single field construction with dimensions determined via rules of thumb determined in equation (18).

$$W_p = 3m \quad (17)$$

$$H_p = \frac{W_p}{22} = 0.136m \quad (18)$$

Finally, the initial dimensions of the main structural components have been defined, the top view and the lateral cross sections of the bridge can be seen in Figures 33, 34 and 35.

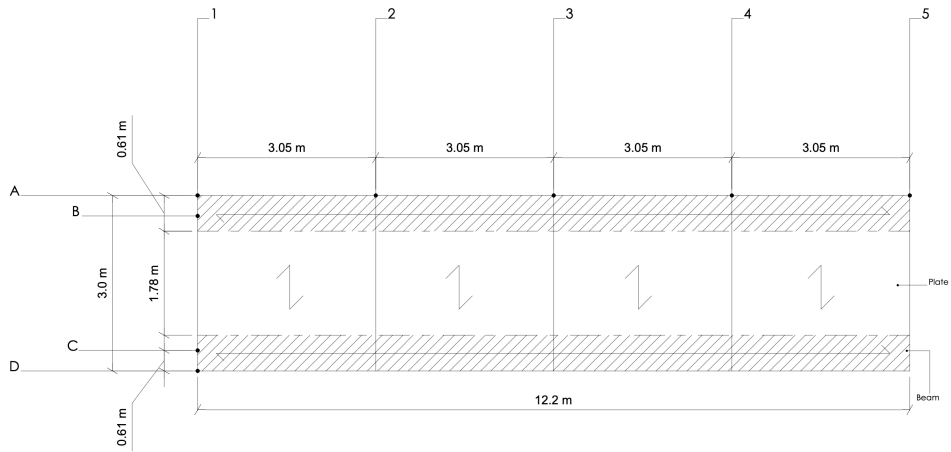


FIGURE 33: Preliminary Design - Top View

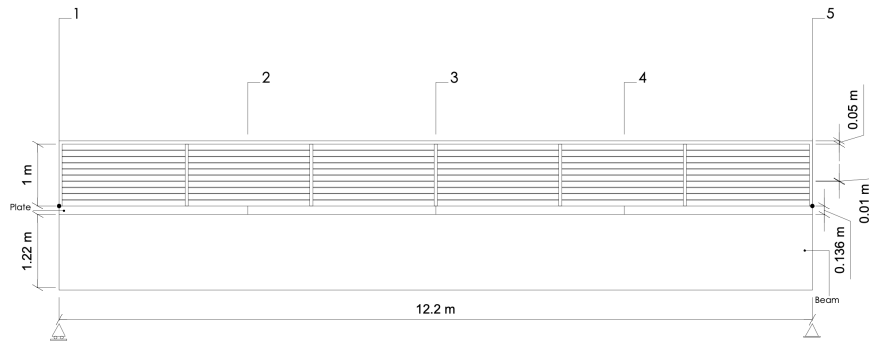


FIGURE 34: Preliminary Design - Side View

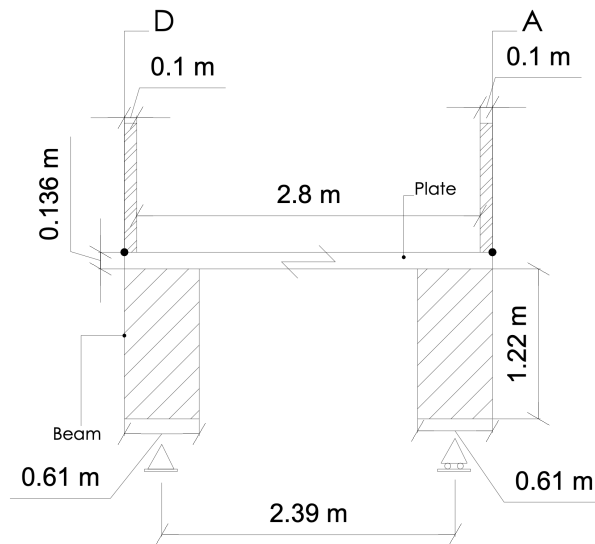


FIGURE 35: Preliminary Design - Front View

B.3 Active and Dead Loads

The structural design of the concrete bridge must meet the Dutch regulations set by the eurocodes. Therefore, calculations for active and dead loads acting on the structure are following the prescribed requirements by (NEN, 2022). Active loads acting on the bridge are caused by snow load, imposed load (caused by pedestrians and cyclists), and wind load. Dead loads are caused by the weight of the structural components, mainly railings, plates, and beams.

B.3.1 Snow Load

The snow load is acting on the bridge structure when a large mass of snow lies on the bridge plates. According to (NEN, 2022) the snow load depends on the following parameters and can be calculated via the equation (19) found in (NEN1991-1-3+C1+A1):

$$s = \mu_i * C_{e,snow} * C_{t,snow} * s_k \quad (19)$$

Where:

μ = Snow load shape coefficient

$C_{e,snow}$ = Exposure coefficient

$C_{t,snow}$ = Thermal coefficient

s_k = Characteristic value of snow load on the ground

Snow load shape coefficient:

Exposure coefficient depends on the shape of the roof (plates), since the structure's inclination angle is 0° the exposure coefficient equals to 0.8. (NEN1991-1-3)

Exposure coefficient:

Exposure coefficient for every location in the Netherlands equals to 1.0. (NEN1991-1-3)

Thermal coefficient:

Thermal coefficient for every building in the Netherlands equals to 1.0. (NEN1991-1-3)

Characteristic value of snow load on the ground:

The characteristic value of the snow load on the ground in the Netherlands equals to 0.7 kN/m^2 . (NEN1991-1-3)

As a result the total snow load will be equal to:

$$s = \mu_i * C_{e,snow} * C_{t,snow} * s_k = 0.56 \text{ kN/m}^2 \quad (20)$$

B.3.2 Imposed Load (caused by cyclists/pedestrians)

According to ("NEN 1991-1-2", 2021), vertical load caused by pedestrians and cyclists equals to:

$$Q_k = 5 \text{ kN/m}^2 \quad (21)$$

B.3.3 Wind Load

The wind load acts in multiple directions, mainly on the x-axis, y-axis, and z-axis. Nevertheless, the lateral (load on the x-axis) and longitudinal (load on the y axis) magnitudes are neglected for the bridge structure since other active and dead loads act perpendicularly to the bridge beams (load on the z-axis) which makes lateral and longitudinal loads insignificant for total loads combination calculations, therefore these parameters are excluded from the calculation. Thus, the wind load magnitude will be considered to act strictly perpendicularly to the bridge beams.

The wind load on the z-axis is calculated via the equation(27):

$$F_{w,z} = \frac{1}{2} * \rho * v_w^2 * C_z * A_{ref,z} \quad (22)$$

Where:

ρ = Density of air

v_w = Wind velocity

C_z = Wind load factor, on z-axis

$A_{ref,z}$ = Reference area, on z-axis

The density of air and the wind velocity are fixed values, thus these can be found in NEN:

$\rho = 1.25kg/m^3$ (NEN1991-1-4+A1+C2)

$v_w = 1.25kg/m^3$ (NEN1991-1-4+A1+C2)

To find the wind load factor on the z-axis (C_z) (see equation (25)), several equation components are to be calculated, mainly the exposure factor of the bridge (C_e), and the force coefficient on the z-axis ($C_{f,z}$).

$$C_{f,z} = 0.9kg/m^3 \text{ (NEN1991-1-4+A1+C2)}$$

The exposure factor of the bridge can be found by the division of the extreme thrust ($q_p(z)$) by the basic thrust (q_w), (see equation (24)) found in (NEN1991-1-4+A1+C2).

The extreme thrust is a fixed value, thus this can be found in NEN:

$$q_p(z) = 0.58 \text{ (NEN1991-1-4+A1+C2)}$$

To find the basic thrust, the equation (23) found in (NEN1991-1-4+A1+C2) is used:

$$q_w = \frac{1}{2} * \rho * v_w^2 = 455.6kN/m^2 \quad (23)$$

$$C_e = \frac{q_p(z)}{q_w} = 0.00127 \quad (24)$$

Now since all equation components are found, the wind load factor on z-axis (C_z) can be calculated according to the equation (25) found in (NEN1991-1-4+A1+C2):

$$C_z = C_{f,z} * C_e = 0.00115 \quad (25)$$

Before proceeding to the calculation of the wind load on the z-axis, the reference surface area ($A_{ref,z}$) has to be calculated. The reference area represents the area of the plates from the top view (see Figure 33), in other words, a multiplication of the bridge's length (L_{bridge}) with the bridge's width (W_{bridge}), (see equation (26)).

$$A_{ref,z} = L_{bridge} * W_{bridge} = 0.00115 \quad (26)$$

Finally, since all components are found, the wind load can be calculated:

$$F_{w,z} = \frac{1}{2} * \rho * v_w^2 * C_z * A_{ref,z} = 19.11kN \quad (27)$$

To ease further calculations, the wind load ($q_{w,z}$) will be represented in kN/m^2 , therefore we use the equation (28) where the reference surface area was excluded:

$$q_{w,z} = \frac{1}{2} * \rho * v_w^2 * C_z = 0.522kN/m^2 \quad (28)$$

B.3.4 Railings Load

The railings systems are attached perpendicularly to the floor plates and are located on both edges of the bridge, see Figure 34. To find the load of the railing on the entire structure, the volume and the density of the material used for railings need to be known. Next, to design safe and functional railings, the dimensions of the railings have to comply with the Dutch building decree, thus according to (Boubesluit C3 2012) the minimum railing height should be 1m. Additionally, since the railings are placed over the entire length of the bridge, the length of the railing top component will equal the length of the bridge, 12.2m.

A closer look at the railings system design can be seen in Figures 34 and 36, it consists of 2 railing top components, 14 railing columns, and 18 cables. There are 7 railing columns on each side of the bridge, these structural components are distributed over the entire length of the bridge having equal distance between each other. Other dimensions of structural components can be seen in Figure 36 and as well in Table 30.

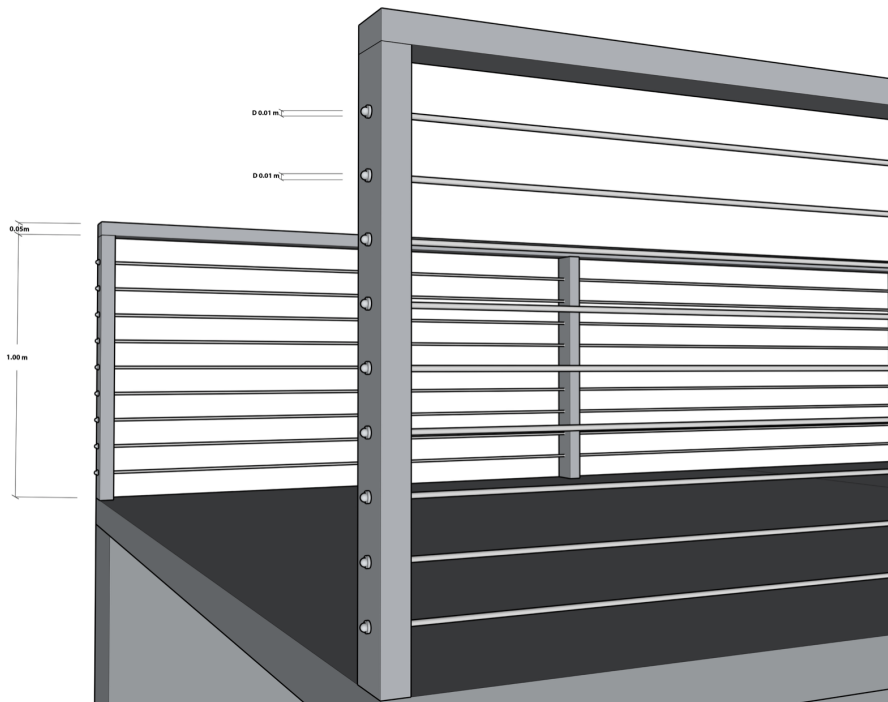


FIGURE 36: Railings detailed perspective

The geometry of all railing components is considered a cuboid except for cables that have a cylindrical shape. Consequently, knowing the dimensions of railing elements the total volume of the railing structure can be calculated, (see Table 30).

| Railing Component | Length [m] | Width [m] | Hight [m] | Volume [m ³] | Amount | Total volume |
|---------------------|------------|---------------|---------------|--------------------------|--------|--------------|
| Railing top | 12.2 | 0.1 | 0.05 | 0.061 | 2 | 0.122 |
| Railing column | 0.05 | 0.1 | 1 | 0.005 | 14 | 0.07 |
| Railing cables | 12.2 | diameter 0.01 | diameter 0.01 | 0.00095 | 18 | 0.0172 |
| Total Volume | | | | | | 0.209 |

TABLE 30: Volume of Railing Components

Given that the concrete railings would require bigger volumes of material for constructing a safe structure, it has been decided to use stainless steel for the railing structure. Thus, the railing components will be made of stainless steel Grade 316 (Davis, 1998) with a density of 8000kg/m^3 .

Given the volume and density of the railing system, we can calculate the total mass of railing elements according to the equation (29).

$$m_{railing} = V_{railing} * \rho_{steel} = 0.209\text{m}^3 * 8000\text{kg/m}^3 = 1673.9\text{kg} \quad (29)$$

For ease of the calculations, the magnitude of the railings will be considered as a point load acting on the edge of the beam, thus represented in kN. In the next sections, the railings magnitude will be adjusted concerning the calculation units, see equation (30) where gravitational acceleration $g = 9.81\text{m/s}^2$.

$$F_{railing} = \frac{m_{railing} * g}{1000} = 16.42\text{kN} \quad (30)$$

B.3.5 Railings Load

To ease further calculations the permanent load caused by beams load, plates load, and railing load is calculated in kN. Given that the gravitation acceleration $g = 9.81\text{m/s}^2$ and the density of concrete $\rho = 2400\text{kg/m}^3$, to find the mass of structural elements the volume of one beam and one plate is calculated according to the equations (31) and (32):

$$V_{beam} = L_{beam} * W_{beam} * H_{beam} = 9.07\text{m}^3 \quad (31)$$

$$V_{plate} = L_{plate} * W_{plate} * H_{plate} = 1.24\text{m}^3 \quad (32)$$

Next, the mass of one beam and one plate can be calculated according to equations (33) and (34):

$$m_{beam} = V_{beam} * \rho_{concrete} = 21790\text{kg} \quad (33)$$

$$m_{plate} = V_{plate} * \rho_{concrete} = 2994\text{kg} \quad (34)$$

Having the mass of both structural components the point force in kN can be calculated according to equations (35) and (36):

$$F_{beam} = \frac{m_{beam} * g}{1000} = 213.7\text{kN} \quad (35)$$

$$F_{plate} = \frac{m_{plate} * g}{1000} = 29.4\text{kN} \quad (36)$$

Finally, the permanent weight or the self-weight of the entire structure can be calculated (see equation (37)) by multiplying forces per component by the total number of elements in the structure, mainly 2 beams and 4 plates. The load-caused railings does not require to be multiplied with any constants since it represents the load caused by the entire railing system.

$$P = 2 * F_{beam} * 4 * F_{plate} + F_{railing} = 561.5\text{kN} \quad (37)$$

B.4 Loads combination

Since all loads acting on the bridge are calculated, their combinations are to be analyzed to find out the maximum load combination. Obviously, the combination calculations comply with the NEN codes and combine the dead load coming from the weight of the structural elements of the bridge and active loads. Several scenarios are analyzed, inherently implying that not all loads apply simultaneously on the bridge, for example, it is not likely that the bridge is full of people while there is a wind storm that creates the highest possible wind magnitude. Therefore, per each scenario, one of the active loads is applied while other active loads are reduced via ψ factor. Consequently, the maximum possible load combination is evaluated for further calculations.

For the load combinations, the equation (38) (“NEN 1992 1-1+C2/NB+A1”, 2020) is used:

$$\Sigma j \geq 1\gamma_{G,j}G_{k,j} + \gamma_p P + \gamma_{Q,1}Q_{k,1} + \Sigma j > 1\gamma_{Q,i}\psi_{0,i}Q_{k,i} \quad (38)$$

Where:

$\psi_{0,people}$ = Factor for combination value of a variable action = 0.4

$\psi_{0,snow}$ = Factor for combination value of a variable action = 0.8

$\psi_{0,wind}$ = Factor for combination value of a variable action = 0.3

$\gamma_{G,sup}$ = Partial factor for permanent action = 1.05

γ_Q = Partial factor for permanent action = 1.35

Nevertheless, before starting the calculate the loads' combinations, all loads have to be translated to the same units, mainly for the beams in kN/m and kN/m^2 for the plates.

Since the self-weight of the floor plates affects the beams, the loads are initially calculated for the plates. Additionally, the loads are calculated per one type of structural element, particularly for 1 plate and for 1 beam.

From loads calculations in previous sections, only the self-weight of the plate needs to be translated from kN to kN/m^2 , however, firstly the implication of the railings has to be applied, see equation (39):

$$P_p = F_{plate} + \frac{F_{railing}}{4} = 29.37kN \quad (39)$$

Now the self-weight of 1 plate can be simply translated from kN to kN/m^2 by dividing the self-weight by the area of the plate, see equation (40):

$$P_{plate} = \frac{P_{plate}}{L_{plate} * W_{plate}} = 3.21kN/m^2 \quad (40)$$

An additional check of the calculation is made before proceeding to loads combination calculation, basically, the self-weight of 1 plate in kN/m^2 is calculated via different formula, see equation (41):

$$P_{plate} = \frac{\rho * g * H_{plate}}{1000} + \frac{F_{railing}}{4 * L_{plate} * W_{plate}} = 3.21kN/m^2 \quad (41)$$

Clearly, both results are equal, thus numerical values of the loads on 1 plate can be inserted in Table 31.

| Type of Load | Values | Units | New value | New Units |
|--------------|--------|-------------------|-----------|-------------------|
| Self weight | 29.37 | kN | 3.21 | kN/m ² |
| Imposed load | 5 | kN/m ² | 5 | kN/m ² |
| Snow load | 0.56 | kN/m ² | 0.56 | kN/m ² |
| Wind load | 0.522 | kN/m ² | 0.522 | kN/m ² |

TABLE 31: Parameterize Loads on 1 Plate to kN/m²

Once the calculation and translation into the necessary units for loads on 1 plate are finished, a similar procedure can be applied for the loads acting on 1 beam. Note that for the beam, all 4 different types of loads need to be adjusted to kN/m.

The self-weight of 1 beam is calculated according to the following equation (42)

$$P_b = \frac{P}{2} = 280.7kN \quad (42)$$

To prove the correctness of the calculation procedure, two different calculation methods are used to translate the self-weight of 1 beam from kN to kN/m. Starting with dividing the self-weight of 1 beam over its length, see equation (43):

$$P_{beam} = \frac{P_b}{L_{beam}} = 23kN/m \quad (43)$$

Secondly, to translate the self-weight of 1 beam from kN to kN/m the following calculation procedure is applied, see equation (44):

$$P_{beam} = (H_{beam} * W_{beam} * 2.4 * g) + \frac{W_{plate} * P_{plate}}{2} = 23kN/m \quad (44)$$

Notice that both active loads, the imposed and the snow load are in kN/m². Therefore, to translate them into kN/m, their numerical values are multiplied by the bridge's width, resulting in a uniformly distributed load over the entire length of the beam, see equation (45) and (46):

$$Q_{k,beam} = Q_k * W_{bridge} = 15kN/m \quad (45)$$

$$s_{beam} = s * W_{bridge} = 1.68kN/m \quad (46)$$

Lastly, the wind load is given in kN/m², thus it has to be concentrated such that the load is distributed over the span of the canal or simply saying the length of the beam. Since the loads acting on the plates are distributed over the beams, the wind load acting on the 4 plates can be spread on the beam by using the equation (47):

$$q_{w,z,beam} = \frac{q_{w,z} * L_{plate} * W_{plate} * 4}{2 * L_{beam}} = 0.783kN/m \quad (47)$$

| Type of Load | Values | Units | New value | New Units |
|--------------|--------|-------------------|-----------|-----------|
| Self weight | 280.7 | kN | 23 | kN/m |
| Imposed load | 5 | kN/m ² | 15 | kN/m |
| Snow load | 0.56 | kN/m ² | 1.68 | kN/m |
| Wind load | 0.522 | kN/m ² | 0.783 | kN/m |

TABLE 32: Parameterize Loads on 1 Beam to kN/m

After translating all loads acting on 1 beam and 1 plate to the required units (see Tables 31 and 32) the loads' combination scenarios can be deducted using the equation (38). Given that there are 3 active loads, a similar number of scenarios will be analyzed for each structural element of the bridge.

The 1st Scenario represents the dominance of the snow load, thus, the imposed load and the wind load are reduced by the ψ factor, see equations (48) and (49):

$$q_{1,beam} = \gamma_{G,sup} * P_{beam} + \gamma_Q * Q_{k,beam} + \gamma_Q * \psi_{0,snow} * s_{beam} + \gamma_Q * \psi_{0,wind} * q_{w,z,beam} = 46.6kN/m \quad (48)$$

$$q_{1,plate} = \gamma_{G,sup} * P_{plate} + \gamma_Q * Q_{k,plate} + \gamma_Q * \psi_{0,snow} * s_{plate} + \gamma_Q * \psi_{0,wind} * q_{w,z,plate} = 10.93kN/m^2 \quad (49)$$

The 2nd *Scenario* implies that the imposed load is dominant while other active loads acting on the bridge are decreased by the ψ factor, see equations (50) and (51):

$$q_{2,beam} = \gamma_{G,sup} * P_{beam} + \gamma_Q * s_{beam} + \gamma_Q * \psi_{0,people} * Q_{k,beam} + \gamma_Q * \psi_{0,wind} * q_{w,z,beam} = 34.84kN/m \quad (50)$$

$$q_{2,plate} = \gamma_{G,sup} * P_{plate} + \gamma_Q * s_{plate} + \gamma_Q * \psi_{0,people} * Q_{k,plate} + \gamma_Q * \psi_{0,wind} * q_{w,z,plate} = 7.04kN/m^2 \quad (51)$$

The 3^d *Scenario* sets the wind load as a dominant load, therefore the imposed load and the snow load are reduced by the ψ factor, see equations (52) and (53):

$$q_{3,plate} = \gamma_{G,sup} * P_{plate} + \gamma_Q * q_{w,z,plate} + \gamma_Q * \psi_{0,people} * Q_{k,plate} + \gamma_Q * \psi_{0,snow} * s_{plate} = 7.38kN/m^2 \quad (52)$$

$$q_{3,beam} = \gamma_{G,sup} * P_{beam} + \gamma_Q * q_{w,z,beam} + \gamma_Q * \psi_{0,people} * Q_{k,beam} + \gamma_Q * \psi_{0,snow} * s_{beam} = 35.13kN/m \quad (53)$$

From the above calculations, the highest load on both plate and beam takes place when the imposed load is dominant (2nd *scenario*) resulting in:

$$\text{Highest load on beam} = 46.63kN/m \quad (54)$$

$$\text{Highest load on plate} = 10.93kN/m^2 \quad (55)$$

B.5 Principal Reinforcement Beams

The highest load combination allows for determining the maximum shear force and moment acting on the beam. Consequently, the preliminary area of the principal reinforcement is calculated.

As aforementioned, given the maximum uniformly distributed load over the length of the beam (see Figure 37, 38 and 39), the shear force and the moment can be determined with equations (56) and (57):

$$V_{beam} = \frac{L_{beam} * q_{beam}}{2} = 285.4kN \quad (56)$$

$$M_{max,beam} = \frac{1}{8} * q_{beam} L_{beam}^2 = 867.5kNm \quad (57)$$

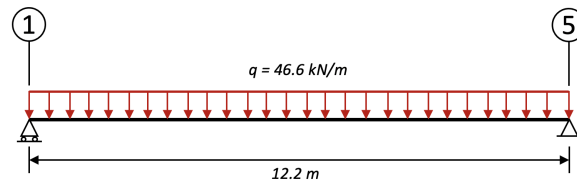


FIGURE 37: Uniformly distributed load diagram for beam

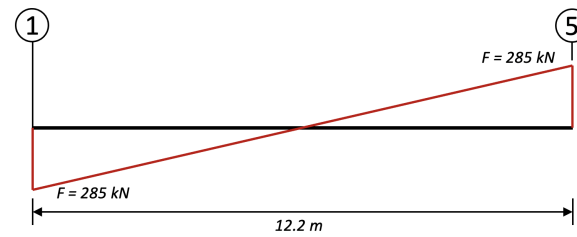


FIGURE 38: Shear force diagram for beam

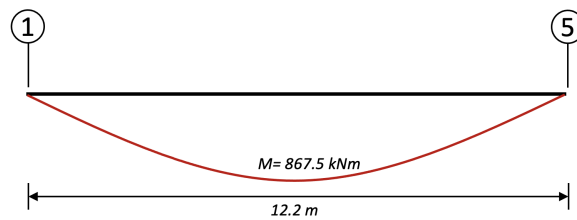


FIGURE 39: Moment diagram for beam

Once the magnitudes of the shear force and the maximum moment are determined, the dimensions of the principal reinforcement in beams can be determined. Initially, the exposure and the structural class of concrete used for the bridge construction has to be chosen.

Considering that the bridge is in periodic contact with water the *XC4* is selected as the exposure class. According to (“NEN 1991-1-2”, 2021) *XC4* is used for structures that are cyclic wet, and dry, but not subject to long-term contact with water. Besides, the structural class of the concrete has to be established concerning the life span of the bridge structural components that have to last for 100 years,

the structural class *S5* is considered. Therefore these exposure classes are completely suitable for later calculation of the cover in beams. These leads to the strength class of C20/25.

Following the exposure and structural class the minimal value for the beam cover can be determined, thus the $C_{min} = 35mm$, see Table 33.

| Requirment for c(min) [mm] | | | | | | | |
|----------------------------|----------------|-----|---------|-----|---------|---------|---------|
| Structural class | Exposure class | | | | | | |
| | XO | XC1 | XC2/XC3 | XC4 | XD1/XS1 | XD2/XS2 | XD3/XS3 |
| S1 | 10 | 10 | 10 | 15 | 20 | 25 | 25 |
| S2 | 10 | 10 | 15 | 20 | 25 | 30 | 30 |
| S3 | 10 | 10 | 20 | 25 | 30 | 35 | 35 |
| S4 | 10 | 15 | 25 | 30 | 35 | 40 | 40 |
| S5 | 15 | 20 | 30 | 35 | 40 | 45 | 45 |
| SO | 20 | 25 | 35 | 40 | 45 | 50 | 50 |

TABLE 33: Thickness of cover

According to (NEN 1992-1-1 NB, 4.4) the allowed deviation for the cover calculation is equal to 5mm. From a safety perspective, the permitted cover deviation will be summed with the minimal required cover dimensions, thus the final cover dimensions can be calculated with the equation (58).

$$c = c_{min} + \Delta c_{dev} = 35 + 5 = 40mm \quad (58)$$

Next, the distance between the top edge of the beam to the center of the reinforcement mentioned as distance *d* (see Figure 40) can be determined with the equation (59) and two additional assumptions. First, the diameter of the stirrups is assumed to be 10mm, and secondly, the diameter of the principal reinforcement equals 20mm.

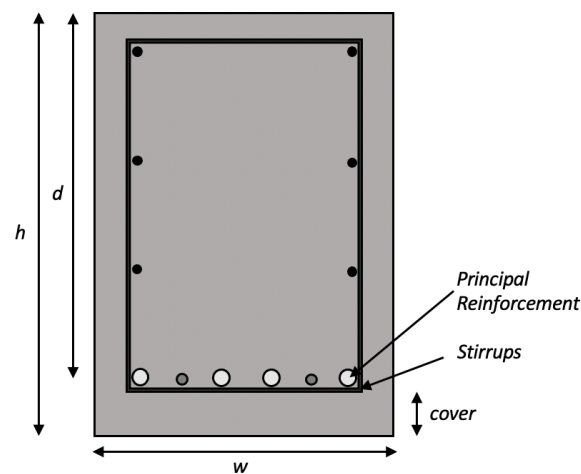


FIGURE 40: Distance *d*

$$d_{beam} = H_{beam} - c - \varnothing_{stirrups} - \frac{1}{2}\varnothing_{principal\ reinforcement} = 1160mm \quad (59)$$

Before proceeding to the calculation of the area of principal reinforcement (see equation (60)), the *z/d* ratio has to be calculated. However, to ease the calculation this ratio is assumed to be 0.8. Accordingly, an additional inspection of the reinforcement area will be provided in the next sections to minimize the implication of the assumed *z/d* ratio.

$$A_{s,beam} = \frac{M_{max,beam}}{\frac{z}{d} * d_{beam} * f_{yd}} \quad (60)$$

Where:

$A_{s,beam}$ = Area of principal reinforcement in beam

$M_{max,beam}$ = The maximum moment on beam

$f_{y,d}$ = Yield strength of steel reinforcement (435N/mm²)

d_{beam} = Distance from the top edge of the beam to the center of the reinforcement

Using the aforementioned numerical values, the area of the principal reinforcement is determined:

$$A_{s,beam} = \frac{M_{max,beam}}{0.8 * d_{beam} * f_{yd}} = 2149.1mm^2 \quad (61)$$

The reinforcement area of the principal reinforcement equals to, using the Table 34 (Snellink, 2021) and following the assumed dimensions of the principal reinforcement to be 20mm, an equal or higher numerical value for the reinforcement area has to be chosen. 7 bars with a diameter of 20mm that result in $A_{s,beam,table} = 2199mm^2$ for reinforcement area completely suits structural properties of the beam.

| bars | $\phi(mm)$ | | | | | | | | |
|------|------------|-----|-----|------|------|------|------|------|-------|
| | 6 | 8 | 10 | 12 | 16 | 20 | 25 | 32 | 40 |
| 1 | 28 | 50 | 79 | 113 | 201 | 314 | 491 | 804 | 1257 |
| 2 | 57 | 101 | 157 | 226 | 402 | 628 | 982 | 1608 | 2513 |
| 3 | 85 | 151 | 236 | 339 | 603 | 942 | 1473 | 2413 | 3770 |
| 4 | 113 | 201 | 314 | 452 | 804 | 1257 | 1963 | 3217 | 5027 |
| 5 | 141 | 251 | 393 | 565 | 1005 | 1571 | 2454 | 4021 | 6283 |
| 6 | 170 | 302 | 471 | 679 | 1206 | 1885 | 2945 | 4825 | 7540 |
| 7 | 198 | 352 | 550 | 792 | 1407 | 2199 | 3436 | 5630 | 8796 |
| 8 | 226 | 402 | 628 | 905 | 1608 | 2513 | 3927 | 6434 | 10053 |
| 9 | 254 | 452 | 707 | 1018 | 1810 | 2827 | 4418 | 7238 | 11310 |
| 10 | 283 | 503 | 785 | 1131 | 2011 | 3142 | 4909 | 8042 | 12566 |

TABLE 34: Area of Reinforcement bars [mm²]

B.6 Principal Reinforcement Plates

Similar to the previous section, the area of the principal reinforcement for the plates is to be determined with the same calculation procedures.

Initially, to determine the shear force and the maximum moment acting on the bridge's plates the load acting on the plate has to be translated from kN/m^2 to kN/m , thus, in the following calculations, it is assumed that the load of $10.93kN/m^2$ acts on a slice of 1m width resulting in similar numerical value but with different units, $10.93kN/m$.

Having the uniformly distributed load over the width of the plate, the shear force and the maximum moment can be calculated, however, before that, an important calculation attribute must be encountered. Due to the fact that the line of action develops through the center point of the beam, (see the location of pin and roller supports in Figure 35) the following calculations will be using the distance between pin supports ($d_{pin,supports}$) instead of the total width of the plate.

The shear force and the maximum moment acting on the plate (see Figures 41, 42, and 43) can be calculated with equations (62) and (63).

$$V_{plate} = \frac{d_{pin,supports} * q_{plate}}{2} = 13.1kN \quad (62)$$

$$M_{max,plate} = \frac{1}{8} * q_{plate}d_{pin,supports}^2 = 7.8kNm \quad (63)$$

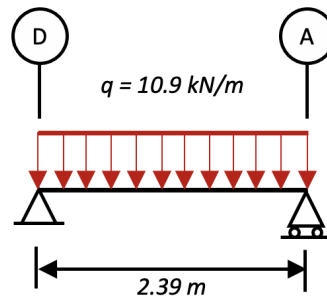


FIGURE 41: Uniformly distributed load diagram for plate

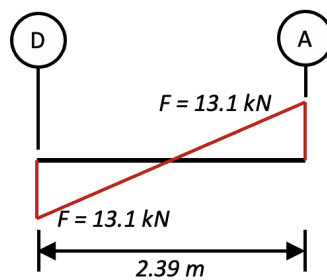


FIGURE 42: Shear force diagram for plate

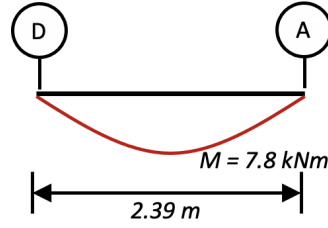


FIGURE 43: Moment diagram for plate

Likewise, for the beams, the cover for the principal reinforcement of plates equals 40mm. Since the overall load acting on the plate is significantly lower compared to the load-acting beam, the assumed diameter of the principal reinforcement will be reduced to 8mm.

$$d_{plate} = H_{plate} - c - \frac{1}{2} \phi_{principal\ reinforcement} = 92.3mm \quad (64)$$

Before calculating the reinforcement area, the z/d ratio has to be assumed. Concerning the magnitude of the load acting on the plate and the dimensions of the element, the z/d ration is presumed to be 0.9. Just like for the beams, additional inspection of the reinforcement area will be provided in the next sections.

$$A_{s,plate} = \frac{M_{max,beam}}{\frac{z}{d} * d_{plate} * f_{yd}} \quad (65)$$

Where:

$A_{s,plate}$ = Area of principal reinforcement in plate

$M_{max,plate}$ = The maximum moment on plate

$f_{y,d}$ = Yield strength of steel reinforcement (435N/mm²)

d_{plate} = Distance from the top edge of the plate to the center of the reinforcement

Using the aforementioned numerical values, the area of the principal reinforcement is determined:

$$A_{s,plate} = \frac{M_{max,plate}}{0.9 * d_{plate} * f_{yd}} = 242.9mm^2 \quad (66)$$

According to the $A_{s,plate}$ result and the assumed dimensions for the reinforcements, following the Table 35 (Snellink, 2021) indicates that principal reinforcement with a c.o.c distance of 200 mm and certainly $\phi 8$ gives a reinforcement area of $A_{s,plate,table} = 251mm^2$ which closely corresponds to the obtained result for the reinforcement area.

| c.o.c distance [mm] | ϕ [mm] | | | | | | | | |
|------------------------|-------------|-----|-----|------|------|------|------|------|-------|
| | 6 | 8 | 10 | 12 | 16 | 20 | 25 | 32 | 40 |
| 100 | 283 | 503 | 785 | 1131 | 2011 | 3142 | 4909 | 8042 | 12566 |
| 125 | 226 | 402 | 628 | 905 | 1608 | 2513 | 3927 | 6434 | 10053 |
| 150 | 188 | 335 | 524 | 754 | 1340 | 2094 | 3272 | 5362 | 8378 |
| 200 | 141 | 251 | 393 | 565 | 1005 | 1571 | 2454 | 4021 | 6283 |
| 250 | 113 | 201 | 314 | 452 | 804 | 1257 | 1963 | 3217 | 5027 |
| 300 | 94 | 168 | 262 | 377 | 670 | 1047 | 1636 | 2681 | 4189 |

TABLE 35: Area of reinforcement bars in [mm²] for plates

B.7 Reinforcement Optimization

After calculating the principal reinforcement area the reinforcement ratio has to be determined. Ideally, the reinforcement area should weigh 1% of the total area of the beam, obviously, since the initial dimensions of the structural components have been adjusted via rules of thumb, the dimensions of the bridge's elements are to be calibrated.

The principal reinforcement for beams has an area of ($A_{s,beam,table}$) $2199mm^2$, while for plates ($A_{s,plate,table}$) $251mm^2$. Thus, the reinforcement ratio for both beam and plate can be determined with the equations (67) and (68).

$$\text{Reinforcement ratio beams} = \frac{A_{s,beam,table}}{W_{beam} * d_{beam}} = 0.310\% \quad (67)$$

$$\text{Reinforcement ratio plates} = \frac{A_{s,plate,table}}{W_{plate} * d_{plate}} = 0.09\% \quad (68)$$

Both numerical values of the reinforcement ratios are below 1%. This implies that the dimensions of the concrete in comparison to the steel reinforcement are too large, thus dimensions of both structural elements must be reduced to achieve the desired reinforcement ratio.

Before adjusting the dimensions of the beams and plates, variables that are strongly related to the bridge dimensions are analyzed. Firstly, the length of the beams, length, and width of the plates can not be changed. This implication reduces the flexibility of the following iterations. Any variance in other dimensions affects the permanent load of the beam and plates, however, all active loads remain similar. Next, any change in the dimensions would impact the highest loads and moment applied to the structural elements leading to a different surface of principal reinforcement and therefore a different reinforcement ratio.

Since loads of the plates impact the beams, the optimization of the plates is applied first. Additionally, a systematic approach of iterations is applied, aiming to increase the reinforcement ratio, the dimensions of the plates are to be reduced by several percent, see Table 36.

| Iteration | % | Height | Area [mm^2] | Reinforcement ration % |
|-----------|------|---------|-----------------|------------------------|
| 1 | 100 | 0.136 | 251 | 0.061 |
| 2 | 70 | 0.0952 | 397 | 0.139 |
| 3 | 66 | 0.08976 | 438 | 0.163 |
| 4 | 65 | 0.0884 | 450 | 0.17 |
| 3 | 73.5 | 0.1 | 421 | 0.25 |

TABLE 36: Plates dimensions iterations

The reinforcement ratio for the plates remains smaller than 1%. The ratio between concrete and steel for the plates results in 0.25% and can not be increased. The main reason for the impossible increase in the reinforcement ratio for the floor plates is the dimension of the concrete cover of 40mm on both sides of the plates. Considering the space for the reinforcement, an additional 20mm is encountered as a boundary condition which implies that the minimum height of the plate is 100mm. On the other side, any increase in the height of the plate reduces the reinforcement ratio meaning that a reinforcement area for the plates of 1% can not be achieved.

In this situation, the numerical value for the principal reinforcement area of the plates is $421mm^2$. The c.o.c. distances are chosen such that one is a multiple of the other, thus a principal reinforcement of Ø8 with a c.o.c. distance of 150mm and Ø6 with a c.o.c. distance of 300mm is applied, giving an area of $429mm^2$, (see Table 35).

Since the dimensions of the plates are optimized, the height and width of the beam can be adjusted respectively. Several iterations (see Table 37) are analyzed which implies that the beam reinforcement

ratio is highly sensitive to the beam height. This is inherent evidence since any alteration of the beam's height affects the load and consequently, the maximum moment magnitude increasing reinforcement area. Therefore, from the economical perspective, the main goal of the optimization is to keep the reinforcement area as low as it is possible and the reinforcement ratio equal to or slightly above 1%. The beam's width can not be significantly reduced due to the cover dimensions. The cover dimensions from both sides of the beam equal 40mm, concerning the space for the reinforcement and the space between them to allow the aggregates to penetrate through the fittings the smallest beam width is 350mm. Therefore, the total number of reinforcement bars has to be kept at a minimum.

| Iteration | Height [m] | Width [m] | Area [mm ²] | Reinforcement ratio % |
|-----------|------------|-----------|-------------------------|-----------------------|
| 1 | 0.8 | 0.4 | 2456 | 0.828 |
| 2 | 0.76 | 0.4 | 2566 | 0.914 |
| 3 | 0.8 | 0.35 | 2384 | 0.918 |
| 4 | 0.75 | 0.4 | 2556 | 0.938 |
| 5 | 0.77 | 0.35 | 2465 | 0.99 |
| 6 | 0.76 | 0.35 | 2556 | 1.043 |

TABLE 37: Beams dimensions iterations

As a result, the reinforcement ratio for the beams is equal to 1.04%, and the required reinforcement area of 2556mm². In this situation, in order to reduce the anchorage length that strongly affects the final price of the construction phase, it is more logical to keep the same diameter as it was used for the maximum moment, (20mm) (Snellink, 2021). Thus 4 bars with a diameter of 25mm and 2 bars with a diameter of 20mm are selected which gives a reinforcement area equal to 2591mm², (see Table 34).

In the Table 38, new dimensions of the structural elements as well as the achieved reinforcement area and the parameters of the reinforcement bars. The combinations of the reinforcement bars result are higher than the minimum required for the reinforcement area to be certainly strong.

| Structural elements | Height | Width | Length | R.ratio % | Reinforcement components | Total R. Area [mm ²] |
|---------------------|--------|-------|--------|-----------|---------------------------------|----------------------------------|
| Plate | 100 | 3000 | 3050 | 0.25 | Ø6 c.o.c. 300 and Ø8 c.o.c. 150 | 429 |
| Beam | 760 | 350 | 12200 | 1.043 | 4Ø25 and 2Ø20 | 2591 |

TABLE 38: Optimal dimensions of structural components

Since the new dimensions of the structural elements are set, to ensure that the connection between the reinforcement bars does not change the location of the bars during the concrete works, the plates require to be reinforced perpendicularly to the newly determined principal reinforcement.

The reinforcement must be equal to 20% of the principal reinforcement area of plates, see equation (69):

$$A_{s,plate,cracks} = A_{s,plate,new} * 0.2 = 85.8mm^2 \quad (69)$$

Considering this, bars of Ø6 with a c.o.c. a distance of 300mm can be placed perpendicularly to the principal reinforcement bars in plates, resulting in 94mm².

Finally, given the new dimensions of the structural components, the highest load on the beam and plate are recalculated, (see equations (70) and (71)). In a matter of fact, the highest load magnitudes take place again when the imposed loads are dominant.

$$\text{NEW highest load on beam} = 33.46kN/m \quad (70)$$

$$\text{NEW highest load on plate} = 10.5kN/m^2 \quad (71)$$

B.8 Shear force reinforcement in Beam

The new dimensions of the beam are set, thus the capacity of the shear force reinforcement (see equation (72)) in beams can be determined. Consequently, the dimensions of the stirrups are calculated.

$$v_{rd} = \frac{V_{new,beam}}{W_{beam} * d_{beam}} \quad (72)$$

Where:

v_{rd} = Capacity of shear force reinforcement

$V_{new,beam}$ = The new maximum shear force acting on the beam

d_{beam} = New distance from the top edge of the beam to the center of the reinforcement

W_{beam} = New width of the beam = 350mm

The value of the maximum shear force applied on the beam as well as the d_{beam} are modified since the load magnitude and the height of the beam have been adjusted. Therefore, the aforementioned parameters can be calculated with the equation (73) and (74):

$$d_{new,beam} = H_{new,beam} - c - \emptyset_{stirrups} - \frac{1}{2}\emptyset_{principal\ reinforcement} = 760 - 40 - 10 - \frac{1}{2} * 20 = 700mm \quad (73)$$

$$V_{new,beam} = \frac{L_{new,beam} * q_{new,beam}}{2} = 204.1kN \quad (74)$$

Once the new maximum shear force acting on the beam and the d_{beam} are known, the capacity of the shear force reinforcement is found with equation (75):

$$v_{rd} = \frac{V_{new,beam}}{W_{new,beam} * d_{new,beam}} = 0.83N/mm^2 \quad (75)$$

With the capacity of the shear force reinforcement and the new width of the beam (W_{beam}), the dimensions of the stirrups are selected. Table 39 shows the shear force capacity for multiple types of stirrups. Given that the initial calculations assumed the diameter of stirrups to be 10mm, therefore only the spacing of the stirrups is modified concerning the beam's width ($W_{beam} = 760mm$). In this situation, stirrups ($\emptyset 10$ and spacing 200mm) give a shear force capacity of $0.88N/mm^2$, (see Table 39) (Snellink, 2021). Given that the resulting value of the capacity of shear force reinforcement is $0.83N/mm^2$ the dimensions of stirrups are chosen appropriately.

Installing similar stirrups throughout the length of the beam would assure a safe structure, however, this would strongly deviate from the applied shear force. In other words, in the middle of the beam, the shear force would be equal to 0kN and linearly increases to the edges of the beam, thus complying with the safety and economic optimization of the stirrups' dimensions located in the middle part of the beam can be reduced.

To find out the amount of shear force on the middle segment of the beam the shear force diagram is used (Figure 44), where the yellowish part represents the distribution of the shear force over the beam), thus the shear force capacity on the middle segment of the beam equals $0.42N/mm^2$. Following the types of stirrups from Table 72, this shear force capacity can be achieved with stirrups with a diameter of 6mm and spacing equal to 150mm. For a better understanding the side view of the stirrups placed in the beam can be seen in Figure 45.

| | Width of Beam | | | | | | | |
|-----------------|---------------|------------|------------|------------|------------|------------|------------|------------|
| | [mm] | [mm] | [mm] | [mm] | [mm] | [mm] | [mm] | [mm] |
| Stirrups | 150 | 200 | 250 | 300 | 350 | 400 | 450 | 500 |
| ϕ 6-100 | 1.48 | 1.11 | 0.89 | 0.74 | 0.63 | 0.55 | 0.49 | 0.44 |
| ϕ 6-150 | 0.98 | 0.74 | 0.59 | 0.49 | 0.42 | 0.37 | 0.33 | 0.30 |
| ϕ 6-200 | 0.74 | 0.55 | 0.44 | 0.37 | 0.32 | 0.28 | 0.25 | 0.22 |
| ϕ 6-250 | 0.59 | 0.44 | 0.35 | 0.30 | 0.25 | 0.22 | 0.20 | 0.18 |
| ϕ 6-300 | 0.49 | 0.37 | 0.30 | 0.25 | 0.21 | 0.18 | 0.16 | 0.15 |
| ϕ 8-100 | 2.62 | 1.97 | 1.57 | 1.31 | 1.12 | 0.98 | 0.87 | 0.79 |
| ϕ 8-150 | 1.75 | 1.31 | 1.05 | 0.87 | 0.75 | 0.66 | 0.58 | 0.52 |
| ϕ 8-200 | 1.31 | 0.98 | 0.79 | 0.66 | 0.56 | 0.49 | 0.44 | 0.39 |
| ϕ 8-250 | 1.05 | 0.79 | 0.63 | 0.52 | 0.45 | 0.39 | 0.35 | 0.31 |
| ϕ 8-300 | 0.87 | 0.66 | 0.52 | 0.44 | 0.37 | 0.33 | 0.29 | 0.26 |
| ϕ 10-100 | 4.10 | 3.07 | 2.46 | 2.05 | 1.76 | 1.54 | 1.37 | 1.23 |
| ϕ 10-150 | 2.73 | 2.05 | 1.64 | 1.37 | 1.17 | 1.02 | 0.91 | 0.82 |
| ϕ 10-200 | 2.05 | 1.54 | 1.23 | 1.02 | 0.88 | 0.77 | 0.68 | 0.61 |
| ϕ 10-250 | 1.64 | 1.23 | 0.98 | 0.82 | 0.70 | 0.61 | 0.55 | 0.49 |
| ϕ 10-300 | 1.37 | 1.02 | 0.82 | 0.68 | 0.59 | 0.51 | 0.46 | 0.41 |
| ϕ 12-100 | 5.90 | 4.43 | 3.54 | 2.95 | 2.53 | 2.21 | 1.97 | 1.77 |
| ϕ 12-150 | 3.94 | 2.95 | 2.36 | 1.97 | 1.69 | 1.48 | 1.31 | 1.18 |
| ϕ 12-200 | 2.95 | 2.21 | 1.77 | 1.48 | 1.27 | 1.11 | 0.98 | 0.89 |
| ϕ 12-250 | 2.36 | 1.77 | 1.42 | 1.18 | 1.01 | 0.89 | 0.79 | 0.71 |
| ϕ 12-300 | 1.97 | 1.48 | 1.18 | 0.98 | 0.84 | 0.74 | 0.66 | 0.59 |

TABLE 39: Shear force capacity for stirrups B500 in N/mm^2

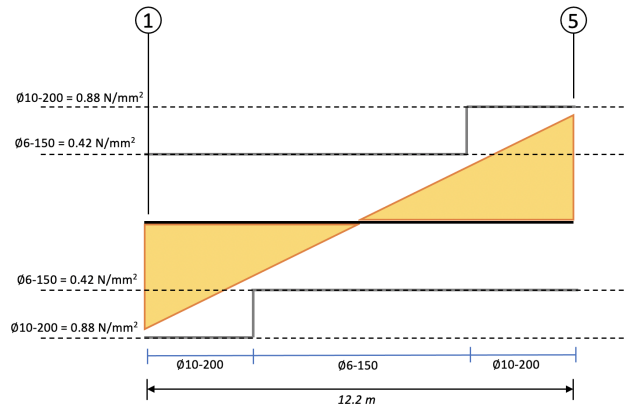


FIGURE 44: Shear force reinforcement beam

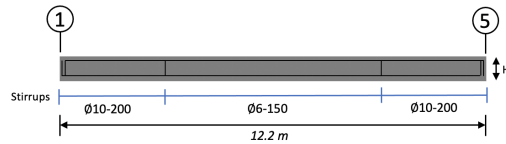


FIGURE 45: Side view of beam, location of stirrups

B.9 Shear force reinforcement in Plates

Similar to the previous section, the shear force reinforcement for plates is to be determined with the same calculation procedures. Besides, due to the optimization of the plate dimensions, the maximum shear force and the distance d are modified, therefore the new values of the aforementioned variables can be found with equations(76) and (77):

$$d_{new,plate} = H_{new,plate} - c - \frac{1}{2} \phi_{principal\ reinforcement} = 100 - 40 - \frac{1}{2} * 8 = 56mm \quad (76)$$

$$V_{new,plate} = \frac{L_{new,plate} * q_{new,plate}}{2} = 13.9kN \quad (77)$$

Once the new maximum shear force acting on the plate and the d_{plate} are known, the capacity of the shear force reinforcement is found with the equation (78):

$$v_{rd} = \frac{V_{new,plate}}{W_{new,beam} * d_{new,plate}} = 0.08N/mm^2 \quad (78)$$

Before analyzing the shear force capacity of the plates, the concrete class has to be specified. According to previous sections, the concrete class is C20/25. Considering that the required shear force reinforcement capacity for the plate equals $0.08N/mm^2$, Table 40 (Snellink, 2021) is used to inspect the minimum value of shear force capacity with respect to distance ($d_{new,plate} = 56mm$). The minimum distance ($d_{new,plate}$) presented in the Table 40 is 200mm and indicates that the minimum shear force capacity should be $0.44N/mm^2$ for the similar concrete class (C20/25). Additionally, the numerical values for the minimum shear force capacity in Table 40 are decreasing with the increase in the distance ($d_{new,plate}$). Given that the new distance ($d_{new,plate}$) used for the bridge calculations is 56mm, the minimum permitted shear force capacity value becomes larger.

| | d [mm] | 200 | 225 | 250 | 300 | 350 | 400 | 500 | 600 | 750 | 1000 |
|---------------|--------------------------------|------|------|------|------|------|------|------|------|------|------|
| | k | 2.00 | 1.94 | 1.89 | 1.82 | 1.76 | 1.71 | 1.63 | 1.58 | 1.52 | 1.45 |
| Class | $f_{c,k}$ [N/mm ²] | | | | | | | | | | |
| C12/15 | 12 | 0.34 | 0.33 | 0.32 | 0.30 | 0.28 | 0.27 | 0.25 | 0.24 | 0.23 | 0.21 |
| C16/20 | 16 | 0.40 | 0.38 | 0.37 | 0.34 | 0.33 | 0.31 | 0.29 | 0.28 | 0.26 | 0.24 |
| C20/25 | 20 | 0.44 | 0.42 | 0.41 | 0.38 | 0.36 | 0.35 | 0.33 | 0.31 | 0.29 | 0.27 |
| C25/30 | 25 | 0.49 | 0.47 | 0.46 | 0.43 | 0.41 | 0.39 | 0.37 | 0.35 | 0.33 | 0.30 |
| C30/37 | 30 | 0.54 | 0.52 | 0.50 | 0.47 | 0.45 | 0.43 | 0.40 | 0.38 | 0.36 | 0.33 |
| C35/45 | 35 | 0.59 | 0.56 | 0.54 | 0.51 | 0.48 | 0.46 | 0.43 | 0.41 | 0.39 | 0.36 |
| C40/50 | 40 | 0.63 | 0.60 | 0.58 | 0.54 | 0.52 | 0.49 | 0.46 | 0.44 | 0.41 | 0.39 |
| C45/55 | 45 | 0.66 | 0.64 | 0.61 | 0.57 | 0.55 | 0.52 | 0.49 | 0.47 | 0.44 | 0.41 |
| C50/60 | 50 | 0.70 | 0.67 | 0.65 | 0.61 | 0.58 | 0.55 | 0.52 | 0.49 | 0.46 | 0.43 |

TABLE 40: Minimal value of concrete shear force capacity

Therefore, according to the calculation results, the bridge's plates do not require shear force reinforcement. This is inherently beneficial for the overall price of the construction due to the high costs of the reduction of shear force in plates which is calibrated through the optimization of plates thickness, (Snellink, 2021).

B.10 Structure's strength control (S/R)

To check the structure's strength a systematic numerical quantitative approach is applied to the beam and plate. The structural system faces multiple types of loads that cause the moment, therefore the S/R ratio check is applied that can be defined as a ratio between the actual maximal moment that occurs in the system and the maximum moment that the structural components can bear. The equation (79) presents the calculation procedure of the S/R ratio which must be bounded between 0.8 and 1. The reason for this numerical boundary can be seen as follows, if the calculated ratio result overcomes 1 it is equivalent to an unsafe and weak structure, on the other hand, if the ratio result is below 0.8 the structure is significantly stronger than required. Therefore, the following calculations aim for the S/R ratio to be close to the numerical value of 0.9. Luckily, according to previous calculations, the structure is safe, nevertheless, an additional calculation is made to exclude any errors and chance of overengineering.

$$0.8 < \frac{S}{R} = \frac{M_d}{M_u} < 1 \quad (79)$$

Where:

M_d = Maximal Moment that can occur in the system

M_u = Maximal Moment that the structure can handle

B.10.1 Beam Check

The dimensions of the beams have been modified, thus the maximal moment that occurs in the beams is changed, its magnitude can be determined with equation (80):

$$M_{d,beam} = M_{new,max,beam} = \frac{1}{8} * q_{new,beam} L_{new,beam}^2 = 622.5kNm \quad (80)$$

Consequently, in order to find the actual moment that the beam can handle the Table 41 (Snellink, 2021) and two equations, mainly the new reinforcement beam ratio $\frac{A_{s_s}}{W*d}$ and $\frac{M_u}{W*d}$.

Considering that in the previous section "Principal Reinforcement Beams" the z/d (see Table 41) was assumed to be 0.8, using the aforementioned method is preferable since the z constant is determined exactly. Besides, an additional inspection concerning the z/d assumption takes place.

$$\text{New reinforcement ratio beams} = \frac{A_{new,s,beam}}{W_{beam} * d_{beam}} = 1.058\% \quad (81)$$

According to the new reinforcement ratio for beams and Table 41, the z/d ratio is bounded between 0.651 and 0.674. Obviously, this is a large deviation from the previously made assumption ($z/d=0.8$), thus using the new values retains the correctness of further calculations.

With the information from Table 41, the $\frac{M_u}{W*d}$ can be calculated:

$$\frac{M_{u,beam}}{W_{new,beam} * d_{new,beam}} = 3600 + (1.058 - 0.996) * \frac{3800 - 3600}{1.066 - 0.996} = 3775.8kN/m^2 \quad (82)$$

Therefore, by applying the reverse calculation procedure the M_u gives the following result, (see equation (83)):

$$M_{u,beam} = 3775.8 * 0.35 * 0.7^2 = 647.5kNm \quad (83)$$

Obtaining both types of moments M_u and M_d , instantly allows to calculate and analyze the S/R ratio:

$$\frac{S}{R} = \frac{M_{u,beam}}{M_{d,beam}} = \frac{622.5}{647.5} = 0.961 \quad (84)$$

The calculation shows that the S/R result is within the accepted boundary. Additionally, the result of 0.96 indicates that the system is safe since all forces are born by the structure, and it is not over-designed meaning that the strength is endured efficiently.

B.10.2 Plate Check

Similarly to the beam, the dimensions of the plate have been changed resulting in a new magnitude for the maximal moment, equation (85):

$$M_{d,plate} = M_{new,max,plate} = \frac{1}{8} * q_{new,plate} d_{new,pin,supports}^2 = 9.225kNm \quad (85)$$

To determine the M_u following the equation the new reinforcement plate ratio $\frac{A_{s,i}}{W*d}$ and $\frac{M_u}{W*d}$.

$$\text{New reinforcement ratio plate} = \frac{A_{new,s,plate}}{W_{plate} * d_{plate}} = 0.2554\% \quad (86)$$

The result of the new reinforcement plate ratio indicated the z/d ratio is bounded by 0.905 and 0.922 (see Table 41) which almost perfectly corresponds to the assumption made in section "Principal Reinforcement Plates" where the z/d was assumed to be 0.9.

Given the new reinforcement ratio for the plate and information provided in Table 41 the $\frac{M_u}{W*d}$ can be determined:

$$\frac{M_{u,plate}}{W_{new,plate} * d_{new,plate}} = 1000 + (0.255 - 0.240) * \frac{1200 - 1000}{0.290 - 0.240} = 1061.4kN/m^2 \quad (87)$$

By a reverse calculation the M_u can be found, (see equation(88)):

$$M_{u,plate} = 1061.4 * 3 * 0.056^2 = 9.986kNm \quad (88)$$

Obtaining both types of moments M_u and M_d , instantly allows to determine and analyze the S/R ratio:

$$\frac{S}{R} = \frac{M_{u,plate}}{M_{d,plate}} = \frac{9.225}{9.986} = 0.92 \quad (89)$$

Similarly to the beam, the S/R ratio for the plates implies that the bridge's plates have been designed strong enough to bear the applied forces as well as avoid overengineering since the strength is endured efficiently.

| C20/25 | | fcd=13.3 N/mm2 | |
|---------------|------------|-----------------------|------------|
| Mu/wd2 | x/d | As/wd | z/d |
| 200 | 0.020 | 0.046 | 0.985 |
| 400 | 0.041 | 0.093 | 0.969 |
| 600 | 0.062 | 0.141 | 0.954 |
| 800 | 0.083 | 0.190 | 0.938 |
| 1000 | 0.104 | 0.240 | 0.922 |
| 1200 | 0.127 | 0.290 | 0.905 |
| 1400 | 0.149 | 0.342 | 0.888 |
| 1600 | 0.172 | 0.394 | 0.871 |
| 1800 | 0.195 | 0.448 | 0.854 |
| 2000 | 0.219 | 0.503 | 0.836 |
| 2200 | 0.244 | 0.559 | 0.817 |
| 2400 | 0.269 | 0.616 | 0.798 |
| 2600 | 0.294 | 0.675 | 0.779 |
| 2800 | 0.321 | 0.735 | 0.759 |
| 3000 | 0.348 | 0.798 | 0.739 |
| 3200 | 0.376 | 0.861 | 0.718 |
| 3400 | 0.404 | 0.928 | 0.697 |
| 3600 | 0.434 | 0.996 | 0.674 |
| 3800 | 0.465 | 1.066 | 0.651 |
| 4000 | 0.497 | 1.140 | 0.627 |
| 4200 | 0.530 | 1.216 | 0.602 |
| 4225 | 0.535 | 1.226 | 0.599 |

TABLE 41: Table used to calculate Mu, (Snellink, 2021)

B.11 Anchorage

To ensure the structural elements' safety, the anchorage must be implemented to principal reinforcement for beams and plates. Thus, the following section determines the required amount of reinforcement and assures that the reinforcements are located correctly.

B.11.1 Beams

The Figure 46 represents the moment diagram for the beam, the moment magnitude at different locations can be recognized by the yellowish color. For example, the highest magnitude of the moment acting on the beam takes place in the center of the beam's length. Considering the calculations from previous sections, two different types of reinforcement bars will be used in the beam. Throughout the whole length of the beam, 4 bars with $\text{Ø}25\text{mm}$ are applied, additionally, 2 more bars with $\text{Ø}20\text{mm}$ are placed closer to the center of the beam to endure the larger moment magnitude.

The anchoring location for beams is determined with the following steps:

Firstly, the moment diagram is enlarged on both sides with the distance $d = 700\text{mm}$.

Next, on the segment of 1963mm^2 (see Figure 46), the reinforcement bars are shifted with the distance l_b which can be determined with the equation (90):

$$l_{b,min,beam} > \max(0.3l_{b,rqd}; 10\text{Ø}; 100) \quad (90)$$

The $l_{b,rqd}$ is determined using the Table 42:

| Concrete class | Good bonding conditions | Bad bonding conditions |
|----------------|-------------------------|------------------------|
| C12/15 | 66Ø | 94Ø |
| C16/20 | 54Ø | 78Ø |
| C20/25 | 47Ø | 67Ø |
| C25/30 | 40Ø | 58Ø |
| C30/37 | 36Ø | 51Ø |
| C35/45 | 32Ø | 46Ø |
| C40/50 | 30Ø | 42Ø |
| C45/55 | 27Ø | 39Ø |
| C50/60 | 25Ø | 36Ø |
| C55/67 | 25Ø | 35Ø |
| C60/75 | 24Ø | 34Ø |

TABLE 42: Bonding conditions

Given the concrete class C20/25 and assuming good bonding conditions:

$$l_{b,rqd} = 47\text{Ø} * \frac{A_{main\ reinforcement,beam}}{A_{new,s,beam}} = 47 * 20 + \frac{1963}{2591} = 712\text{mm} \quad (91)$$

$$0.3 * l_{b,rqd} = 213.6\text{mm} \quad (92)$$

$$10 * \text{Ø} = 200\text{mm} \quad (93)$$

$$l_{b,min,beam} > \max(0.3l_{b,rqd}; 10\text{Ø}; 100) \Rightarrow 213.6\text{mm} \quad (94)$$

Thirdly, on the segment of 2591mm^2 , the reinforcement bars are shifted with the distance $l_{b,rqd,beam}$ which is calculated using the equation (95):

$$l_{b,rqd} = 47\text{Ø} * \frac{A_{new,s,beam,table}}{A_{new,s,beam}} = 47 * 20 + \frac{2556}{2591} = 927.3\text{mm} \quad (95)$$

The anchoring locations are determined, and can be seen in Figure 46, the anchorage is installed at the locations where the moment diagram is enlarged. Consequently, the segment of the required reinforcement is represented in grey color.

The illustration of cross-sections of the beam are represented, where 4 Ø25mm reinforcement bars (represented with white circles) span throughout the full length of the beam adding to the reinforcement area $1963mm^2$. Closer to the middle part of the beam where the anchorage shifts from $1963mm^2$ segment to $2591mm^2$ segment, additional reinforcement bars are placed, mainly 2 Ø20mm (represented with gray circles) giving an additional reinforcement area of $628mm^2$. Finally, the total surface area of the reinforcement bars equals $2591mm^2$.

In the cross-sections of the beam (see Figure 46) the stirrups and top flanges (represented with a black circle) have a diameter of 10mm. The distance between flanges at the top corner and the middle edge of the stirrups is equally distributed on both sides of the beam and equals 270mm.

According to (NEN1991-1-1 C8.4), the minimum distance between the reinforcement bars is defined as:

$$k_1 + \varnothing = 1 + 25 = 26mm \quad (96)$$

Where:

k_1 = National Annex constant = 1mm

\varnothing = The diameter of the largest bar used for the beam's reinforcement = 25mm

The distance between the reinforcement bars is 27mm which implies that the concrete aggregates can penetrate through the reinforcements.

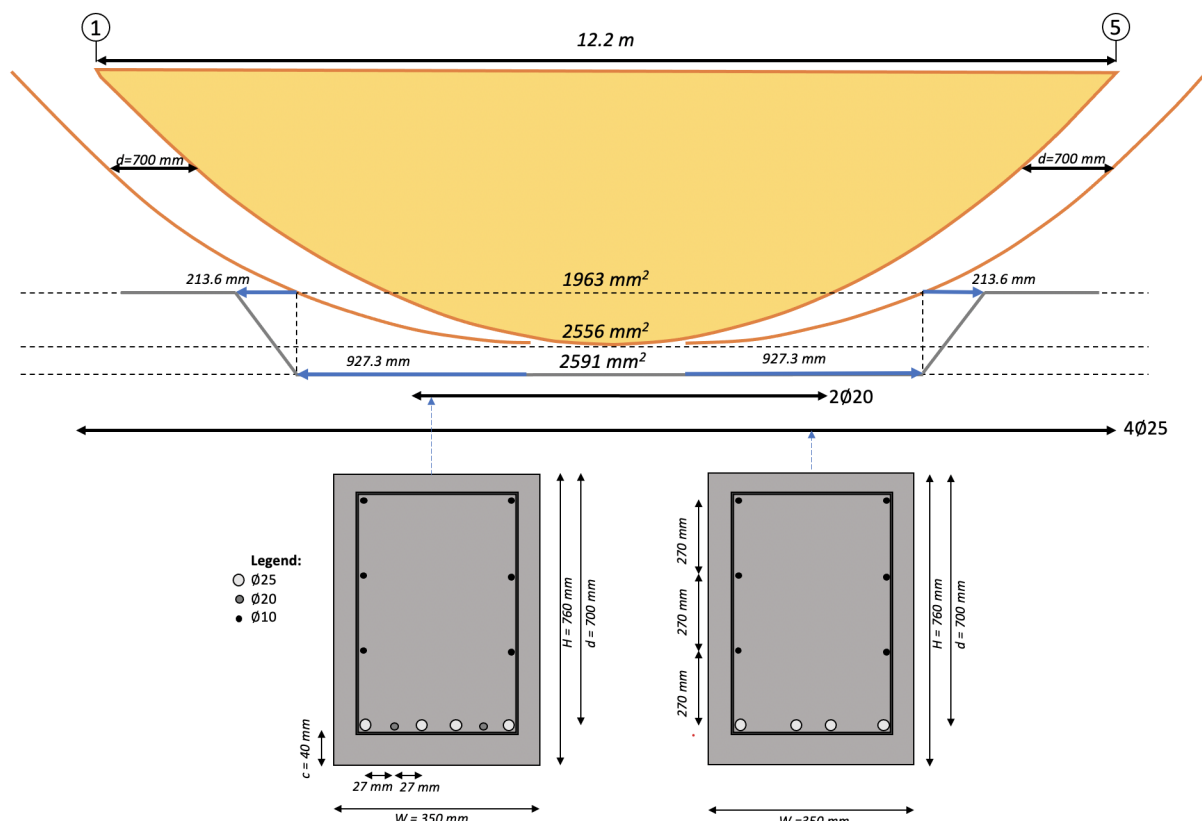


FIGURE 46: Anchoring Beam

B.11.2 Plates

A similar procedure is used to find the location of the anchorage for the plates. For the reinforcement of the plates, multiple types of reinforcement bars are applied. Throughout the whole width of the plate ($W_{plate} = 3m$) bars of $\text{Ø}8$ c.o.c. 150mm are applied which give a reinforcement area of $251mm^2$. To ensure that the plate can fully endure the highest moment (see Figure 47) that occurs in the middle of the plate's width, additional reinforcement bars are added, mainly $\text{Ø}6$ c.o.c. 300 which have a surface area of $94mm^2$.

The anchoring location for beams is determined with the following steps:

The moment diagram is enlarged on both sides with the distance $d = 56mm$.

On the segment of $335mm^2$ (see Figure 47), the reinforcement bars are shifted with the distance l_b which can be determined with the equation (97):

$$l_{b,min,plate} > \max(0.3l_{b,rqd}; 10\text{Ø}; 100) \quad (97)$$

The $l_{b,rqd}$ is determined using the Table (42):

Given the concrete class C20/25 and assuming good bonding conditions:

$$l_{b,rqd} = 47\text{Ø} * \frac{A_{main\ reinforcement,plate}}{A_{new,s,plate}} = 47 * 6 + \frac{335}{429} = 220.2mm \quad (98)$$

$$0.3 * l_{b,rqd} = 66mm \quad (99)$$

$$6 * \text{Ø} = 60mm \quad (100)$$

$$l_{b,min,plate} > \max(0.3l_{b,rqd}; 10\text{Ø}; 100) \Rightarrow 100mm \quad (101)$$

On the segment of $429mm^2$, the reinforcement bars are shifted with the distance $l_{b,rqd,plate}$ which is calculated using the equation (95):

$$l_{b,rqd} = 47\text{Ø} * \frac{A_{new,s,beam,table}}{A_{new,s,plate}} = 47 * 6 + \frac{421}{429} = 276.7mm \quad (102)$$

The cross-section of the plates can be seen in Figure 47, the basic reinforcement bars are placed throughout the total plate's width (represented with silver color) and the additional reinforcement bars are placed closer to the center of the plate's width (represented with gray color), resulting in a total reinforcement area of $429mm^2$.

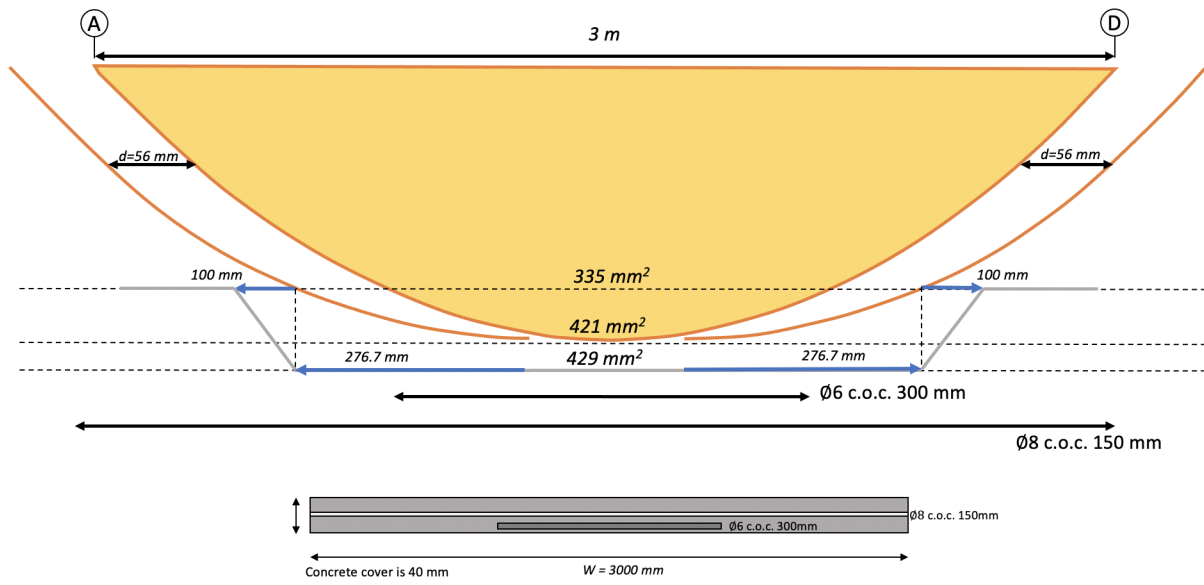


FIGURE 47: Anchoring Plate

B.12 Crack Control

The bridge elements made of concrete belong to the exposure class XC4. Considering this, to reduce the chance of cracks in the system, a calculation procedure verifies if the actual bar spacing is smaller than the maximum allowed bar spacing. Both beam and plate exposure class is XC4, therefore the cracks' maximum acceptable length equals 0.3mm, ("NEN 1992 1-1+C2/NB+A1", 2020).

B.12.1 Beam

Table 43 ("NEN 1990 1-1+C2/NB+A1", 2020) is used to determine the maximum bar spacing with respect to the steel stress which can be determined with equation (103):

$$\sigma_{s,freq,beam} = f_{yd} * \frac{q_{freq,beam}}{q_{d,beam}} * \frac{A_{new,s,beam,table}}{A_{new,s,beam}} \quad (103)$$

Where according to (NEN-EN-1990-2002):

$\sigma_{s,freq,beam}$ = Steel stress, beam

f_{yd} = Yield strength steel reinforcement = 435N/mm²

$q_{freq,beam}$ = Serviceability load per frequency, beam

$q_{d,beam}$ = Strength load per frequency, beam

$A_{new,s,beam,table}$ = Area of reinforcement per beam table value = 2556mm²

$A_{new,s,beam}$ = Total new reinforcement area for beam = 2591mm²

Serviceability:

γ_g = The partial factor for permanent actions = 1

γ_q = The partial factor for variable actions = 1

ψ_1 = The factor for the frequent value of a variable action = 0.5

Strength:

γ_g = The partial factor for permanent actions = 1.35

γ_q = The partial factor for variable actions = 1.5

The strength and serviceability constants are found in ("NEN 1992 1-1+C2/NB+A1", 2020), the $q_{freq,beam}$ and $q_{d,beam}$ can be determined with equations (104) and (105).

$$q_{freq,beam} = \gamma_g P_{beam,new} + \psi_1 \gamma_q A_{q,beam} = 1 * 10.46 + 0.5 * 1 * 17.46 = 19.2kN/m \quad (104)$$

$$q_{d,beam} = \gamma_g P_{beam,new} + \gamma_q A_{q,beam} = 1 * 10.46 + 1.5 * 17.46 = 40.3kN/m \quad (105)$$

Where:

$P_{beam,new}$ = New self-weight of beam = 10.46 kN/m²

$A_{q,beam}$ = Total active loads on the beam = 17.46 kN/m²

With this information the $\sigma_{s,freq,beam}$ can be calculated:

$$\sigma_{s,freq,beam} = f_{yd} * \frac{q_{freq,beam}}{q_{d,beam}} * \frac{A_{new,s,beam,table}}{A_{new,s,beam}} = 435 * \frac{19.2}{40.3} * \frac{2556}{2591} = 204.3MPa \quad (106)$$

Following the calculated steel stress $\sigma_{s,freq,beam}$, and using the Table 43 ("NEN 1992 1-1+C2/NB+A1", 2020) where the steel stress is selected as 250 MPa, the maximum bar spacing corresponds to 200 mm. Considering that the beam's width equals 350 mm and 6 bars are used as reinforcement, the width between the bars will be certainly less than 200 mm, therefore, the reinforcement design complies with the imposed standards.

| Steel stress [MPa] | Maximum bar spacing [mm] | | |
|--------------------|--------------------------|-------------|-------------|
| | wk=0,4 [mm] | wk=0,3 [mm] | wk=0,2 [mm] |
| 160 | 300 | 300 | 200 |
| 200 | 300 | 250 | 150 |
| 240 | 250 | 200 | 100 |
| 280 | 200 | 150 | 50 |
| 320 | 150 | 100 | - |
| 360 | 100 | 50 | - |

TABLE 43: Maximum bar spacing, (Snellink, 2021)

B.12.2 Plate

The same steps for the crack control for plates. The cracks' maximum acceptable length equals 0.3mm, (NEN 1992-1-1), thus steel stress needs to be determined to find out the allowed maximum bar spacing. A similar calculation procedure as for the beam will follow for the plates. Nevertheless, $q_{freq,plate}$ and $q_{d,plate}$ will be given in kN/m^2 , however sine these factors are reduced one by another (see equation (107)) no modifications are being applied throughout the calculation steps.

$$\sigma_{s,freq,plate} = f_{yd} * \frac{q_{freq,plate}}{q_{d,plate}} * \frac{A_{new,s,plate,table}}{A_{new,s,plate}} \quad (107)$$

Where according to ("NEN 1990 1-1+C2/NB+A1", 2020):

$\sigma_{s,freq,plate}$ = Steel stress, plate

f_{yd} = Yield strength steel reinforcement = $435N/mm^2$

$q_{freq,plate}$ = Serviceability load per frequency, plate

$q_{d,plate}$ = Strength load per frequency, plate

$A_{new,s,plate,table}$ = Area of reinforcement per plate table value = $421mm^2$

$A_{new,s,plate}$ = Total new reinforcement area for plate = $429mm^2$

Serviceability:

γ_g = The partial factor for permanent actions = 1

γ_q = The partial factor for variable actions = 1

ψ_1 = The factor for the frequent value of a variable action = 0.5

Strength:

γ_g = The partial factor for permanent actions = 1.35

γ_q = The partial factor for variable actions = 1.5

The strength and severability constants are found in ("NEN 1990 1-1+C2/NB+A1", 2020), the $q_{freq,plate}$ and $q_{d,plate}$ can be determined with equations (108) and (109).

$$q_{freq,plate} = \gamma_g P_{plate,new} + \psi_1 \gamma_q A_{q,plate} = 1 * 2.8 + 0.5 * 1 * 6.08 = 5.84kN/m \quad (108)$$

$$q_{d,plate} = \gamma_g P_{plate,new} + \gamma_q A_{q,plate} = 1 * 2.8 + 1.5 * 6.08 = 12.9kN/m \quad (109)$$

Where:

$P_{plate,new}$ = New self-weight of plate = $2.8 kN/m^2$

$A_{q,plate}$ = Total active loads on the plate = $6.08kN/m^2$

Then the $\sigma_{s,freq,plate}$ can be is determined:

$$\sigma_{s,freq,plate} = f_{yd} * \frac{q_{freq,plate}}{q_{d,plate}} * \frac{A_{new,s,plate,table}}{A_{new,s,plate}} = 435 * \frac{5.84}{12.9} * \frac{421}{429} = 193MPa \quad (110)$$

Considering the determined steel stress and following the Table 43, the maximum bar spacing equals 250mm. The maximum bar spacing in plates is 150mm, subsequently indicating that the design requirement is satisfied.

B.13 Conclusion

To conclude, all structural elements of the bridge design comply with all required Dutch construction norms. Additionally, the system has been checked on its strength and it can withstand all potential combinations of loads that can be applied. The final dimensions of the bridge can be seen in Figures 48, 49, and 50. Additionally, the final reinforcement of the beam and plate is represented in Figures 51 and 52.

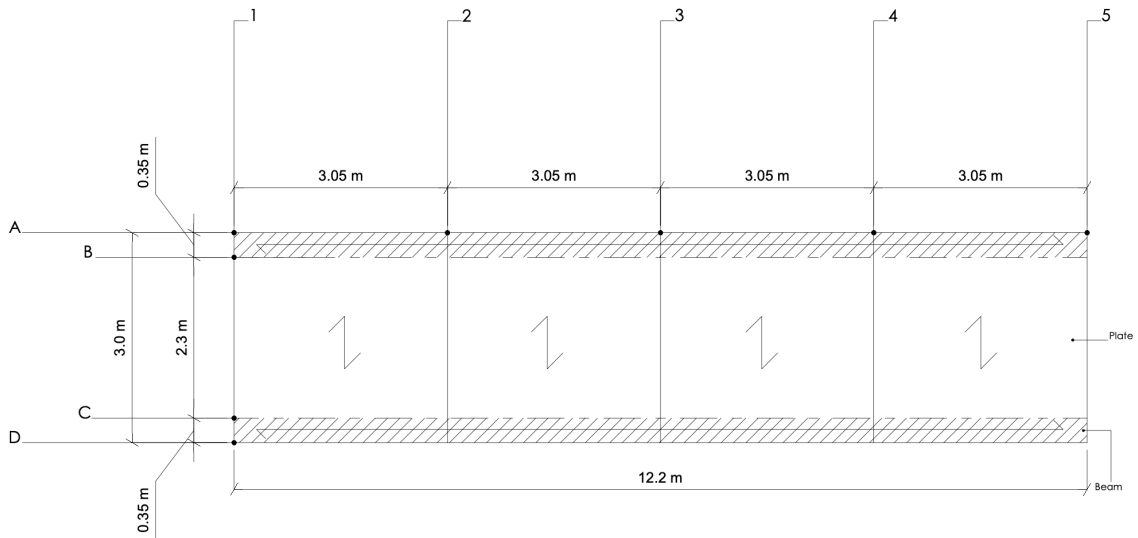


FIGURE 48: Final Design - Top View

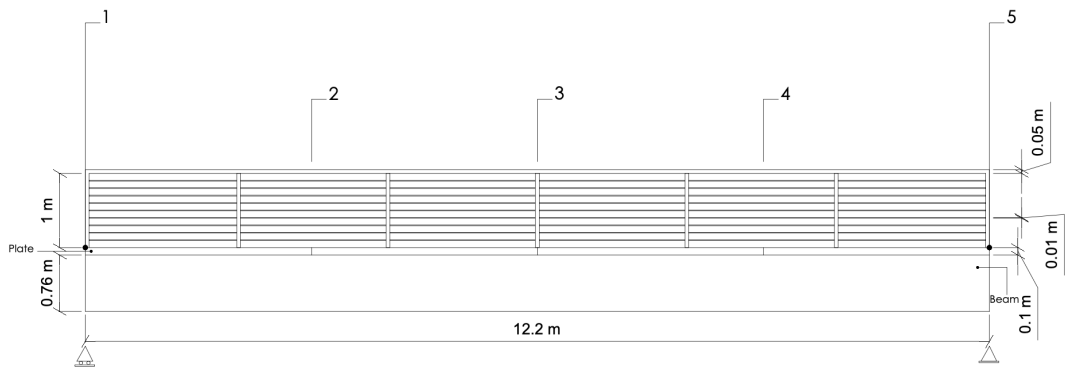


FIGURE 49: Final Design - Side View

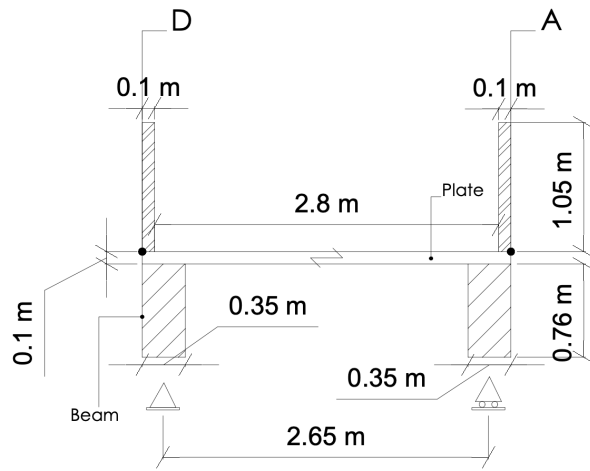


FIGURE 50: Final Design - Front View

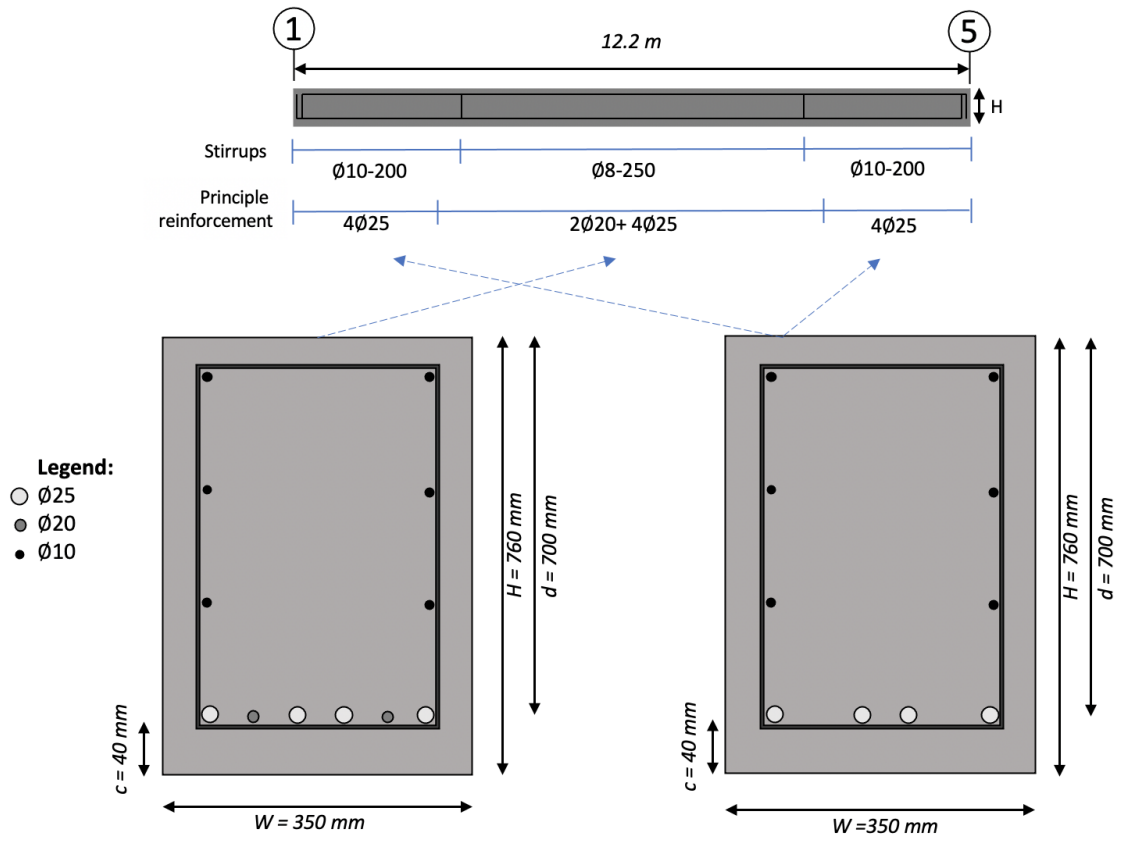


FIGURE 51: Beam with final reinforcement

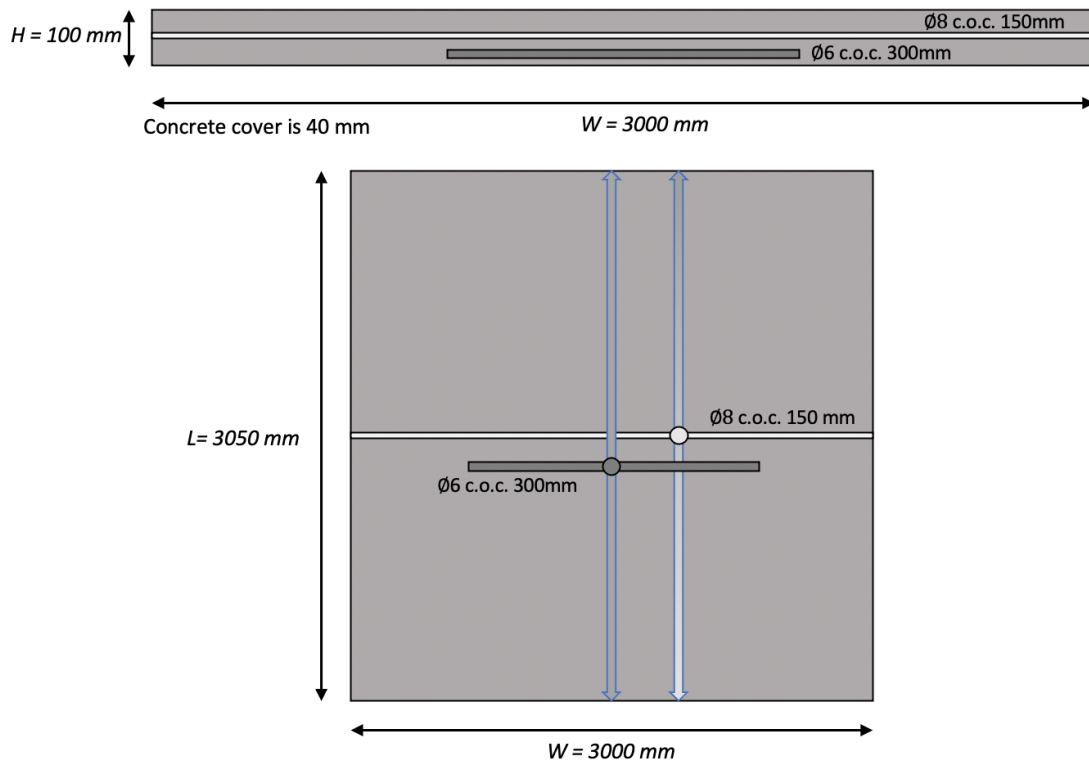


FIGURE 52: Plate with final reinforcement

C LCC results of Case Study

C.1 Production and Construction phase costs



FIGURE 53: Histogram Production-Construction phase costs

C.2 Use phase costs

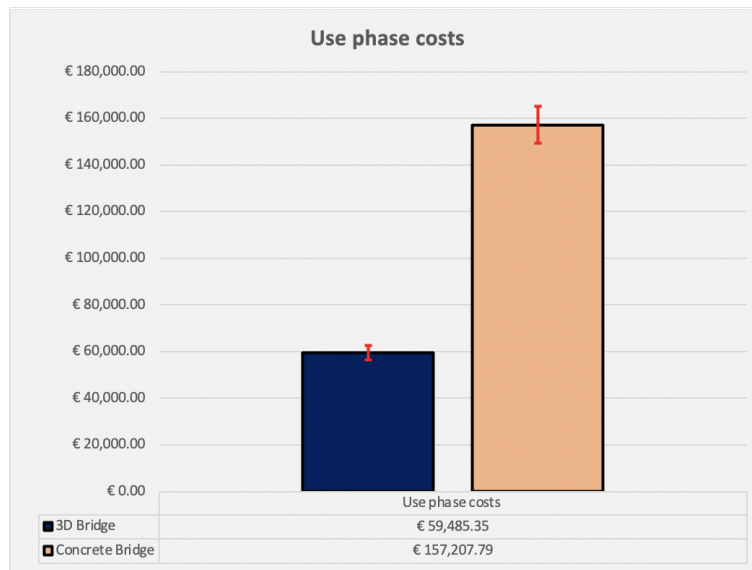


FIGURE 54: Histogram Use phase costs

C.3 End-of-life phase costs



FIGURE 55: Histogram End-of-life phase costs

C.4 Concrete bridge activities distribution

| Component/Activity |
|---|
| Beams reinforced |
| Plates reinforced |
| Railings |
| Reinforced Concrete Material |
| Stainless steel G304 (railings) Material |
| Truck driven from the factory to the bridge and back, steel and concrete construction phase |
| Crane driven from the origin and back construction phase |
| Crane operated during construction phase |
| Machinery 1 (used by construction crew) construction phase |
| Machinery 2 (used by construction crew) construction phase |
| Crane rental construction-phase |
| Truck driven from the factory to the bridge and back, steel and concrete construction phase |
| Crane driven from the origin and back construction phase |
| Construction crew (6 people) construction phase |
| Cleaning machinery (pressure washer) concrete use phase |
| Plastering machnie (painting) concrete use phase |
| Repairing machinery (saw) (construction crew) reinforcement use phase |
| Removal machinery (corosion cleaner) corosion use phase |
| Cleaning machinery (pressure washer) parapet and rainwaterdischarge use phase |
| Water for the cleaning machinery concrete cleaning Material |
| Concrete Paint (2.5l/m ²) Material |
| Water for the cleaning machinery concrete cleaning Material |
| Repair Mortar (polymer) Material |
| Cleaning machinery (pressure washer)(cleaner) concrete use phase |
| Plastering machnie (painting)(maintenance workers) concrete use phase |
| Repairing machinery (saw) (construction crew) reinforcement use phase |
| Removal machinery (corosion cleaner)(maintenance workers) corosion use phase |
| Cleaning machinery (pressure washer)(cleaner) parapet and rainwaterdischarge use phase |
| Concrete repair works |
| Truck driven from the factory to the bridge and back, steel and concrete end of life phase |
| Crane driven from the origin and back end-of-life phase |
| Crane operated during end-of-life phase phase |
| Machinery 1 (used by construction crew) end-of-life phase |
| Machinery 2 (used by construction crew) end-of-life phase |
| Machinery 4 (drill used by construction crew) end-of-life phase |
| Machinery 5 (saw used by construction crew) end-of-life phase |
| Crane rental end-of -life phase |
| Truck driven from the factory to the bridge and back, steel and concrete end of life phase |
| Crane driven from the origin and back end-of-life phase |
| Construction crew (6 people) end-of-life phase |
| Concrete Disposal |
| Steel Recycling |

FIGURE 56: Concrete bridge activities distribution per costs categories

C.5 3D printed bridge activities distribution

| Component/Activity |
|--|
| Bridge production phase |
| Stainless steel grade 304L |
| Boat driven from the MX3D to the bridge and back construction phase |
| Crane driven from the origin and back construction phase |
| Crane operated during construction phase |
| Machinery 1 (used by construction crew) construction phase |
| Machinery 2 (used by construction crew) construction phase |
| 3D printing |
| Crane rental construction-phase |
| Boat driven from the MX3D to the bridge and back construction phase |
| Crane driven from the origin and back end-of-life phase |
| Construction crew (10 people) construction phase |
| Bridge Deck power wash with water to remove salt residue (pressure washer) Use phase |
| Expansion Joints power wash with water to remove debris, sand and salt residue (pressure washer) Use phase |
| Bridge Seats clean around bearings by flushing with (air blast) Use phase |
| Paint isolated areas of rusted steel (painting) (once in 2-4years) Use phase |
| Removal machinery (corosion cleaner) corosion Use phase |
| Water for Deck power wash with water to remove salt residue |
| Water for Expansion Joints power wash |
| Paint isolated areas of rusted steel |
| Bridge Deck power wash with water to remove salt residue (pressure washer) |
| Expansion Joints power wash with water to remove debris, sand and salt residue (pressure washer) |
| Bridge Seats clean around bearings by flushing with (air blast) |
| Paint isolated areas of rusted steel (painting) (once in 2-4years) |
| Removal machinery (corosion cleaner) corosion use phase |
| Truck driven from the factory to the bridge and back, steel and concrete end of life phase |
| Crane driven from the origin and back end-of-life phase |
| Crane operated during end-of-life phase |
| Machinery 1 (used by construction crew) end-of-life phase |
| Machinery 2 (used by construction crew) end-of-life phase |
| Machinery 4 (drill used by construction crew) end-of-life phase |
| Machinery 5 (saw used by construction crew) end-of-life phase |
| Crane rental end-of -life phase |
| Truck driven from the factory to the bridge and back, steel and concrete end of life phase |
| Crane driven from the origin and back end-of-life phase |
| Construction crew (10 people) end-of-life phase |
| Steel Recycling |

FIGURE 57: 3D printed bridge activities distribution per costs categories

C.6 Cost Categories

| |
|-----------------------|
| Components Category |
| Construction/disposal |
| Transportation |
| Electricity |
| Labour/rental |
| Material |

FIGURE 58: Costs categories

C.7 Concrete bridge Uncertainty

| Variables | Activity Name | Initial values | Unit | Type of distribution | Deviation from mean value (minimum to maximum value) | Minimal value | Maximal Value | Unit | 50% from Minimal deviation | 50% from Maximal deviation | | | |
|---|---|---|----------------------|----------------------|--|----------------|----------------|-------------|----------------------------|----------------------------|----------------|---------------------|--------|
| Activity duration | Amount of time Truck transports Beams and returns to the origin construction phase | 3.5 | h | Triangular | (-10% to +10%) | -10 | 10 | 3.15 | 3.85 | h | 3.325 | 3.675 | |
| | Amount of time Truck transports Plates and returns to the origin construction phase | 3.5 | h | | (-10% to +10%) | -10 | 10 | 3.15 | 3.85 | h | 3.325 | 3.675 | |
| | Amount of time Truck transports Railings and returns to the origin construction phase | 1.5 | h | | (-10% to +10%) | -10 | 10 | 1.35 | 1.65 | h | 1.425 | 1.575 | |
| | Amount of time Crane travels and returns to the origin construction phase | 1 | h | | (-10% to +10%) | -10 | 10 | 0.9 | 1.1 | h | 0.95 | 1.05 | |
| | Amount of time Crane is used at the construction site construction phase | 5 | h | | (-10% to +10%) | -10 | 10 | 4.5 | 5.5 | h | 4.75 | 5.25 | |
| | Cleaning machinery (pressure washer) concrete use phase | 1.5 | h | | (-10% to +10%) | -10 | 10 | 1.35 | 1.65 | h | 1.425 | 1.575 | |
| | Activity distance to travel | Distance to travel Beams construction phase | 80 | km | Triangular | (-40% to +40%) | -40 | 40 | 48 | 112 | km | 64 | 96 |
| | | Distance to travel Plates construction phase | 80 | km | | (-40% to +40%) | -40 | 40 | 48 | 112 | km | 64 | 96 |
| | | Distance to travel Railings construction phase | 30 | km | | (-40% to +40%) | -40 | 40 | 18 | 42 | km | 24 | 36 |
| | | Distance to travel Crane construction phase | 18 | km | | (-40% to +40%) | -40 | 40 | 10.8 | 25.2 | km | 14.4 | 21.6 |
| | | Distance from Beams construction phase | 80 | km | | (-40% to +40%) | -40 | 40 | 48 | 112 | km | 64 | 96 |
| | | Distance from Plates construction phase | 80 | km | | (-40% to +40%) | -40 | 40 | 48 | 112 | km | 64 | 96 |
| Activity unit price | | Truck Driver wage | 14.8 | euro/h | Triangular | (-10% to +10%) | -10 | 10 | 13.32 | 16.28 | euro/h | 14.06 | 15.54 |
| | | Crane Driver wage | 23.5 | euro/h | | (-10% to +10%) | -10 | 10 | 21.15 | 25.85 | euro/h | 22.325 | 24.675 |
| | | Contractor (contractor from the construction crew) wage | 21.7 | euro/h | | (-10% to +10%) | -10 | 10 | 19.53 | 23.87 | euro/h | 20.615 | 22.785 |
| | | Cleaner (pressure washer) wage | 12.2 | euro/h | | (-10% to +10%) | -10 | 10 | 10.98 | 13.42 | euro/h | 11.59 | 12.81 |
| | | Concrete maintenance worker wage | 20.1 | euro/h | | (-10% to +10%) | -10 | 10 | 18.09 | 22.11 | euro/h | 19.095 | 21.105 |
| | | Reinforced Concrete Material | 480 | euro/m ³ | | Triangular | (-10% to +10%) | -10 | 10 | 432 | 528 | euro/m ³ | 456 |
| | Stainless steel (304) (railings) Material | 1,625 | euro/kg | (-10% to +10%) | -10 | | 10 | 1,462.5 | 1,787.5 | euro/kg | 1,543.75 | 1,706.25 | |
| | Crane rental construction phase | 146 | euro/h | (-10% to +10%) | -10 | | 10 | 131.4 | 160.6 | euro/h | 138.7 | 153.3 | |
| | Crane rental end-of-life phase | 146 | euro/h | (-10% to +10%) | -10 | | 10 | 131.4 | 160.6 | euro/h | 138.7 | 153.3 | |
| | Beams reinforced concrete | 6.4904 | m ³ | Triangular | (-25% to +25%) | | -25 | 25 | 4.8678 | 8.113 | m ³ | 5.6791 | 7.3017 |
| | Plates reinforced concrete | 3.86 | m ³ | | (-10% to +10%) | | -10 | 10 | 3.294 | 4.026 | m ³ | 3.477 | 3.843 |
| | Reinforcements Beams | 0.0156 | m ³ | | (-0.04% to +0.04%) | -0.04 | 0.04 | 0.0150964 | 0.0159036 | m ³ | 0.0155032 | 0.0156968 | |
| Reinforcements Plates | 0.000744 | m ³ | (-0.002% to +0.002%) | | -0.002 | 0.002 | 0.000743985 | 0.000744015 | m ³ | 0.000743993 | 0.000744007 | | |
| Stirrups Beams | 0.00824 | m ³ | (-0.03% to +0.03%) | | -0.03 | 0.03 | 0.008237528 | 0.008242472 | m ³ | 0.008238764 | 0.008241236 | | |
| Railings | 0.20924729 | m ³ | (-60% to +60%) | | -60 | 60 | 0.08368832 | 0.334792727 | m ³ | 0.16447313 | 0.272011258 | | |
| Number of workers required per activity | Construction crew (8 people) construction phase | 8 | # | Triangular | (-3 worker to +3 worker) | -3 | 3 | 5 | 11 | # | 6.5 | 9.5 | |
| | Plastering machine (painting) concrete use phase | 2 | # | | (-1 worker to +1 worker) | -1 | 1 | 1 | 3 | # | 1.5 | 2.5 | |
| | Repairing machinery (lawn) (construction crew) reinforcement use phase | 4 | # | | (-1 worker to +1 worker) | -1 | 1 | 3 | 5 | # | 3.5 | 4.5 | |
| | Removal machinery (concrete cleaner) concrete use phase | 2 | # | | (-1 worker to +1 worker) | -1 | 1 | 1 | 3 | # | 1.5 | 2.5 | |
| | Construction crew (6 people) end-of-life phase | 6 | # | | (-2 worker to +2 worker) | -2 | 2 | 4 | 8 | # | 5 | 7 | |
| Activity frequency | Cleaning machinery (pressure washer) concrete use phase | 100 | times in 100y | Triangular | (-20% to +20%) | -20 | 20 | 80 | 120 | times in 100y | | | |
| | Plastering machine (painting) concrete use phase | 20 | times in 100y | | (-5% to +5%) | -5 | 5 | 19 | 21 | times in 100y | | | |
| | Repairing machinery (lawn) (construction crew) reinforcement use phase | 7 | times in 100y | | (-5% to +5%) | -5 | 5 | 6.55 | 7.45 | times in 100y | | | |
| | Removal machinery (concrete cleaner) concrete use phase | 50 | times in 100y | | (-10% to +10%) | -10 | 10 | 45 | 55 | times in 100y | | | |
| | Cleaning machinery (pressure washer) parapet and rainwater discharge use phase | 100 | times in 100y | | (-20% to +20%) | -20 | 20 | 80 | 120 | times in 100y | | | |
| Dimensions of structural elements | Concrete repair works | 7 | times in 100y | Triangular | (-5% to +5%) | -5 | 5 | 6.65 | 7.35 | times in 100y | | | |
| | Beam width | 0.35 | m | | (-25% to +25%) | -25 | 25 | 0.2625 | 0.4375 | m | 0.3025 | 0.3975 | |
| Price for steel recycling | Beam height | 0.76 | m | Triangular | (-25% to +25%) | -25 | 25 | 0.57 | 0.95 | m | 0.665 | 0.855 | |
| | Price for steel recycling | 6800 | euro/m ³ | | (-20% to +20%) | -20 | 20 | 5440 | 8160 | euro/m ³ | 4760 | 8840 | |
| Discount Rate | Discount rate | 2.5 | % | Triangular | (-40% to +40%) | -40 | 40 | 1.5 | 3.5 | euro/m ³ | 2 | 3 | |
| | | | | | | | | | | | | | |

FIGURE 59: Uncertainty Concrete bridge

C.8 3D printed bridge Uncertainty

| Variables | Activity Name | Initial values | Unit | Type of distribution | Deviation from mean value (minimum to maximum value) | Minimal value | Maximal Value | Unit | |
|--|--|-----------------------------|------------|----------------------|--|---------------|---------------|--------|-----------------------|
| Activity duration | Amount of time Boat transports Bridge and returns to the origin construction phase | 5 h | | Triaogular | (-10% to +10%) | -10 | 4.5 | 5.5 h | |
| | Amount of time Crane travels and returns to the origin construction phase | 1 h | | | (-10% to +10%) | -10 | 0.9 | 1.1 h | |
| | Amount of time Crane is used at the construction sight construction phase | 4 h | | | (-10% to +10%) | -10 | 3.6 | 4.4 h | |
| | Machinery 1 (used by construction crew) construction phase | 5 h | | Triaogular | (-10% to +10%) | -10 | 4.5 | 5.5 h | |
| | Machinery 2 (used by construction crew) construction phase | 5 h | | | (-10% to +10%) | -10 | 4.5 | 5.5 h | |
| | Bridge Deck power wash with water to remove salt residue (pressure washer) Use phase | 1.5 h | | | (-10% to +10%) | -10 | 1.35 | 1.65 h | |
| | Expansion joints power wash with water to remove debris, sand and salt residue (pressure washer) Use phase | 1 h | | Triaogular | (-10% to +10%) | -10 | 0.9 | 1.1 h | |
| | Bridge Seats clean around bearings by flushing with (air blast) Use phase | 1 h | | | (-10% to +10%) | -10 | 0.9 | 1.1 h | |
| | Paint isolated areas of rusted steel (painting) (once in 2-4years) Use phase | 2 h | | | (-10% to +10%) | -10 | 1.8 | 2.2 h | |
| | Removal machinery (corrosion cleaner) corrosion Use phase | 2.5 h | | Triaogular | (-10% to +10%) | -10 | 2.25 | 2.75 h | |
| | Amount of time Truck transports Bridge to the recycling point end-of-life phase | 3 h | | | (-10% to +10%) | -10 | 2.7 | 3.3 h | |
| | Amount of time Crane travels and returns to the origin end-of-life phase | 1 h | | | (-10% to +10%) | -10 | 0.9 | 1.1 h | |
| Amount of time Crane is used at the construction sight end-of-life phase | 6 h | | Triaogular | (-10% to +10%) | -10 | 5.4 | 6.6 h | | |
| Distance to travel Crane construction phase | 18 km | | | (-40% to +40%) | -10.8 | 25.2 km | | | |
| Distance from Crane construction phase | 18 km | | | (-40% to +40%) | -10.8 | 25.2 km | | | |
| Activity distance to travel | Distance to travel Truck | 79 km | | Triaogular | (-40% to +40%) | -47.4 | 110.6 km | | |
| | Distance to travel Crane end-of-life phase | 18 km | | | (-40% to +40%) | -10.8 | 25.2 km | | |
| | Distance from Truck end-of-life phase | 79 km | | Triaogular | (-40% to +40%) | -47.4 | 110.6 km | | |
| | Distance from Crane end-of-life phase | 18 km | | | (-40% to +40%) | -10.8 | 25.2 km | | |
| Activity unit price | Truck Drive wage | 14.8 euro/h | | Triaogular | (-10% to +10%) | 13.32 | 16.28 | euro/h | |
| | Boat Driver wage | 21.5 euro/h | | | (-10% to +10%) | -10 | 19.35 | 23.65 | euro/h |
| | Crane Driver wage | 23.5 euro/h | | | (-10% to +10%) | -10 | 21.15 | 25.85 | euro/h |
| | Constructor (constructor from the construction crew) wage | 21.7 euro/h | | Triaogular | (-10% to +10%) | -10 | 19.53 | 23.87 | euro/h |
| | Cleaner (pressure washer) wage | 12.2 euro/h | | | (-10% to +10%) | -10 | 10.98 | 13.42 | euro/h |
| | Steel maintenance worker wage | 20.1 euro/h | | | (-10% to +10%) | -10 | 18.09 | 22.11 | euro/h |
| | Stainless steel grade 304L | 1.8 euro/kg | | Triaogular | (-10% to +10%) | -10 | 1.62 | 1.98 | euro/kg |
| | Crane rental construction-phase | 146 euro/h | | Triaogular | (-10% to +10%) | -10 | 131.4 | 160.6 | euro/h |
| | Crane rental end-of-life phase | 146 euro/h | | Triaogular | (-10% to +10%) | -10 | 131.4 | 160.6 | euro/h |
| | Paint isolated areas of rusted steel | 3.06 (euro/m ²) | | Triaogular | (-10% to +10%) | -10 | 2.754 | 3.366 | euro/m ² |
| Number of workers required per activity | Construction crew (10 people) construction phase | 10 # | | Triaogular | (-3 worker to +3 worker) | -3 | 7 | 13 # | |
| | Paint isolated areas of rusted steel (painting) (once in 2-4years) | 2 # | | | (-1 worker to +1 worker) | -1 | 1 | 3 # | |
| | Removal machinery (corrosion cleaner) corrosion use phase | 2 # | | | (-1 worker to +1 worker) | -1 | 1 | 3 # | |
| | Construction crew (10 people) end-of-life phase | 10 # | | Triaogular | (-3 worker to +3 worker) | -3 | 7 | 13 # | |
| Activity frequency | Bridge Deck power wash with water to remove salt residue (pressure washer) Use phase | 100 times in 100y | | Triaogular | (-20% to +20%) | -20 | 20 | 80 | |
| | Expansion joints power wash with water to remove debris, sand and salt residue (pressure washer) Use phase | 100 times in 100y | | | (-20% to +20%) | -20 | 20 | 80 | |
| | Bridge Seats clean around bearings by flushing with (air blast) Use phase | 100 times in 100y | | | (-20% to +20%) | -20 | 20 | 80 | |
| | Paint isolated areas of rusted steel (painting) (once in 2-4years) Use phase | 34 times in 100y | | | (-30% to +30%) | -30 | 30 | 24 | |
| | Removal machinery (corrosion cleaner) corrosion Use phase | 25 times in 100y | | | (-10% to +10%) | -10 | 10 | 23 | |
| 3D Printing | Arc Voltage [V] | 19.5 V | | Triaogular | (-8% to +8%) | -1.8 | 1.8 | 21 V | |
| | Arc Voltage [A] | 120 A | | | (-17% to +17%) | -17 | 17 | 140 A | |
| | Deposition rate | 1.25 kg/h | | | (-40% to +60%) | -40 | 60 | 0.5 | 2 kg/h |
| Geometric characteristics | Mass | 7800 kg | | Triaogular | (-20% to +20%) | -20 | 20 | 6240 | |
| | Total Area of the bridge (m ²) | 141.65 m ² | | | (-20% to +20%) | -20 | 20 | 113.32 | 169.98 m ² |
| Price for steel recycling | Price for steel recycling | -6800 euro/m ³ | | Triaogular | (-20% to +20%) | -20 | 20 | -5440 | |
| Discount Rate | Discount rate | 2.5 % | | Triaogular | (-40% to +40%) | -40 | 40 | 1.5 | |

FIGURE 60: Uncertainty 3D printed bridge

C.9 LCC variation of 3D and Concrete bridges

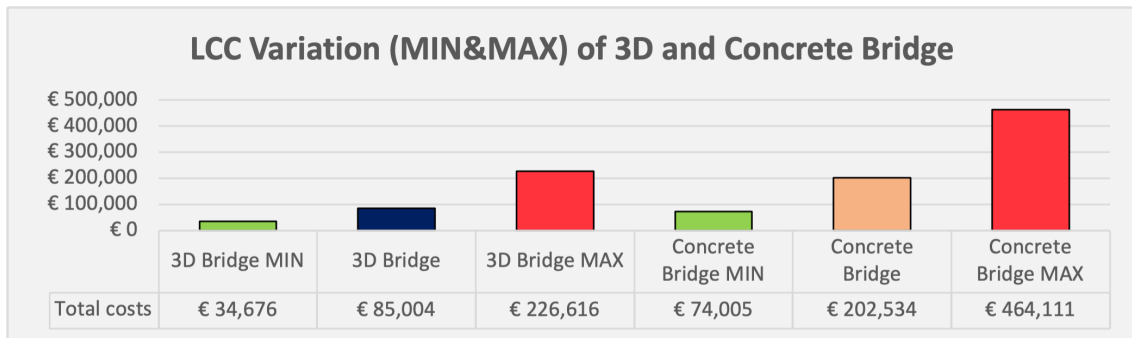


FIGURE 61: Maximum and Minimum LCC deviation from the mean value

C.10 Maximum and Minimal LCC deviation for Concrete bridge

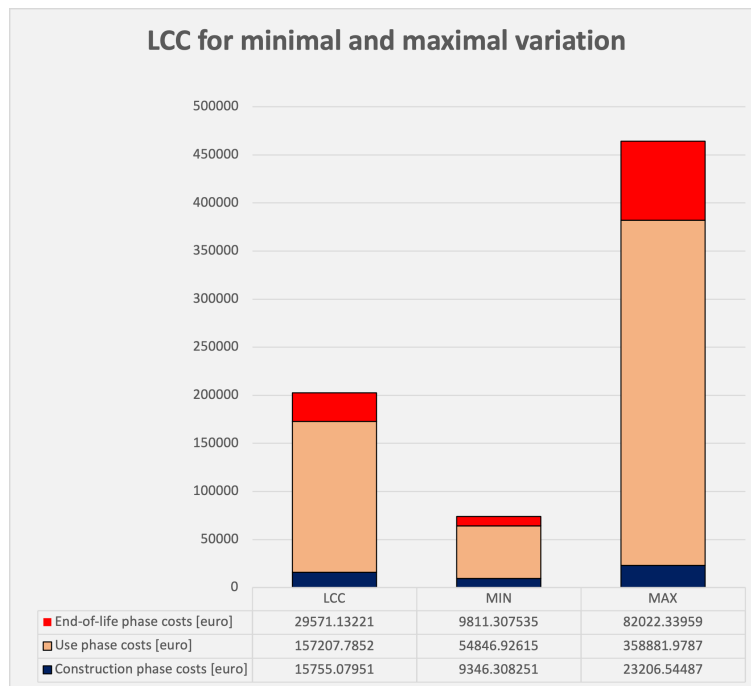


FIGURE 62: Maximum and Minimal LCC deviation, Concrete bridge

C.11 Maximum and Minimal LCC deviation for 3D printed bridge

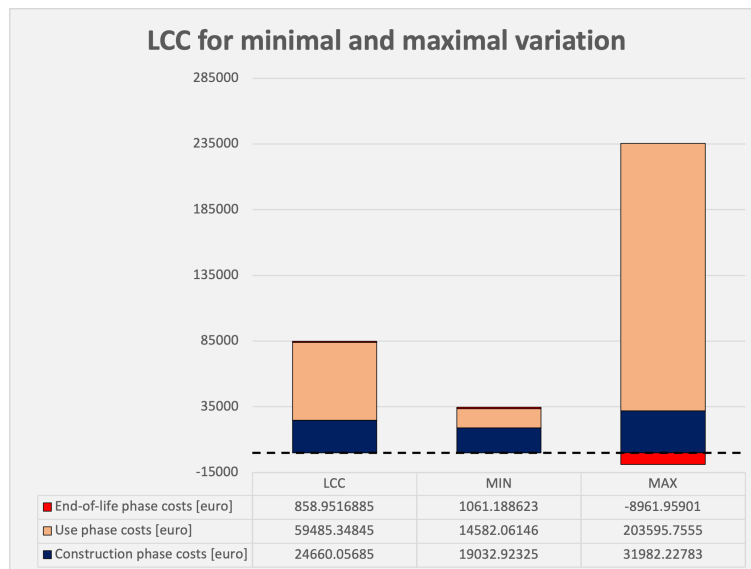


FIGURE 63: Maximum and Minimal LCC deviation, 3D printing bridge

C.12 Initial deviation for Concrete bridge

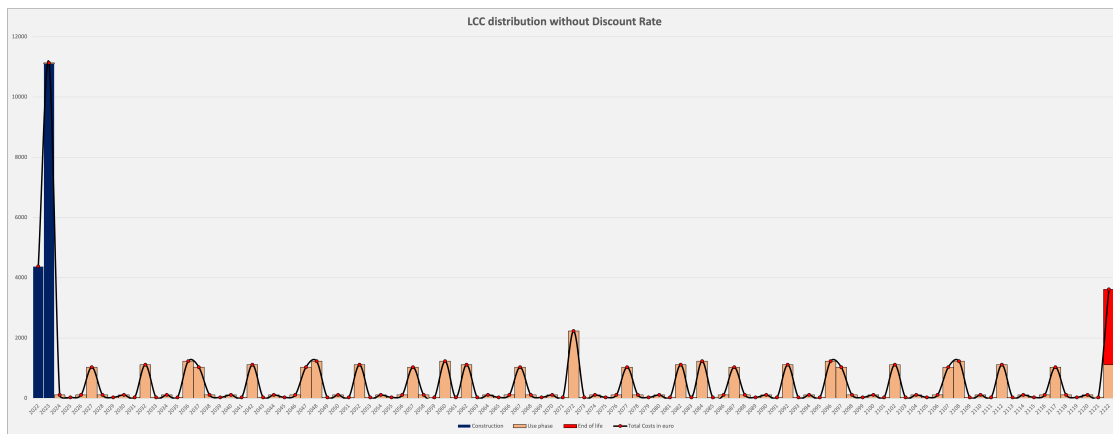


FIGURE 64: Initial LCC (no discount factor application) Concrete bridge

C.13 Initial deviation for 3D Printed bridge

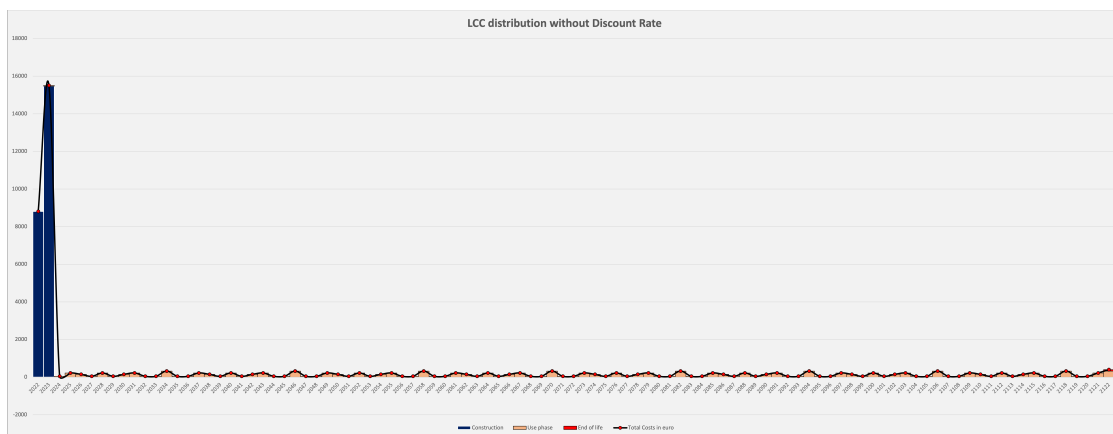


FIGURE 65: Initial LCC (no discount factor application) 3D printed bridge

C.14 LCC comparison for Concrete and 3D Printed bridges

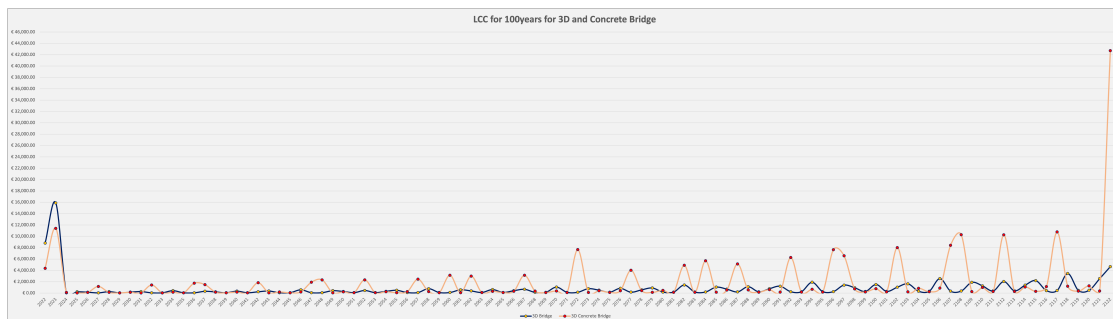


FIGURE 66: LCC comparison for Concrete and 3D printed bridges

C.15 Concrete bridge activity costs calculation

| | LCC | | | | | | | |
|--|---|--|-------------------|--------------|--------------|--------------------------------------|------------------------------------|--------------------------------------|
| | Component/Activity | Cost of 1 unit | Frequency in 100y | Total cost | Duration [y] | Starting year of the first iteration | Ending year of the first iteration | Time boundary between iterations [y] |
| Production | Beams reinforced | 250.5081313 | 1 | 250.5081313 | 2 | 2022 | 2023 | 100 |
| | Plates reinforced | 141.2639838 | 1 | 141.2639838 | 2 | 2022 | 2023 | 100 |
| | Railings | 767.8539989 | 1 | 767.8539989 | 2 | 2022 | 2023 | 100 |
| | Reinforced Concrete Material | 4872.192 | 1 | 4872.192 | 2 | 2022 | 2023 | 100 |
| | Stainless steel G304 (railings) Material | 2720.215278 | 1 | 2720.215278 | 2 | 2022 | 2023 | 100 |
| Construction | Truck driven from the factory to the bridge and back, steel and concrete construction phase | 232.96 | 1 | 232.96 | 1 | 2023 | 2023 | 100 |
| | Crane driven from the origin and back construction phase | 14.688 | 1 | 14.688 | 1 | 2023 | 2023 | 100 |
| | Crane operated during construction phase | 122.4 | 1 | 122.4 | 1 | 2023 | 2023 | 100 |
| | Machinery 1 (used by construction crew) construction phase | 2.31 | 1 | 2.31 | 1 | 2023 | 2023 | 100 |
| | Machinery 2 (used by construction crew) construction phase | 2.75 | 1 | 2.75 | 1 | 2023 | 2023 | 100 |
| | Crane rental construction-phase | 876 | 1 | 876 | 1 | 2023 | 2023 | 100 |
| | Truck driven from the factory to the bridge and back, steel and concrete construction phase | 125.8 | 1 | 125.8 | 1 | 2023 | 2023 | 100 |
| | Crane driven from the origin and back construction phase | 141 | 1 | 141 | 1 | 2023 | 2023 | 100 |
| | Construction crew (6 people) construction phase | 5208 | 1 | 5208 | 1 | 2023 | 2023 | 100 |
| | Cleaning machinery (pressure washer) concrete use phase | 0.6765 | 100 | 67.65 | 1 | 2023 | 2023 | 1 |
| Use | Plastering machine (painting) concrete use phase | 0.924 | 20 | 18.48 | 1 | 2027 | 2027 | 5 |
| | Repairing machinery (saw) (construction crew) reinforcement use phase | 0.528 | 7 | 3.696 | 1 | 2036 | 2036 | 12 |
| | Removal machinery (corrosion cleaner) corrosion use phase | 0.616 | 50 | 30.8 | 1 | 2024 | 2024 | 2 |
| | Cleaning machinery (pressure washer) parapet and rainwaterdischarge use phase | 0.451 | 100 | 45.1 | 1 | 2023 | 2023 | 1 |
| | Water for the cleaning machinery concrete cleaning Material | 0.01044 | 100 | 1.044 | 1 | 2023 | 2023 | 1 |
| | Concrete Paint (2.5l/m ²) Material | 838.6272 | 20 | 16772.544 | 1 | 2027 | 2027 | 5 |
| | Water for the cleaning machinery concrete cleaning Material | 0.01044 | 100 | 1.044 | 1 | 2023 | 2023 | 1 |
| | Repair Mortar (polymer) Material | 376.782848 | 7 | 2637.479936 | 1 | 2036 | 2036 | 12 |
| | Cleaning machinery (pressure washer)(cleaner) concrete use phase | 18.3 | 100 | 1830 | 1 | 2023 | 2023 | 1 |
| | Plastering machine (painting)(maintenance workers) concrete use phase | 160.8 | 20 | 3216 | 1 | 2027 | 2027 | 5 |
| | Repairing machinery (saw) (construction crew) reinforcement use phase | 173.6 | 7 | 1215.2 | 1 | 2036 | 2036 | 12 |
| | Removal machinery (corrosion cleaner)(maintenance workers) corrosion use phase | 80.4 | 50 | 4020 | 1 | 2024 | 2024 | 2 |
| | Cleaning machinery (pressure washer)(cleaner) parapet and rainwaterdischarge use phase | 12.2 | 100 | 1220 | 1 | 2023 | 2023 | 1 |
| | Concrete repair works | 566.64 | 7 | 3966.48 | 1 | 2036 | 2036 | 12 |
| | End | Truck driven from the factory to the bridge and back, steel and concrete end of life phase | 130.968 | 1 | 130.968 | 1 | 2122 | 2122 |
| Crane driven from the origin and back end-of-life phase | | 14.688 | 1 | 14.688 | 1 | 2122 | 2122 | 100 |
| Crane operated during end-of-life phase | | 122.4 | 1 | 122.4 | 1 | 2122 | 2122 | 100 |
| Machinery 1 (used by construction crew) end-of-life phase | | 2.31 | 1 | 2.31 | 1 | 2122 | 2122 | 100 |
| Machinery 2 (used by construction crew) end-of-life phase | | 2.75 | 1 | 2.75 | 1 | 2122 | 2122 | 100 |
| Machinery 4 (drill used by construction crew) end-of-life phase | | 0.66 | 1 | 0.66 | 1 | 2122 | 2122 | 100 |
| Machinery 5 (saw used by construction crew) end-of-life phase | | 0.792 | 1 | 0.792 | 1 | 2122 | 2122 | 100 |
| Crane rental end-of-life phase | | 876 | 1 | 876 | 1 | 2122 | 2122 | 100 |
| Truck driven from the factory to the bridge and back, steel and concrete end of life phase | | 103.6 | 1 | 103.6 | 1 | 2122 | 2122 | 100 |
| Crane driven from the origin and back end-of-life phase | | 141 | 1 | 141 | 1 | 2122 | 2122 | 100 |
| Construction crew (6 people) end-of-life phase | | 2343.6 | 1 | 2343.6 | 1 | 2122 | 2122 | 100 |
| Concrete Disposal | | 354.40356 | 1 | 354.40356 | 1 | 2122 | 2122 | 100 |
| Steel Recycling | | -1590.053038 | 1 | -1590.053038 | 1 | 2122 | 2122 | 100 |

C.16 3D printed bridge activity costs calculation

| | LCC | | | | | | | | |
|--|--|--|-------------------|------------|--------------|--------------------------------------|------------------------------------|--------------------------------------|-----|
| | Component/Activity | Cost of 1 unit | Frequency in 100y | Total cost | Duration [y] | Starting year of the first iteration | Ending year of the first iteration | Time boundary between iterations [y] | |
| Production | Bridge production phase | 3577.86 | 1 | 3577.86 | 2 | 2022 | 2023 | 100 | |
| | Stainless steel grade 304L | 14040 | 1 | 14040 | 2 | 2022 | 2023 | 100 | |
| Construction | Boat driven from the MX3D to the bridge and back construction phase | 71.4 | 1 | 71.4 | 1 | 2023 | 2023 | 100 | |
| | Crane driven from the origin and back construction phase | 14.688 | 1 | 14.688 | 1 | 2023 | 2023 | 100 | |
| | Crane operated during construction phase | 97.92 | 1 | 97.92 | 1 | 2023 | 2023 | 100 | |
| | Machinery 1 (used by construction crew) construction phase | 2.09 | 1 | 2.09 | 1 | 2023 | 2023 | 100 | |
| | Machinery 2 (used by construction crew) construction phase | 2.31 | 1 | 2.31 | 1 | 2023 | 2023 | 100 | |
| | 3D printing | 1606.176 | 1 | 1606.176 | 1 | 2023 | 2023 | 100 | |
| | Crane rental construction-phase | 730 | 1 | 730 | 1 | 2023 | 2023 | 100 | |
| | Boat driven from the MX3D to the bridge and back construction phase | 107.5 | 1 | 107.5 | 1 | 2023 | 2023 | 100 | |
| | Crane driven from the origin and back end-of-life phase | 117.5 | 1 | 117.5 | 1 | 2023 | 2023 | 100 | |
| | Construction crew (10 people) construction phase | 3906 | 1 | 3906 | 1 | 2023 | 2023 | 100 | |
| Use | Bridge Deck power wash with water to remove salt residue (pressure washer) Use phase | 0.6765 | 100 | 67.65 | 1 | 2023 | 2023 | 1 | |
| | Expansion Joints power, sand and salt residue (pressure washer) Use phase | 0.451 | 100 | 45.1 | 1 | 2023 | 2023 | 1 | |
| | Bridge Seats clean around bearings by flushing with (air blast) Use phase | 0.22 | 100 | 22 | 1 | 2023 | 2023 | 1 | |
| | Paint isolated areas of rusted steel (painting) (once in 2-4years) Use phase | 0.462 | 34 | 15.708 | 1 | 2025 | 2025 | 3 | |
| | Removal machinery (corrosion cleaner) corrosion Use phase | 0.77 | 25 | 19.25 | 1 | 2026 | 2026 | 4 | |
| | Water for Deck power wash with water to remove salt residue | 0.01044 | 100 | 1.044 | 1 | 2023 | 2023 | 1 | |
| | Water for Expansion Joints power wash | 0.01044 | 100 | 1.044 | 1 | 2023 | 2023 | 1 | |
| | Paint isolated areas of rusted steel | 96.8886 | 34 | 3294.212 | 1 | 2025 | 2025 | 3 | |
| | Bridge Deck power wash with water to remove salt residue (pressure washer) | 18.3 | 100 | 1830 | 1 | 2023 | 2023 | 1 | |
| | Expansion Joints power, sand and salt residue (pressure washer) | 12.2 | 100 | 1220 | 1 | 2023 | 2023 | 1 | |
| | Bridge Seats clean around bearings by flushing with (air blast) | 12.2 | 100 | 1220 | 1 | 2023 | 2023 | 1 | |
| | Paint isolated areas of rusted steel (painting) (once in 2-4years) | 80.4 | 34 | 2733.6 | 1 | 2025 | 2025 | 3 | |
| | Removal machinery (corrosion cleaner) corrosion use phase | 100.5 | 25 | 2512.5 | 1 | 2026 | 2026 | 4 | |
| | End-of-life | Truck driven from the factory to the bridge and back, steel and concrete end of life phase | 96.696 | 1 | 96.696 | 1 | 2122 | 2122 | 100 |
| | | Crane driven from the origin and back end-of-life phase | 14.688 | 1 | 14.688 | 1 | 2122 | 2122 | 100 |
| Crane operated during end-of-life phase | | 146.88 | 1 | 146.88 | 1 | 2122 | 2122 | 100 | |
| Machinery 1 (used by construction crew) end-of-life phase | | 1.386 | 1 | 1.386 | 1 | 2122 | 2122 | 100 | |
| Machinery 2 (used by construction crew) end-of-life phase | | 0.99 | 1 | 0.99 | 1 | 2122 | 2122 | 100 | |
| Machinery 4 (drill used by construction crew) end-of-life phase | | 1.584 | 1 | 1.584 | 1 | 2122 | 2122 | 100 | |
| Machinery 5 (saw used by construction crew) end-of-life phase | | 1.584 | 1 | 1.584 | 1 | 2122 | 2122 | 100 | |
| Crane rental end-of-life phase | | 1022 | 1 | 1022 | 1 | 2122 | 2122 | 100 | |
| Truck driven from the factory to the bridge and back, steel and concrete end of life phase | | 44.4 | 1 | 44.4 | 1 | 2122 | 2122 | 100 | |
| Crane driven from the origin and back end-of-life phase | | 164.5 | 1 | 164.5 | 1 | 2122 | 2122 | 100 | |

C.17 Cycle Cost distribution (wider perspective), Concrete bridge

